NASA CR-72786
GE R70 AEG 426

TASK II STAGE DATA AND PERFORMANCE REPORT

FOR

INLET FLOW DISTORTION TESTING

VOLUME I

EVALUATION OF RANGE AND DISTORTION TOLERANCE FOR HIGH MACH NUMBER TRANSONIC FAN STAGES

By

W.A. Tesch and V.L. Doyle

GENERAL ELECTRIC COMPANY
Aircraft Engine Group
Cincinnati, Ohio 45215

Prepared For

NATIONAL AERONAUTICS AND SPACE ADMINISTRATION

January 1971

NASA Lewis Research Center
Contract NAS3-11157
Charles H. Voit Project Manager

12

Requests for copies of this report should be referred to:

National Aeronautics and Space Administration
Office of Scientific and Technical Information
Attention: AFSS-A
Washington, D.C. 20546

NASA CR-72786
GE R70 AEG 426

TASK II STAGE DATA AND PERFORMANCE REPORT
FOR
INLET FLOW DISTORTION TESTING

VOLUME I

EVALUATION OF RANGE AND DISTORTION TOLERANCE FOR HIGH MACH NUMBER TRANSONIC FAN STAGES

By

W.A. Tesch and V.L. Doyle

GENERAL ELECTRIC COMPANY
Aircraft Engine Group
Cincinnati, Ohio 45215

Prepared For

NATIONAL AERONAUTICS AND SPACE ADMINISTRATION

January 1971

NASA Lewis Research Center
Contract NAS3-11157
Charles H. Voit Project Manager

ABSTRACT

A variable geometry stage consisting of a 1500 ft/sec tip speed, medium aspect ratio rotor, a variable camber inlet guide vane and a variable-stagger stator was tested under conditions of tip radial and 90° one-per-rev circumferential distorted inlet flow. Overall performance and stall limits were determined for each inlet condition at 70%, 90% and 100% of design speed. Extensive surveys of flow conditions were made for the case of circumferential distortion. In addition, blade element data were obtained when testing with radial distortion.

Volume I of this report contains a presentation and discussion of the inlet distortion test results while Volume II contains complete tabulations of the data.

PRECEDING PAGE BLANK-NOT FILMED

TABLE OF CONTENTS

VOLUME I

TABLE OF CONTENTS (Concluded)

VOLUME II

LIST OF TABLES

VOLUME I

VOLUME II

LIST OF ILLUSTRATIONS

LIST OF ILLUSTRATIONS (Continued)

LIST OF ILLUSTRATIONS (Continued)

LIST OF ILLUSTRATIONS (Continued)

LIST OF ILLUSTRATIONS (Concluded)

SECTION I

SUMMARY

This report presents the results of the NASA Task II Stage testing with inlet flow distortions. The Task II Stage consisted of a 1500 ft/sec tip-speed rotor, with an aspect ratio of 2.36 and a design pressure ratio of 1.686, together with variable-camber inlet guide vanes and variable-stagger stators.

Testing was performed for two combinations of inlet guide vane and stator setting angles for both tip-radial and circumferential inlet flow distortion. The two tested vane schedules consisted of an inlet guide vane setting angle of 0° with a stator setting angle of 0°, and also an inlet guide vane setting angle of 40° with a stator setting of 8°. Values for the distortion parameter, $(P_{max} - P_{min})/P_{max}$, equal to 0.172 and 0.159 were obtained for radial and circumferential distortion respectively at 100 percent speed.

Overall performance and stall limits were determined with both the tip-radial and circumferential inlet flow distortions at 70%, 90% and 100% speeds. In the case of circumferential distortion, extensive radial and circumferential flow surveys were made. Radial flow surveys and blade element data were also obtained for the radial distortion condition. For all tests, the rotating stalls originated at the rotor tip. With both distortions, the stage suffered significant losses in efficiency. Stage total-pressure ratio and weight flow losses for both inlet flow distortions were appreciably less with the 40° inlet guide vane stage configuration than with the zero turning configuration.

SECTION II

INTRODUCTION

The need to reduce the size and weight of gas turbine engines for advanced military and commercial aircraft has led to the use of high-tip-speed fan and compressor stages. The Task II Stage was designed under NASA Contract NAS3-11157 to obtain data on the efficiency, stall margin and distortion tolerance of high-tip-speed stages and to investigate the use of variable geometry features to maintain performance at off-design operating conditions.

The design of the NASA Task II Stage is presented in Reference 1. Reference 2 documents the testing of the Task II Stage with undistorted inlet flow.

This report presents the performance of the NASA Task II Stage when tested with tip-radial and 90° one-per-rev circumferential inlet flow distortions. Performance was determined for each inlet condition at two combinations of inlet guide vane and stator setting angles. For convenience, the inlet guide vane and stator schedule combination will be abbreviated as the numerical value of the inlet guide vane setting angle followed by the numerical value for the stator vane setting angle. Thus the combination of a 40° IGV (inlet guide vane) setting angle with an 8° stator adjustment would be written as the 40°/8° IGV/stator schedule.

In addition to overall performance and the effect on stall limits, blade element data were obtained for the case of radial distortion. Blade element data used for velocity diagram calculations, were recorded using traverse probes at each blade row inlet and exit. For the case of circumferential distortion, detailed flow surveys were performed at each blade row inlet and discharge. These were obtained by rotating the circumferential distortion screen to various positions relative to the fixed rakes and traverse probes.

SECTION III

APPARATUS AND PROCEDURE

1. TEST COMPRESSOR STAGE

The Task II Stage used for this program consisted of a 1500 ft/sec tip-speed rotor and variable-geometry guide vanes and variable-stagger stators. The Task II Stage test vehicle employed much of the existing hardware from earlier Task I testing performed under this contract, including the stators. New hardware included the IGV assembly and rotor.

Table I is a summary of Task II Stage blade row design parameters and predicted performance. Additional details of the Task II Stage design are given in Reference 1. The inlet corrected weight flow of the Task II Stage was selected to be 226 lbs/sec, with a specific weight flow of 41.62 lbs/sec-sq ft of annulus area. The required Task II rotor tip diffusion factor of 0.35 and the rotor tip speed of 1500 ft/sec dictated that Task II rotor total-pressure ratio to be just under 1.7. The rotor blades employed arbitrarily shaped tip sections to minimize shock losses and excess flow area. These sections were smoothly blended to a double-circular-arc-type section at the hub. The stator had double-circular-arc-type vane sections at the outer part of the blade which blended into arbitrarily shaped hub sections designed especially for low suction surface Mach numbers. Stator hub solidity was 2.155, and aspect ratio was 2.065 with radially non-constant chord. The inlet guide vane was derived from an uncambered NACA series 65 airfoil with a maximum thickness to chord ratio of 10%. The vane was made in two parts to accomplish camber variation. The nose part, whose chord was 20.43% of the total chord, was fixed in the axial direction. The rear flap, with a chord that was 79.57% of the total, could be rotated to vary the trailing edge angle. The solidity, based on the sum of the nose and flap chords, ranged from 1.299 at the tip to 1.788 at the hub.

2. TEST FACILITY

Performance tests were conducted in General Electric's house compressor test facility in Lynn, Massachusetts. The test compressor drew atmospheric

air through two banks of filters. The first filter bank was intended to remove 22% of the particles larger than 3-5 microns (dust spot test), and the second filter bank was intended to remove 90-95% of the remaining particles down to the same size. The air then passed through a coarse-wire inlet screen, into the bellmouth and then through the distortion screen and compressor. In the exit assembly, the compressor discharge flow was split into two concentric streams. The inner air stream was passed into an exit pipe containing a flow straightener and a venturi flow meter and then was exhausted to the atmosphere. The outer air stream passed through a slide cylindrical throttle valve into a collector. Two pipes, each of which contained a flow straightener and a venturi flow meter, then discharged the outer stream to the atmosphere. Power to drive the test compressor was provided by a high-pressure non-condensing steam turbine rated at 15,000 horsepower. A schematic diagram of the test facility is shown in Figure 1.

3. INLET DISTORTION EQUIPMENT

The Task II inlet distortion screens were the same as those used in the Task I distortion testing performed under NASA Contract NAS3-11157. Both radial and circumferential distortions were tested. The radial distortion screen for Task II, shown in Figure 2, covered the outer 40% of the annulus area, while the circumferential screen, shown in Figure 3, spanned a 90° arc from hub to tip. Both screens were made of 20-mesh 0.016-inch diameter wire, giving a screen open area of 0.46. The screen material was selected to give a distortion parameter, $(P_{max} - P_{min})/P_{max}$, equal to 0.20 with a design flow of 226 lbs/sec at 100% design speed.

The support screen, which spanned the entire annulus and to which the distortion screens were attached, was designed to be rotated 360° past the instrumentation for the circumferential inlet distortion testing. The support screen material was one-inch-square mesh with 0.093-inch diameter wire, and gave an open area of 83.4%. The Task II support screen was designed to separate into halves to facilitate installation.

The distortion screens were located one rotor diameter forward of the rotor leading edge, and were mounted in a cylindrical section approximately one-rotor diameter long which was inserted into the test vehicle only during distortion testing.

4. INSTRUMENTATION

A listing of fixed and traverse instruments provided for each phase of the distortion testing is given in Table II. The locations of these instruments, and of hub and casing static taps are shown in the instrumentation schematics, Figures 4 and 5.

All traverse probes were calibrated for Mach number and pitch angle effects, and these calibrations were used in the data reduction calculations. Static wire calibrations for thermocouple sensors were properly accounted for. Fixed temperature and pressure rakes were calibrated for Mach number effects, but these proved to be small enough for the case of pressure elements to be neglected.

Overall performance measurements were obtained from fixed instrumentation at stage inlet and exit, located at seven radial positions on design streamlines passing through the 5%, 10%, 30%, 50%, 70%, 90%, and 95% of annulus height from the tip at Plane 1.51. The inlet total pressure forward of the distortion screen was measured by six 7-element pitot-static rakes located at Plane 0.01. The inlet total temperature was measured with 24 chromel-alumel thermocouples distributed over the face of the vehicle inlet screen. The inlet total pressure aft of the distortion screen was obtained by two 7-element total-pressure distortion rakes located at Plane 0.18 in the 30° and 195° circumferential positions. Figure 6(a) illustrates one of these rakes. Stage exit conditions were measured at Plane 2.20 with seven 14-element total-pressure and total-temperature wake rakes. An example of these rakes can be seen in Figure 6(b). Discharge static pressures were measured by eight hub and eight casing static taps at the exit plane.

Radial distortion blade element immersion data (total pressure, total temperature, static pressure and flow angle) were measured at each blade row inlet and exit by a 4-parameter combination probe designated T-1, T-3, T-8 and T-11 in Figure 5. For circumferential distortion, traverse data were recorded at the 10%, 50% and 90% immersions by the 4-parameter probes instead of at the usual seven immersions. Figure 6(c) is an enlarged photograph of the sensing head on the combination probe. The combination probe designated T-3 at plane 0.95, the inlet guide vane exit, had the capability of traversing circumferentially. This capability insured that measurements taken at the inlet guide vane exit would be taken in mid-channel between adjacent inlet guide vanes and not in a vane wake.

Three hot-wire anemometer probes at Plane 1.51 were used during all stall tests at the 10%, 50% and 90% immersions to determine the initiation of stall and the radial extent of the stall cells. For all other testing the hot-wire probes were removed from the airstream. One of the probes is illustrated in Figure 6(d).

5. DATA REDUCTION METHODS

Three separate computer programs were used to reduce the test data. The Overall Performance Data Program computed average fluid properties at each measuring station from data measured by fixed instruments and calculated overall stage and rotor performance parameters such as total-pressure ratio and adiabatic efficiency. The Blade Element Data Program calculated vector diagram and blade element performance parameters for seven streamline sections. This program reduced data from both fixed and traversing instruments. These two computer programs were used primarily to reduce data obtained during radial inlet flow distortion testing. A special Circumferential Distortion Data Program was used to calculate vector diagram data at numerous circumferential, radial and axial locations during circumferential inlet flow distortion testing. This data reduction computer program also calculated overall performance data from average fluid properties determined by special circumferential/radial mass-averaging methods. Input data were obtained from both fixed and traverse instruments at twelve different circumferential positions of the distortion screen.

Several assumptions were made that were common to all three data reduction programs. First, it was assumed that the radial position and meridional slope angle of each stream surface on which data were recorded were fixed at the design value for all operating conditions. Second, all mass-averaging calculations used to determine average total temperature and total pressure were formulated in terms of enthalpy and entropy. Finally, the real gas properties of dry air were used in all thermodynamic calculations.

Additional details of the data reduction methods used appear in the following sections.

a. OVERALL PERFORMANCE DATA PROGRAM

Average test vehicle inlet conditions ahead of the inlet distortion screen were taken as the arithmetic average of the Plane 0.01 thermocouple and total-pressure rake readings. With radial inlet flow distortion the average stage inlet total temperature was calculated as mentioned above, but inlet total pressure was radially mass-averaged from readings of the two distortion rakes located at Plane 0.18 between the distortion screen and the inlet guide vanes. The static pressure used in the mass-averaging procedure was determined at each of the seven radial instrument positions by linear interpolation versus radius between arithmetically averaged hub and casing wall static pressure values. Total pressure at each radial position was taken as the arithmetic average of the values given by the two inlet distortion rakes. An approximate value of average inlet total pressure was also calculated by this program for the case of circumferential inlet flow distortion. At each radial instrument position, the pressure reading from the Plane 0.18 rake located in the 270° undistorted region was weighted three times as heavily as that from the rake located in the 90° distorted region when calculating the local average pressure with circumferential distortion. These were then mass-averaged radially as in the case of radial inlet flow distortion. With either inlet distortion, the flow at Plane 0.18 was assumed to be axial.

Average stage exit total pressure and total temperature were calculated from data measured by the Plane 2.20 wake rakes. A simultaneous radial and

circumferential mass-averaging procedure was used to properly account for variations of measured properties across the stator spacing as well as radially. The static pressure required at each of the seven radial measurement positions was again obtained by linear interpolation between average wall static pressure values. In addition to overall fluid properties at Plane 2.20, this data reduction program also calculated average total temperature and total pressure at each radial position by mass-averaging circumferentially across each wake rake. Flow angles at Plane 2.20 were assumed to equal zero degrees plus or minus any stator stagger adjustment. In order to calculate more accurate total properties with circumferential distortion at each specific discharge wake rake radial and circumferential location, the static pressure associated with each particular wake rake was interpolated from readings of hub and casing wall static taps located at the same circumferential position as the wake rake. These methods of obtaining discharge conditions were believed to offer excellent accuracy for axisymmetric flow fields expected with radially distorted inlet conditions, but to be only approximate for circumferential distortion testing.

Rotor exit total pressure at each of the seven radial measurement positions was taken as the arithmetic average of the three highest readings on each stage exit wake rake. Total temperature at each radial position was assumed equal to the stage exit value. Average total pressure at the rotor exit station was calculated by a radial mass-averaging procedure which used a weight flow at each radial position calculated from stage exit properties and flow angles.

During undistorted inlet tests, inlet guide vane total-pressure loss coefficients were determined using special test procedures as discussed in Reference 2. The rotor inlet total pressure at each immersion at Plane 0.95 for the distortion testing was determined using a table of inlet guide vane loss coefficients versus inlet Mach number and guide vane turning angle. The guide vane inlet Mach number was calculated using the distortion rake total pressure and the static pressure obtained through a linear interpolation between arithmetically averaged casing and hub measured static pressures.

The average rotor inlet total pressure was calculated using a radial mass-averaging procedure, assuming the flow angle at the rotor inlet, Plane 0.95, equal to the inlet guide vane camber angle. The IGV losses determined from the undistorted inlet tests were used for both radial and circumferential inlet distortion testing. This procedure was only approximate with circumferential distortion due to the guide vane incidence angle variations resulting from the non-axisymmetric flow.

The average total temperatures and total pressures at the stage inlet, rotor inlet, rotor exit and stage exit measurement stations were used to calculate overall performance parameters of total-pressure ratio, total-temperature ratio and adiabatic and polytropic efficiency for the stage as a whole and for the rotor as an isolated blade row. The weight flow was corrected to standard day conditions at Plane 0.18. In addition, the Overall Performance Data Program calculated local average total temperature and total pressure at seven radial positions at each measuring station which could be used as input data to the other data reduction computer programs.

b. BLADE ELEMENT DATA PROGRAM

Blade element and vector diagram data were obtained at seven immersions for rotor, stator and inlet guide vanes during radial distortion tests. Circumferential uniformity was assumed for all such data. The primary data used for blade element calculations were obtained by combination probes at each blade row inlet and exit. These probes measured total temperature and pressure, static pressure and flow angle at Planes 0.18 (IGV inlet), 0.95 (IGV exit/rotor inlet), 1.51 (rotor exit/stator inlet) and 2.20 (stator exit).

After the thermodynamic properties had been determined at seven radial positions at each measuring plane, they were transferred along streamlines to the leading and trailing edges of each blade row. The slopes, radii and streamtube convergence along streamlines between measurement station and blade edge were assumed to remain fixed at the design values for all flow conditions. The tangential velocity was obtained at the edges of the blades by applying the condition of constant moment of angular momentum along each streamline. The calculated meridional Mach number at the measurement station

was used to determine the meridional Mach number at the blade edge from the streamtube convergence relationship illustrated in Figure 7. This method was a good approximation when the radius change between the blade edge of the measurement station was small. However, since there was appreciable swirl velocity at the rotor trailing edge, any large radius changes would adversely affect the approximate results. Table III gives the constants used in these computations for the inlet guide vane, rotor and stator. With the measured total conditions assumed to be constant along the design streamlines and the tangential velocities and meridional Mach numbers determined at blade edges in the above manner, the velocities, Mach numbers and all vector diagram components were determined at the edges of each blade row.

Calculated blade element performance parameters included diffusion factor, static-pressure-rise coefficient, total-pressure loss coefficient and loss parameter, adiabatic and polytropic efficiency, plus total-temperature and total-pressure ratios. Alternate values of rotor and stator total-pressure loss coefficient and loss parameter and of blade element efficiency were calculated by using total temperature and rotor exit total pressure measured by the stage exit wake rakes in place of the combination probe measurements at Plane 1.51.

c. CIRCUMFERENTIAL DISTORTION DATA PROGRAM

With the non-axisymmetric flow produced by circumferential inlet flow distortions, special procedures were required in order to determine the circumferential variation of vector diagram parameters and to calculate overall performance from fluid properties that had been mass-averaged circumferentially as well as radially. At certain operating conditions, compressor speed and weight flow were maintained constant and the distortion screen was rotated to twelve different circumferential positions. Both fixed and traverse instruments were read at each screen position.

Stage exit total temperatures and total pressures, measured at Plane 2.20 by wake rakes, were obtained in the form of local mass-averaged values at 10, 30, 50, 70 and 90% immersions at each screen position by processing the fixed instrument data through the Overall Performance Data Program.

Stage exit static pressure and flow angle were measured by a four-parameter traverse probe at Plane 2.20 immersed to the 10, 50 and 90% immersions at each screen position. At Planes 0.18, 0.95 and 1.51, the stage inlet, rotor inlet and rotor exit planes, the total pressures, static pressures and flow angles were measured at three immersions by four-parameter probes. Rotor exit total temperatures were also obtained from the Plane 1.51 four-parameter probe.

These data were then input to the Circumferential Distortion Data Program. Input data were first corrected for variations in atmospheric conditions by applying temperature and pressure correction factors θ and δ as determined from the Plane 0.01 data listed in the output of the Overall Performance Data Program for the appropriate screen position. The stage inlet temperature was then assumed constant, equal to 518.688°R. Radial interpolations versus radius were used with the data from the traverse probes to determine fluid properties at the 30% and 70% immersions where traverse data were not recorded. The circumferential position of each instrument, and thus of each item of measured data, relative to the distortion screen centerline was then determined. Finally, by linear interpolation versus circumferential position, a value of total temperature, total pressure, static pressure and flow angle was deduced at twelve standard circumferential positions and five radial positions at each of Planes 0.18, 0.95, 1.51 and 2.20.

These four fluid conditions, plus the assumption of design streamline slope angle, were sufficient to calculate all vector diagram components at each of the standard points in the flow field. In addition to calculating vector diagram data, the Circumferential Distortion Data Program also used this extensive set of data to calculate an average value of total temperature and total pressure at each measuring station. These were obtained by a mass-averaging procedure which accounted for circumferential as well as radial variations. These average fluid properties were then used to calculate the total-pressure ratio, total-temperature ratio, and adiabatic and polytropic efficiency for the stage and for the rotor as an isolated blade row. Values of weight flow corrected to standard day conditions, $W\sqrt{\theta}/\delta$, at both IGV

inlet and rotor inlet were calculated using δ values obtained from fully mass-averaged total pressures at Planes 0.18 and 0.95.

6. TEST PROCEDURE

The distortion testing of the NASA Task II Stage was performed at 70%, 90% and 100% of rotor design speed for each of two specified stage configurations with radial and circumferential inlet flow distortions. The two configurations consisted of the nominal (0°/0°) and 40°/8° IGV/stator schedules selected for undistorted inlet testing, as described in Reference 2.

The first part of each test run was concerned with defining the stall points for that particular stage configuration and inlet flow distortion. When determining the stall point, the discharge throttle was closed until strain-gage and hot-wire anemometer signals indicated that rotating stall cells had formed in the rotor. Three shielded hot-wire anemometers were immersed to the 10, 50 and 90% positions at Plane 1.51 and oscillograph traces were obtained which showed the radial extent of the stalled region. The throttle valve was then reset to an unstalled condition close to the stall limit and overall performance data were recorded.

An ICPAC* trace was obtained whenever the vehicle was stalled, and the approximate stalling weight flow was obtained by recording the ICPAC flow at the instant stall was detected. The true stalling weight flow was obtained from a correlation of ICPAC flow versus actual weight flow using values obtained during overall performance testing.

a. RADIAL DISTORTION TESTING

When the stall limits for radial distortion had been established, overall performance data were recorded at 70, 90 and 100% of rotor design

---

* The ICPAC (Instantaneous Compressor Performance Analysis Computer) is an analogue circuit which senses weight flow and pressure ratio, and which plots these quantities nearly instantaneously to provide an approximate on-line compressor performance map.

speed for both IGV/stator schedules at discharge throttle valve settings where maximum flow, near-stall and intermediate flow conditions were expected.

During radial distortion testing, blade element traverse tests were accomplished using the combination probes located at Planes 0.18, 0.95, 1.51 and 2.20 for three flow conditions for each IGV/stator schedule. For the nominal IGV/stator schedule, blade element traverses were performed for flow conditions of 100% design speed at both maximum weight flow and near-stalling flow; a traverse was also obtained at 70% speed at the intermediate flow condition. For the 40°/8° IGV/stator schedule, blade element data were obtained at 70% design speed at maximum flow and near-stalling flow, and also at 100% design speed at the intermediate flow condition. At the conclusion of each blade element traverse, the probes were retracted out of the airstream and overall performance data were recorded.

b. CIRCUMFERENTIAL DISTORTION TESTING

Circumferential distortion overall performance testing methods were similar to those used with radial distortion. Once the stall points had been identified for 70%, 90% and 100% of rotor design speed, overall performance data were obtained for flow conditions of maximum flow near-stall and intermediate flow for each speed at both IGV/stator schedules.

In addition to overall performance testing, detailed radial and circumferential flow surveys were made. These surveys were performed using the distortion screen rotation capability and the combination traverse probes. Screen rotation tests were performed at flow conditions similar to those used for the radial distortion blade element traverses. For each operating condition, at each of twelve circumferential distortion screen positions spaced every 30°, overall performance data were recorded and traverse data were obtained at immersion positions of 10%, 50%, and 90%. At each screen position, following the traverse test, the probes were retracted out of the airstream and overall performance data were recorded. These data were processed using the Circumferential Distortion Data Program as discussed in the Data Reduction Methods section.

SECTION IV

RESULTS AND DISCUSSION

The testing reported herein was conducted on the NASA Task II Stage subjected to inlet flow distortions. The performance of the stage with undistorted inlet flow is documented in Reference 2. The performance obtained with radial and circumferential inlet flow distortion is presented in the following sections.

1. RADIAL DISTORTION TEST DATA

The distortion screen used to produce the tip-radial distortion is shown in Figure 2. At 100% design speed, near the limit of stall-free operation and with the nominal IGV/stator schedule, the severity of the distortion pattern is indicated by the value of the distortion parameter $(P_{max} - P_{min})/P_{max}$, equal to 0.172. Figure 8 shows the distortion parameter variation for both radial and circumferential inlet distortions over the weight flow range at all speeds tested. These data were calculated from overall performance results with radial and circumferential distortions.

a. OVERALL PERFORMANCE DATA

A listing of overall performance readings obtained with radial distortion is given in Table IV(a). The stage performance map based on the overall performance data for the nominal IGV/stator schedule is shown in Figure 9. Similarly, Figure 10 presents the performance map for the 40°/8° IGV/stator schedule. The dashed lines on these maps indicate the performance of the stage with undistorted inlet flow as presented in Reference 2. As can be seen there was a significant reduction in adiabatic efficiency and total-pressure ratio for both stage configurations due to the tip-radial distortion.

The radial distortion stall lines are indicated on the performance maps, Figures 9 and 10, for the two IGV/stator schedules. The stalling weight flow and total-pressure ratio were obtained as discussed in the Test Procedure Section. Rotating stalls were encountered at all speeds. Ocillograph traces obtained from shielded hot-wire anemometers indicated that the rotating stall

cells were most severe at the tip and were very weak at the hub in all instances. At 100% of design rotor speed, the tip-radial distortion resulted in reductions in stalling total-pressure ratio from 1.76 to 1.645 and from 1.425 to 1.37 for the nominal and 40°/8° IGV/stator schedules, respectively, when compared to the undistorted inlet stall line.

b. BLADE ELEMENT DATA

Figures 11(a)-(d) present radial profiles of total and static pressure, total temperature, axial velocity and flow angle obtained from blade element traverse measurements at 100% speed near stall with the nominal (0°/0°) IGV/stator schedule. Figures 12(a)-(d) present similar data obtained at 70% speed near stall with the 40°/8° IGV/stator schedule. Radial distributions of rotor and stator diffusion factors for conditions near stall and maximum flow are presented in Figure 13 for the 0°/0° IGV/stator schedule at 100% speed and in Figure 14 for the 40°/8° IGV/stator schedule at 70% speed. Rotor and stator total-pressure-loss coefficient, total-pressure-loss parameter, and deviation angles calculated by the blade element data program are plotted against diffusion factor over the speed range for each of seven immersions. Figures 15(a)-(g) and 16(a)-(g) show the nominal (0°0°) IGV/stator schedule blade element data, while the results for the 40°/8° IGV/stator schedule are displayed in Figures 17(a)-(g) and 18(a)-(g).

A complete tabulation of blade element data with radial distortion is given for all three blade rows in Appendix B, Volume II of this report.

2. CIRCUMFERENTIAL DISTORTION TEST DATA

The distortion screen used to produce the circumferential distortion is shown in Figure 3. The screen covered a 90° arc of the inlet annulus area at plane 0.10. A value for the distortion parameter, $(P_{max} - P_{min})/P_{max}$, equal to 0.159 was determined from tests for the near-stall limit condition at 100% design speed with the nominal IGV/stator schedule. The nominal distortion screen centerline position was 195° from top center to insure that the center of the screen would be aligned with one of the distortion rakes. Figure 8 shows the variation of the circumferential distortion parameter over the entire weight flow range tested based on

maximum and minimum total pressures on the inlet distortion rakes (R-7 and R-8, Figure 3) with the center of the distortion screen in the nominal position, 195° from top center.

a. OVERALL PERFORMANCE DATA

Table IV(b) contains a listing of the overall performance readings obtained with circumferential inlet distortion. Figure 19 presents the compressor performance map for the nominal (0°/0°) IGV/stator schedule. Similarly, Figure 20 contains the performance map for the 40°/8° IGV/stator schedule. The dashed lines indicate the performance of the stage with undistorted inlet flow. The performance maps were constructed using adjusted overall performance data.

Due to the limited sampling of data for single readings taken with the distortion screen in the nominal position, the Overall Performance Data Program calculated somewhat inaccurate average values of fluid properties and overall performance parameters for circumferentially distorted flow. In order to obtain data more representative of actual flow conditions, overall performance and traverse data were obtained at twelve screen positions for a single operating point as described in the Test Procedure Section. The screen rotation test data were processed using the Circumferential Distortion Data Program to obtain circumferentially as well as radially mass-averaged stage inlet and exit total pressures, and stage exit total temperatures. A correlation was then made between the circumferential distortion output average properties and the corresponding properties obtained from the single overall performance reading at the nominal distortion screen position. Results obtained using readings 10-21, 22-33, 34-45, 77-88, 119-130 and 132-143 were correlated with data from readings 10, 22, 34, 77, 119 and 132, respectively, which were obtained with a nominal (195°) distortion screen centerline position. A set of average correction factors was then obtained for stage pressure ratio and discharge total temperature for each IGV/stator schedule. These corrections were then applied to the readings for which no screen rotation tests were performed and new overall performance parameters were calculated. Table IV(b) and Figures 19 and 20 reflect the corrected overall performance values.

The performance maps show that both configurations suffered significant losses in efficiency due to the circumferential inlet distortion. However, the weight flow and pressure ratio penalties with the 40°/8° IGV/stator schedule were less than with the nominal schedule.

The circumferential distortion stall lines are indicated on the performance maps, Figures 19 and 20, for the two IGV/stator schedules tested. As in the radial distortion case, rotating stall cells were most severe at the rotor tip and weakest at the hub. For the nominal IGV/stator schedule at 100% design speed, the circumferential distortion resulted in a decrease in stalling total-pressure ratio from 1.76 to 1.66 when compared to the clean inlet stall line. Similarly, at 100% design speed, the 40°/8° schedule showed a decrease in stalling total-pressure ratio from 1.425 to 1.38.

b. FLOW SURVEY DATA

Figures 21-23 and 24-26 present circumferential profiles of flow conditions at each plane for the nominal (0°/0°) and 40°/8° IGV/stator schedules, respectively. Data is presented for 10%, 50% and 90% immersions. A detailed listing of flow properties and velocity diagram data is given in Appendix C of Volume II. These data were obtained during screen rotation tests and processed by the Circumferential Distortion Data Program.

APPENDIX A - SYMBOLS

Symbol	Description	Units
A	Annulus or Streamtube Area	in^2.
C	Chord Length of Cylindrical Section	in.
C_h	Enthalpy-Equivalent Static-Pressure-Rise Coefficient, ie for Rotor: $C_h = \frac{2gJc_p t_1 \left[\left(\frac{p_2}{p_1}\right)^{\frac{\gamma-1}{\gamma}} - 1\right] - (U_2^2 - U_1^2)}{V_1'^2}$	---
C_p	Static-Pressure-Rise Coefficient, ie for Rotor: $C_p = \frac{p_2 - p_1}{P_1' - p_1}$.	---
c_p	Specific Heat at Constant Pressure, 0.2399 Btu/lb-°R	
D	Diffusion Factor: $D_{Rotor} = 1 - \frac{V_2'}{V_1'} + \frac{r_2 V_{\theta_2} - r_1 V_{\theta_1}}{2\bar{r}\ \sigma\ V_1'}$ $D_{IGV/Stator} = 1 - \frac{V_2}{V_1} + \frac{r_1 V_{\theta_1} - r_2 V_{\theta_2}}{2\bar{r}\ \sigma\ V_1}$	---
g	Acceleration Due to Gravity, 32.174 ft/sec^2	
i	Incidence Angle; Difference Between Flow Angle and Camber Line Angle at Leading Edge in Cascade Projection	deg
J	Mechanical Equivalent of Heat, 778.161 ft-lb/Btu.	
K_{bl}	Effective Area Coefficient Due to Wall Boundary Layer Blockage	---
M	Mach Number	---
N	Rotational Speed	rpm

APPENDIX A - SYMBOLS (Continued)

Symbol	Description	Units
P	Total or Stagnation Pressure	psia
p	Static Pressure	psia
r	Radius	in.
$\bar{r}$	Mean Radius, Average of Streamline Leading and Trailing Edge Radii	in.
T	Total or Stagnation Temperature	°R
t	Static Temperature	°R
U	Rotor Speed	ft/sec
V	Air Velocity	ft/sec
W	Weight Flow	lbs/sec
Z	Displacement Along Compressor Axis	in.
β	Flow Angle; Angle Whose Tangent is the Ratio of Tangential to Axial Velocity	deg
$\Delta\beta$	Flow Turning Angle, $\Delta\beta = \beta_1 - \beta_2$	deg
γ	Ratio of Specific Heats	---
γ°	Blade-Chord Angle (Stagger), Angle in Cascade Projection Between Blade Chord and Axial Direction	deg
δ	Pressure Correction, $P_{Actual}/14.696$ psia	
δ°	Deviation Angle, Difference Between Flow Angle and Camber Angle at Trailing Edge in Cascade Projection	deg
ϵ°	Slope of Meridional Streamline	deg
η	Efficiency	
θ	Temperature Correction, $T_{Actual}/518.7°R$	
θ°	Circumferential Position From Top Center	deg

Symbol	Description	Units
$K°$	Angle Between Tangent to Blade Meanline and the Axial Direction	deg
σ	Solidity, Ratio of Chord to Blade Spacing	---
$\phi°$	Camber Angle, Difference Between Angles in Cascade Projection of Tangents to Camberline at the Extremes of the Camberline Arc	deg
$\bar{\omega}$	Total Pressure Loss Coefficient Rotor: $\bar{\omega}' = \frac{P_2'_{id} - P_2'}{P_1' - p_1}$, IGV/Stator: $\bar{\omega} = \frac{P_1 - P_2}{P_1 - p_1}$	---
$\frac{\bar{\omega}\text{Cos}\beta_2}{2\sigma}$	Total Pressure Loss Parameter	---

Subscripts

ad	Adiabatic
an	Annulus
d	Downstream Measurement Station (Table III)
e	Edge of Blade (Figure 7)
id	Ideal
j	Immersion
m	Meridional Direction
p	Polytropic
s	Measurement Station (Figure 7)
t	Tip at Station 1.0
u	Upstream Measurement Station (Table III)
z	Axial Direction
θ	Tangential Direction

APPENDIX A - SYMBOLS (Concluded)

Subscripts	Description
1	Leading Edge
2	Trailing Edge
0.01	Measurement Station Designation
0.18	Measurement Station Designation
0.95	Measurement Station Designation
1.51	Measurement Station Designation
2.20	Measurement Station Designation

Superscripts	Description
'	Relative to Rotor
*	Critical Flow Condition

REFERENCES

1. Doyle, V.L. and Koch, C.C.: Evaluation of Range and Distortion Tolerance for High Mach Number Transonic Stages, Design Report, NASA CR-72720, 1970.

2. Bilwakesh, K.R.: Evaluation of Range and Distortion Tolerance for High Mach Number Transonic Fan Stages, Task II Stage Data and Performance Report for Undistorted Inlet Flow Testing, Volumes I and II, NASA CR-72787, 1971.

Table I. Summary of Stage Design Specifications and Performance

	TASK II STAGE
Rotor inlet corrected tip speed, ft/sec	1500
Stage inlet corrected weight flow, lbs/sec	226.0
Stage total-pressure ratio	1.659
Stage adiabatic efficiency	0.854
Number of inlet guide vanes	24
Inlet guide vane total-pressure loss, percent inlet total pressure	0.37
Inlet guide vane exit flow angle, deg.	0
Rotor inlet tip diameter, in.	36.5
Rotor inlet hub: tip radius ratio	0.5
Rotor inlet corrected weight flow per unit annulus area, lbs/sec-sq ft	41.62
Rotor inlet tip relative Mach number	1.526
Rotor tip diffusion factor	0.368
Rotor total-pressure ratio	1.686
Rotor adiabatic efficiency	0.883
Rotor tip solidity	1.4
Rotor aspect ratio	2.36
Number of rotor blades	44
Stator inlet hub absolute Mach number	0.766
Stator exit flow angle, deg.	0
Stator hub diffusion factor	0.435
Stator total-pressure loss, percent stator inlet total pressure	1.22
Stator hub solidity	2.155
Stator aspect ratio	2.065
Number of stator vanes	46

Table II. Summary of Instrumentation Used For Task II Distortion Testing

Location	Instrumentation
0.01 Vehicle Inlet	6 7-element pitot-static rakes 24 total-temperature thermocouples
0.18 Stage Inlet	2 7-element total pressure distortion rakes 1 4-parameter combination probe (total temperature and pressure, static pressure, flow angle)
0.95 Rotor Inlet	1 4-parameter combination probe with circumferential traverse capability
1.51 Stator Inlet	1 4-parameter combination probe 3 hot-wire probes
2.20 Stage Exit	7 14-element wake rakes (total temperature and pressure) 1 4-parameter combination probe

Table III. Summary of Blade Element Data Reduction Constants

(a) IGV - Task II

Parameter	% Immersion	Plane 0.18	Edge 1	Edge 2	Plane 0.95
No K_{bl} included A_j	5	88.40			78.50
	10	133.95			119.70
	30	198.79			177.58
	50	179.55			157.38
	70	163.26			145.51
	90	93.31			86.66
	95	51.94			49.60
r_j	0	18.412	18.408	18.370	18.323
	5	17.893	17.900	17.870	17.835
	10	17.415	17.420	17.450	17.420
	30	15.388	15.39	15.580	15.604
	50	13.300	13.330	13.600	13.797
	70	11.080	11.160	11.590	11.972
	90	8.580	8.700	9.180	9.910
	95	7.781	7.820	8.380	9.285
	100	7.099	7.099	7.680	8.737
ϵ_j°	0	-0.99	-0.01	-1.34	-2.68
	5	-1.05	0.12	-0.78	-2.37
	10	-1.29	0.290	-0.35	-1.91
	30	-1.44	0.90	1.80	1.05
	50	-1.08	1.70	4.46	4.85
	70	-0.66	2.65	7.80	9.38
	90	-0.33	3.05	12.70	15.45
	95	-0.17	2.35	15.15	17.55
	100	0	1.80	17.80	19.59
K_j°	0		0	Equal to guide vane setting angle	
	5		↓		
	10				
	30				
	50				
	70				
	90				
	95				
	100		0		

Parameter	% Immersion	
$\frac{(W_j/W^*)_1}{(W_j/W^*)_u}$	5	0.9864
	10	0.9945
	30	1.0128
	50	1.0237
	70	1.0216
	90	1.0111
	95	1.0063
$\frac{(W_j/W^*)_2}{(W_j/W^*)_d}$	5	0.9756
	10	0.9739
	30	0.9607
	50	0.9663
	70	0.9576
	90	0.9140
	95	0.8830
$\bar{r}_j$ (Used for Diffusion Factor)	5	17.885
	10	17.435
	30	15.485
	50	13.465
	70	11.375
	90	8.940
	95	8.10
σ_j (Used for Diffusion Factor) (Based on total chord)	5	1.309
	10	1.317
	30	1.361
	50	1.419
	70	1.502
	90	1.646
	95	1.716

Radii are in inches
Areas are in square inches

Table III. Summary of Blade Element Data Reduction Constants (Concluded)

(b) Rotor - Task II

Parameter	% Immersion	Plane 0.95	Edge 1	Edge 2	Plane 1.51
No K_{bl} included	5	78.50			62.89
	10	119.70			99.21
	30	177.58			148.69
	50	157.38			133.36
A_j	70	145.51			111.59
	90	86.66			74.96
	95	49.60			36.54
	0	18.323	18.173	17.890	17.838
	5	17.835	17.706	17.525	17.462
	10	17.420	17.350	17.138	17.081
r_j	30	15.604	15.610	15.567	15.568
	50	13.797	13.900	14.008	14.056
	70	11.972	12.150	12.425	12.543
	90	9.910	10.212	10.904	11.030
	95	9.285	9.625	10.500	10.652
	100	8.737	9.125	10.141	10.287
	0	-2.68	-8.77	-5.89	-0.28
	5	-2.37	-6.58	-5.30	-0.70
	10	-1.92	-4.95	-4.47	-0.83
ϵ°_j	30	1.05	0.28	-0.97	0.50
	50	4.85	4.53	2.81	3.14
	70	9.40	9.41	7.20	6.80
	90	15.60	16.20	12.31	11.17
	95	17.55	18.02	13.50	12.28
	100	19.59	19.46	14.86	13.42
	0		63.30	57.27	
	5		61.28	57.52	
	10		60.25	57.18	
K'_j	30		57.07	52.85	
	50		53.90	46.10	
	70		50.80	34.70	
	90		48.58	16.84	
	95		48.02	10.70	
	100		47.50	4.56	

Parameter	% Immersion	
	5	1.0589
	10	1.0602
$(W_j/W^*)_1$	30	1.0555
	50	1.0537
$(W_j/W^*)_u$	70	1.0544
	90	1.0479
	95	1.0378
	5	1.0460
	10	1.0307
$(W_j/W^*)_2$	30	1.0214
	50	1.0200
$(W_j/W^*)_d$	70	1.0013
	90	0.9897
	95	0.9908
	5	17.616
	10	17.244
$\bar{r}_j$	30	15.589
	50	13.954
(Used for	70	12.288
Diffusion	90	10.558
Factor)	95	10.063
	5	1.431
	10	1.461
σ_j	30	1.612
	50	1.773
(Used for	70	1.964
Diffusion	90	2.248
Factor)	95	2.347

Radii are in inches
Areas are in square inches

Table III. Summary of Blade Element Data Reduction Constants (Continued)

(c) Stator - Task II

Parameter	% Immersion	Plane 1.51	Edge 1	Edge 2	Plane 2.20
No K_{bl} included A_j	5	62.89			58.73
	10	99.21			91.59
	30	148.69			134.20
	50	133.36			121.11
	70	111.59			108.78
	90	74.96			64.09
	95	36.54			29.08
r_j	0	17.838	17.836	17.836	17.836
	5	17.462	17.450	17.463	17.478
	10	17.081	17.075	17.125	17.130
	30	15.568	15.610	15.700	15.750
	50	14.056	14.175	14.363	14.420
	70	12.543	12.725	12.980	13.075
	90	11.030	11.300	11.720	11.775
	95	10.652	10.950	11.388	11.475
	100	10.287	10.625	11.100	11.168
ϵ_j°	0	-0.28	0	0	0
	5	-0.70	0.24	0.22	0.12
	10	-0.83	0.50	0.42	0.24
	30	0.50	1.70	1.28	0.71
	50	3.14	3.52	2.18	1.13
	70	6.80	6.04	3.25	1.38
	90	11.17	9.40	4.39	1.14
	95	12.28	10.31	4.80	0.92
	100	13.42	11.38	4.70	0.65
K_j° (At nominal stator setting)	0		40.09	-13.08	
	5		39.47	-11.13	
	10		39.11	-10.10	
	30		39.01	-8.87	
	50		39.80	-8.75	
	70		40.86	-9.10	
	90		42.22	-10.58	
	95		42.76	-12.36	
	100		43.32	-12.88	

Parameter	% Immersion	
$\frac{(W_j/W^*)_1}{(W_j/W^*)_u}$	5	0.9992
	10	1.0043
	30	1.0229
	50	1.0327
	70	1.0385
	90	1.0378
	95	1.0334
$\frac{(W_j/W^*)_2}{(W_j/W^*)_d}$	5	0.9880
	10	0.9873
	30	0.9904
	50	0.9932
	70	0.9987
	90	1.0158
	95	1.0254
$\bar{r}_j$ (Used for Diffusion Factor)	5	17.457
	10	17.100
	30	15.655
	50	14.269
	70	12.853
	90	11.510
	95	11.169
σ_j (Used for Diffusion Factor)	5	1.523
	10	1.544
	30	1.631
	50	1.742
	70	1.880
	90	2.051
	95	2.098

Radii are in inches
Areas are in square inches

Table IV. Summary of Distortion Test Data
(a) Summary of Radial Distortion Data

Reading Number	Percent Design Speed	Discharge Valve Setting	Inlet Corrected Weight Flow	Stage Total Pressure Ratio	Stage Adiabatic Efficiency	Type Point*	IGV/Stator Schedule
96	70	30	169.1	1.211	0.770	OP	0°/0°
97	70	30	133.8	1.120	0.785	OP	40°/8°
98	70	6.5	111.1	1.200	0.788	OP	40°/8°
99	70	13	120.3	1.166	0.787	OP	40°/8°
100	70	9.0	151.0	1.289	0.813	OP	0°/0°
101	70	14	160.1	1.264	0.829	OP	0°/0°
102	90	30	203.4	1.321	0.690	OP	0°/0°
103	90	10.8	196.1	1.490	0.796	OP	0°/0°
104	90	15	199.9	1.426	0.772	OP	0°/0°
105	90	30	157.4	1.190	0.746	OP	40°/8°
106	90	8	143.4	1.323	0.783	OP	40°/8°
107	90	10.5	148.2	1.295	0.791	OP	40°/8°
108	100	30	164.8	1.211	0.690	OP	40°/8°
109	100	12	161.6	1.340	0.773	OP	40°/8°
110	100	15	162.9	1.303	0.760	OP	40°/8°
111	100	30	217.6	1.377	0.667	OP	0°/0°
112	100	10	214.3	1.620	0.773	OP	0°/0°
113	100	15	216.2	1.512	0.745	BE	0°/0°
114	100	30	216.7	1.379	0.671	OP	0°/0°
115	100	15	164.9	1.304	0.762	BE	40°/8°
116	70	30	129.3	1.122	0.795	BE	40°/8°
117	70	6.5	113.1	1.200	0.797	BE	40°/8°
118	70	14	159.6	1.265	0.822	BE	0°/0°

* OP - Overall Performance Reading
BE - Blade Element Performance Reading

Table IV. Summary of Distortion Test Data (Concluded)
(b) Summary of Circumferential Distortion Data

Reading Number	Percent Design Speed	Discharge Valve Setting	Inlet Corrected Weight Flow	Stage Total Pressure Ratio	Stage Adiabatic Efficiency	Type Point*	Distortion Screen Pos. From TDC	IGV/Stator Schedule
1	70	50	172.3	1.197	0.741	OP	195	0°/0°
2	70	4.5	134.4	1.308	0.771	OP	195	
3	70	11	154.6	1.277	0.814	OP	195	
4	90	30	206.7	1.344	0.741	OP	195	
5	90	8.5	190.3	1.525	0.800	OP	195	
6	90	11	197.8	1.491	0.817	OP	195	
7	100	30	221.3	1.407	0.711	OP	195	
8	100	9.5	211.6	1.639	0.796	OP	195	
9	100	12	218.5	1.593	0.801	OP	195	
10-21	100	30	221.5	1.407	0.715	SRT	195-165	
22-33	100	9.5	211.8	1.644	0.748	SRT	195-165	
34-45	70	11	153.8	1.274	0.838	OP	195-165	0°/0°
46	70	50	127.3	1.109	0.840	OP	195	40°/8°
47	70	5	108.5	1.205	0.778	OP	195	
48	70	10	117.2	1.181	0.836	OP	195	
49	90	30	156.9	1.190	0.816	OP	195	
50	90	6	140.4	1.339	0.775	OP	195	
51	90	10	147.7	1.299	0.836	OP	195	
52	100	30	166.1	1.222	0.756	OP	195	
53	100	9.5	160.8	1.372	0.819	OP	195	
54	100	13	163.7	1.328	0.839	OP	195	
77-88	70	30	128.2	1.121	0.830	SRT	195-165	
89	70	30	128.5	1.121	0.838	OP	195	
119-130	70	5	109.5	1.205	0.814	SRT	195-165	
131	70	5	109.4	1.207	0.787	OP	195	
132-143	100	13	164.9	1.326	0.806	SRT	195-165	
144	100	13	164.9	1.325	0.822	OP	195	40°/8°

* OP - Overall Performance Reading
SRT - Screen Rotating Test (12 Circumferential Distortion Screen Positions in 30° Intervals from 195° TDC)

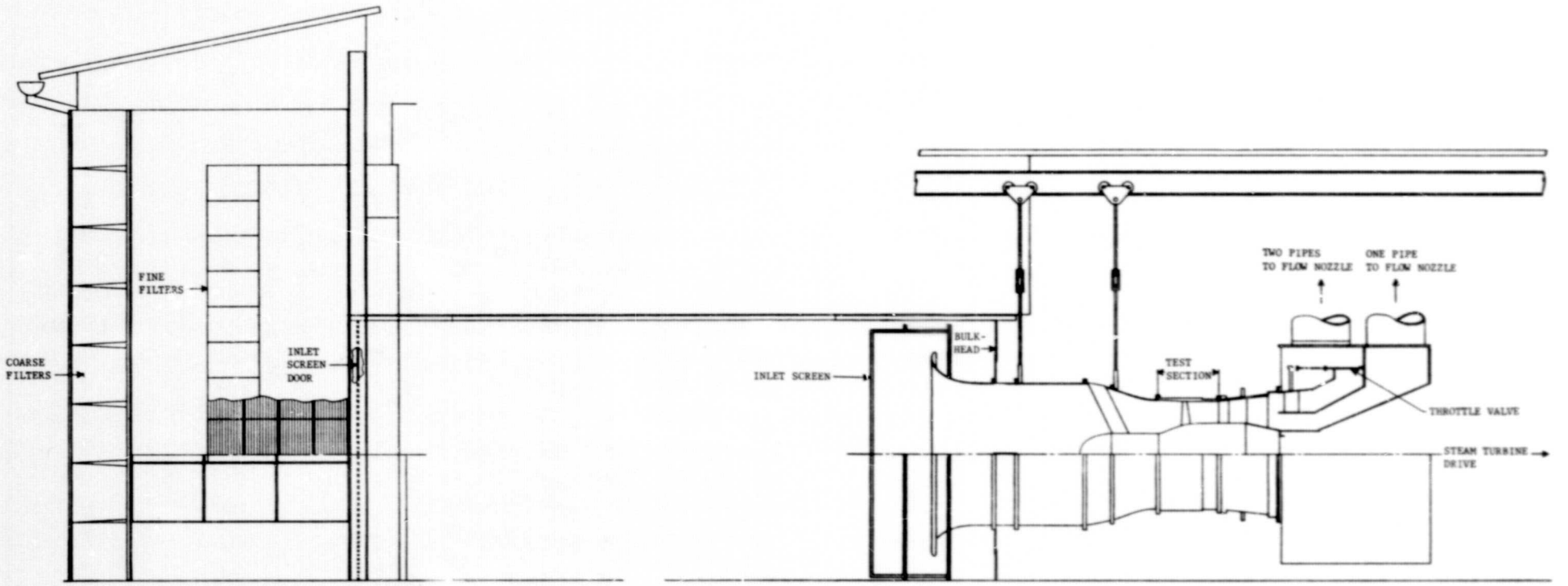

Figure 1. Schematic Diagram of House Compressor Test Facility.

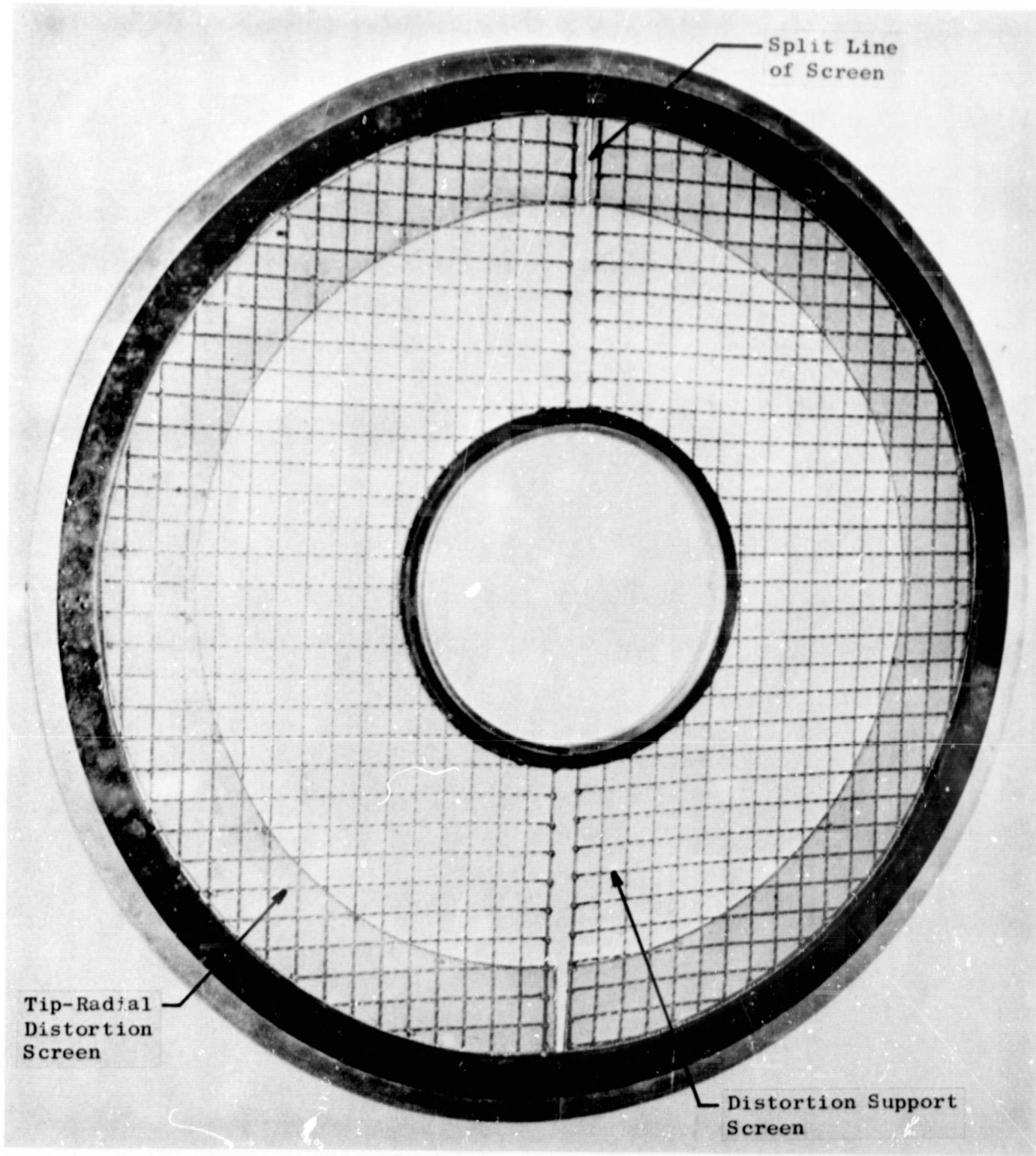

Figure 2. Tip-Radial Distortion Screen.

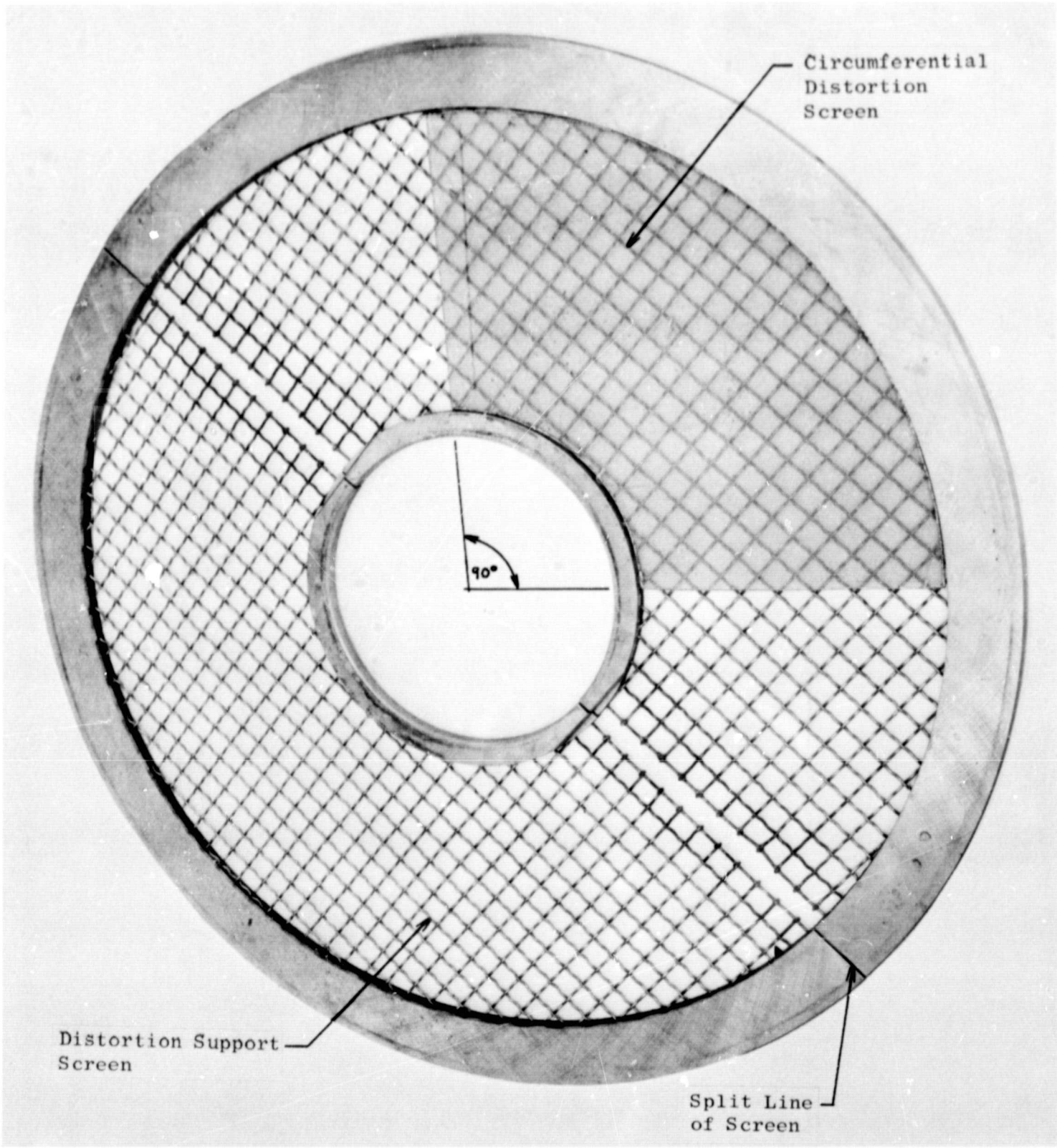

Figure 3. Circumferential Distortion Screen.

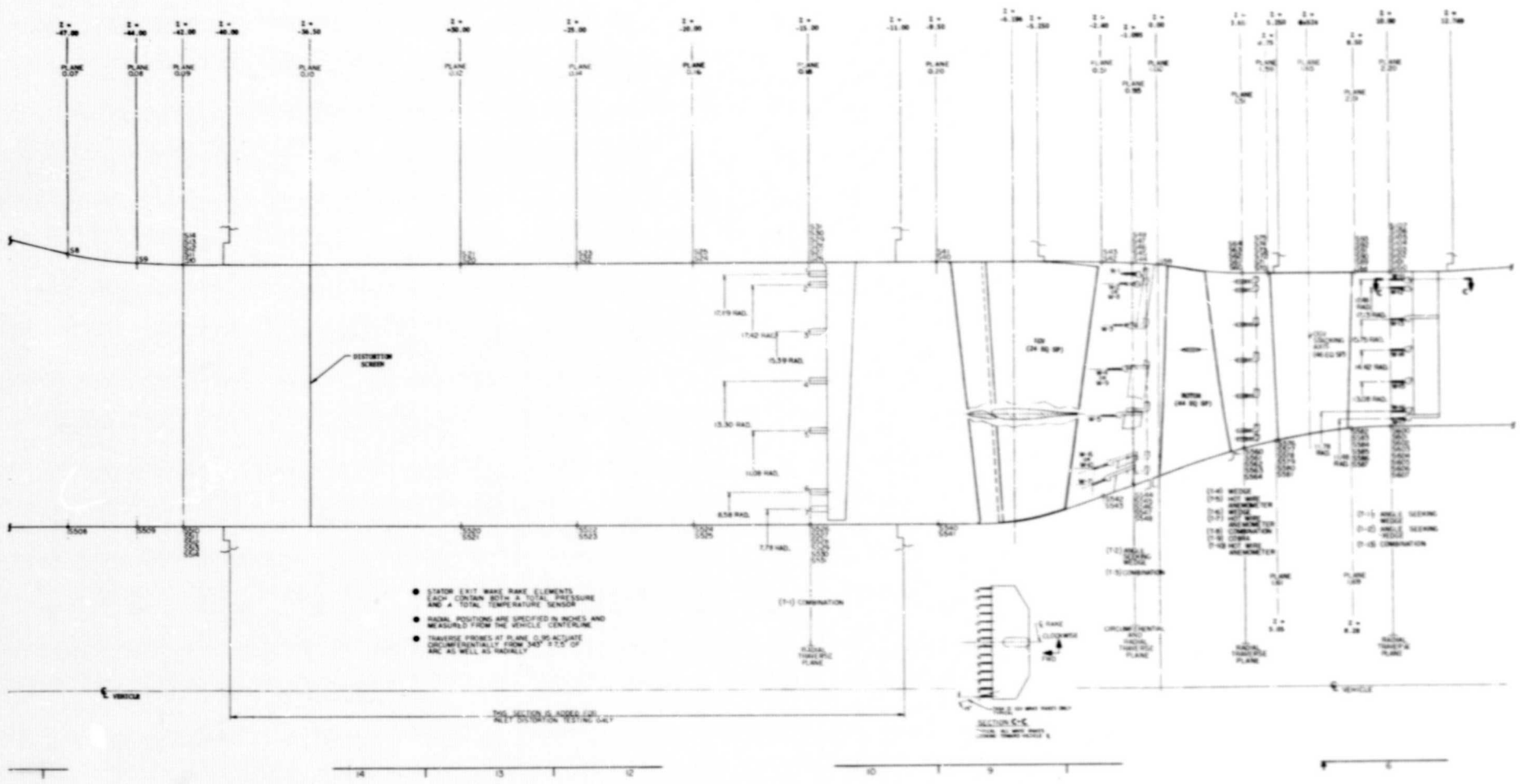

Figure 4. Meridional View Showing Instrumentation Locations.

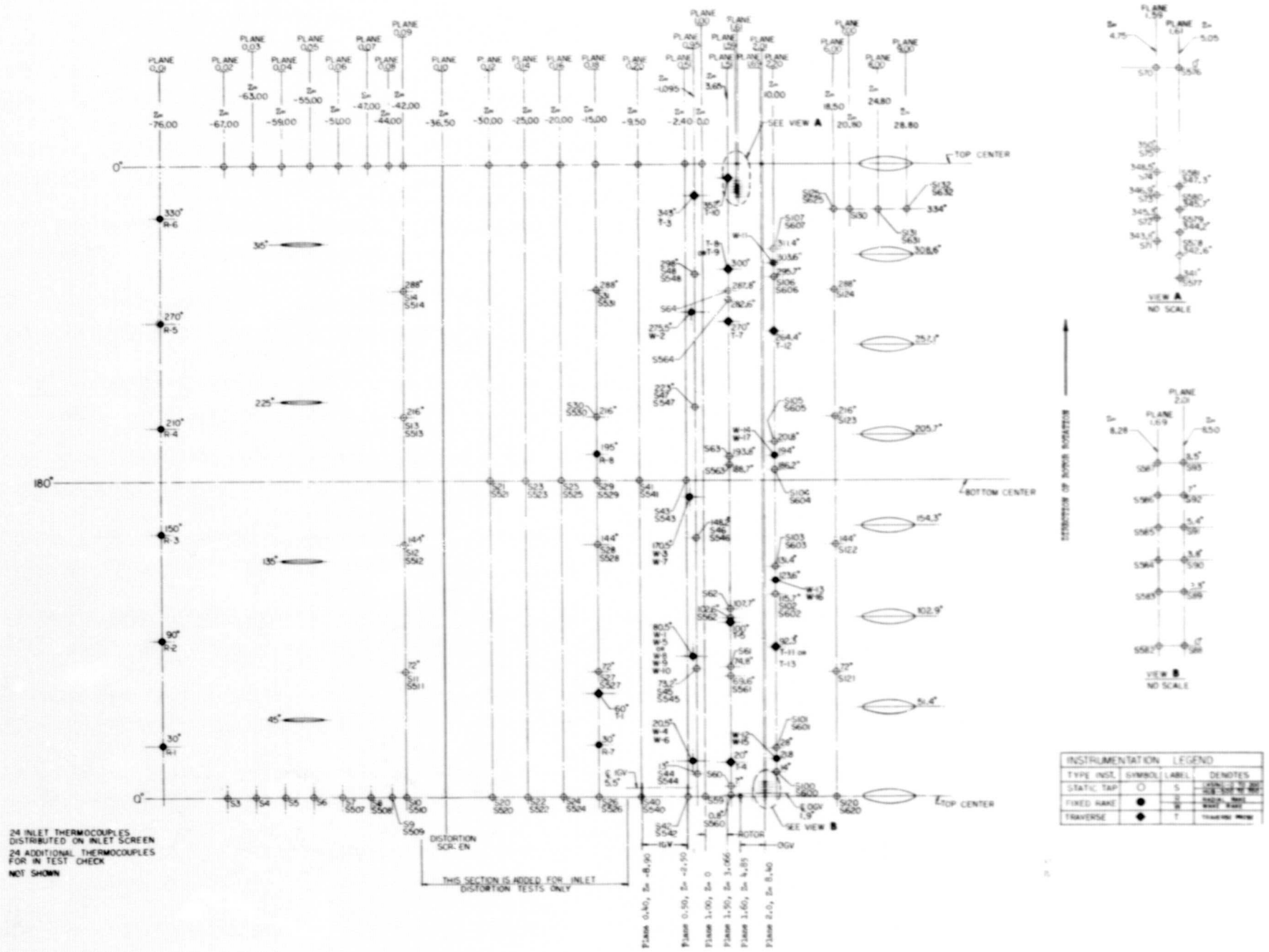

Figure 5. Circumferential Development Showing Instrumentation Locations.

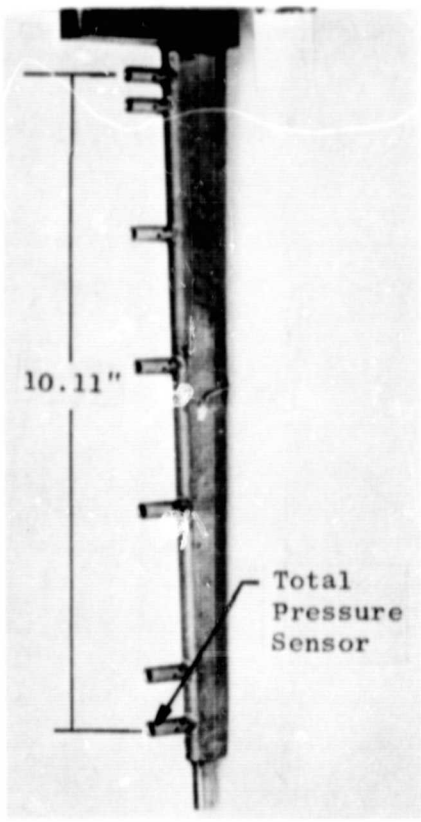

(a) Fixed Inlet Distortion Total-Pressure Rake Located at Plane 0.18

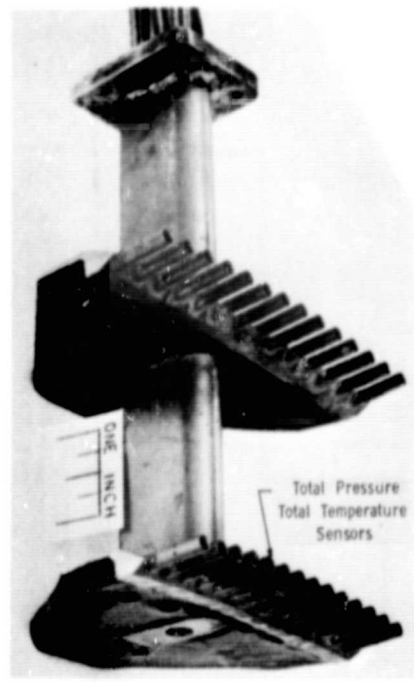

(b) Fixed Discharge Total-Pressure - Total-Temperature Wake Rake Located at Plane 2.20

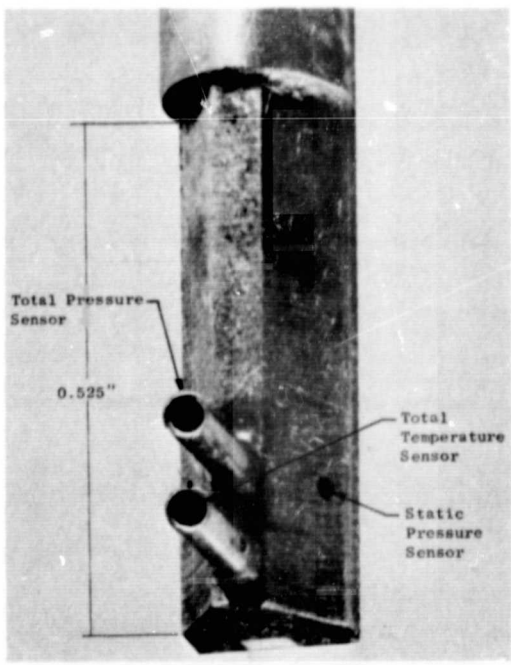

(c) Sensing Element of Four-Parameter Combination Traverse Probe

(d) Sensing Element of Shielded Hot-Wire Anemometer Traverse Probe

Figure 6. Fixed and Traverse Instrumentation Used in Distortion Testing.

(Dashed lines with arrows and inset formulas indicate calculation sequence for sample case.)

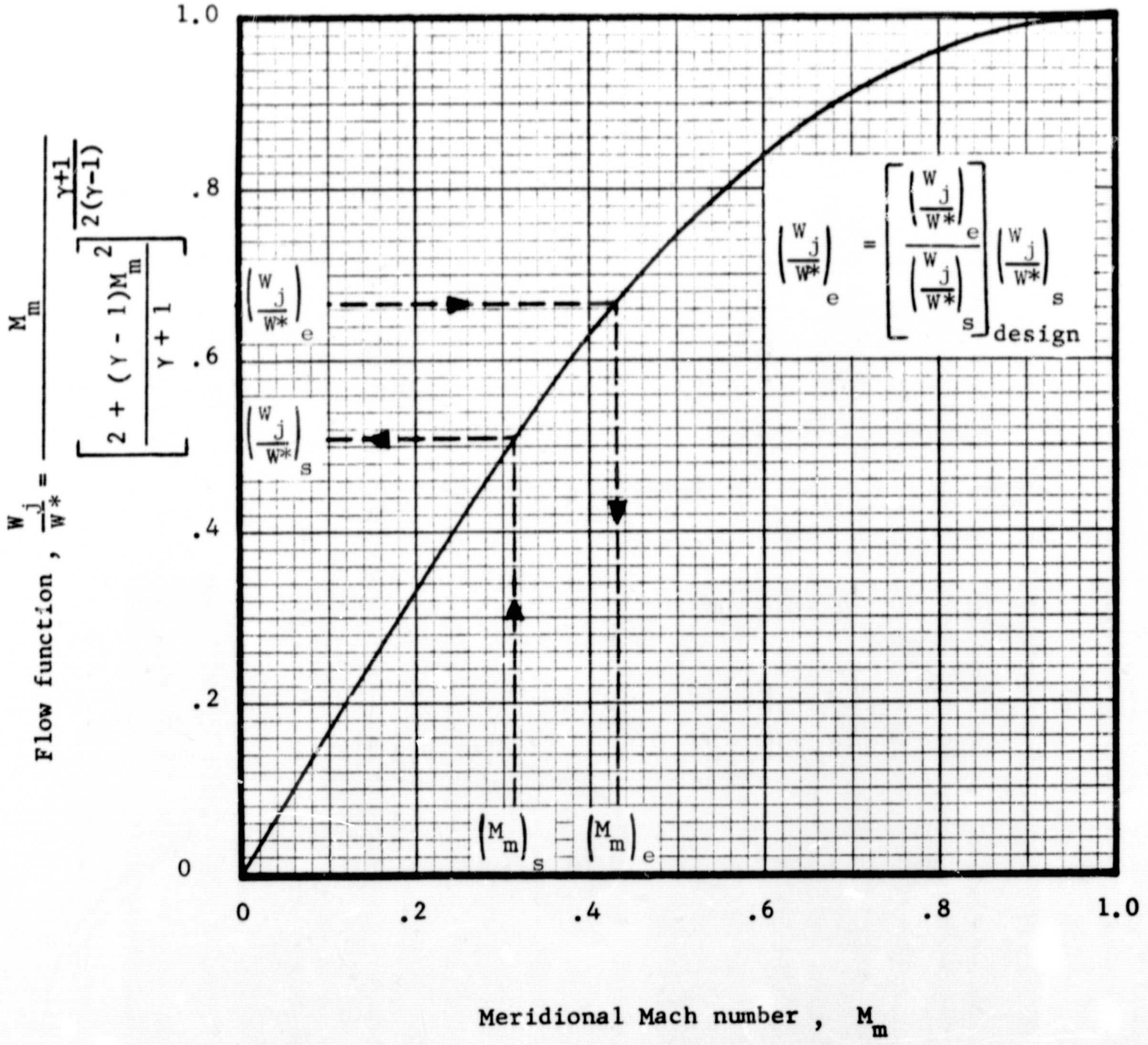

Figure 7. Relationship Between Flow Function and Meridional Mach No. Used for Transferring Traverse Measurements to Blade Edges.

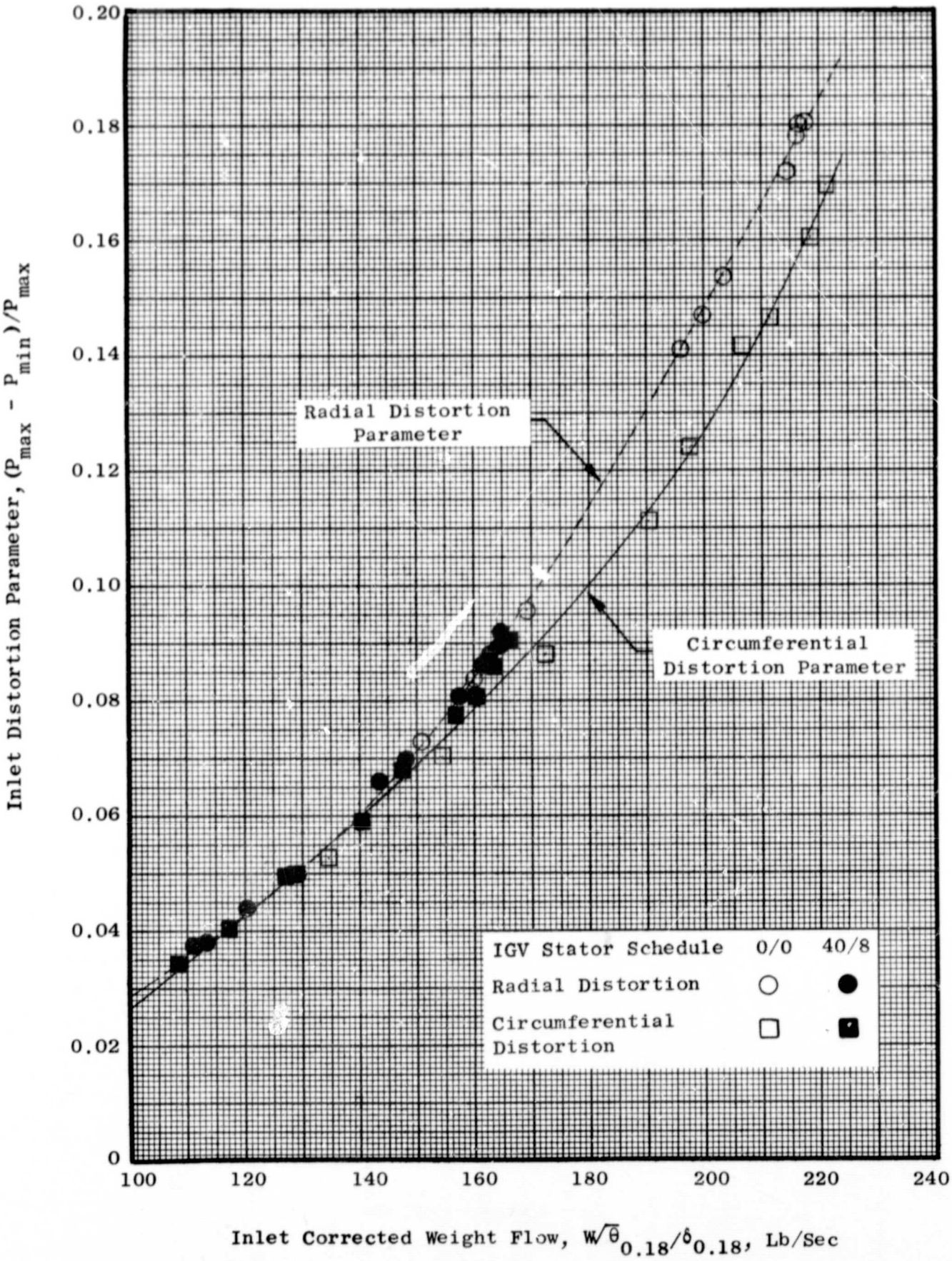

Figure 8. Task II Distortion Parameter Variation for Radial and Circumferential Inlet Distortions.

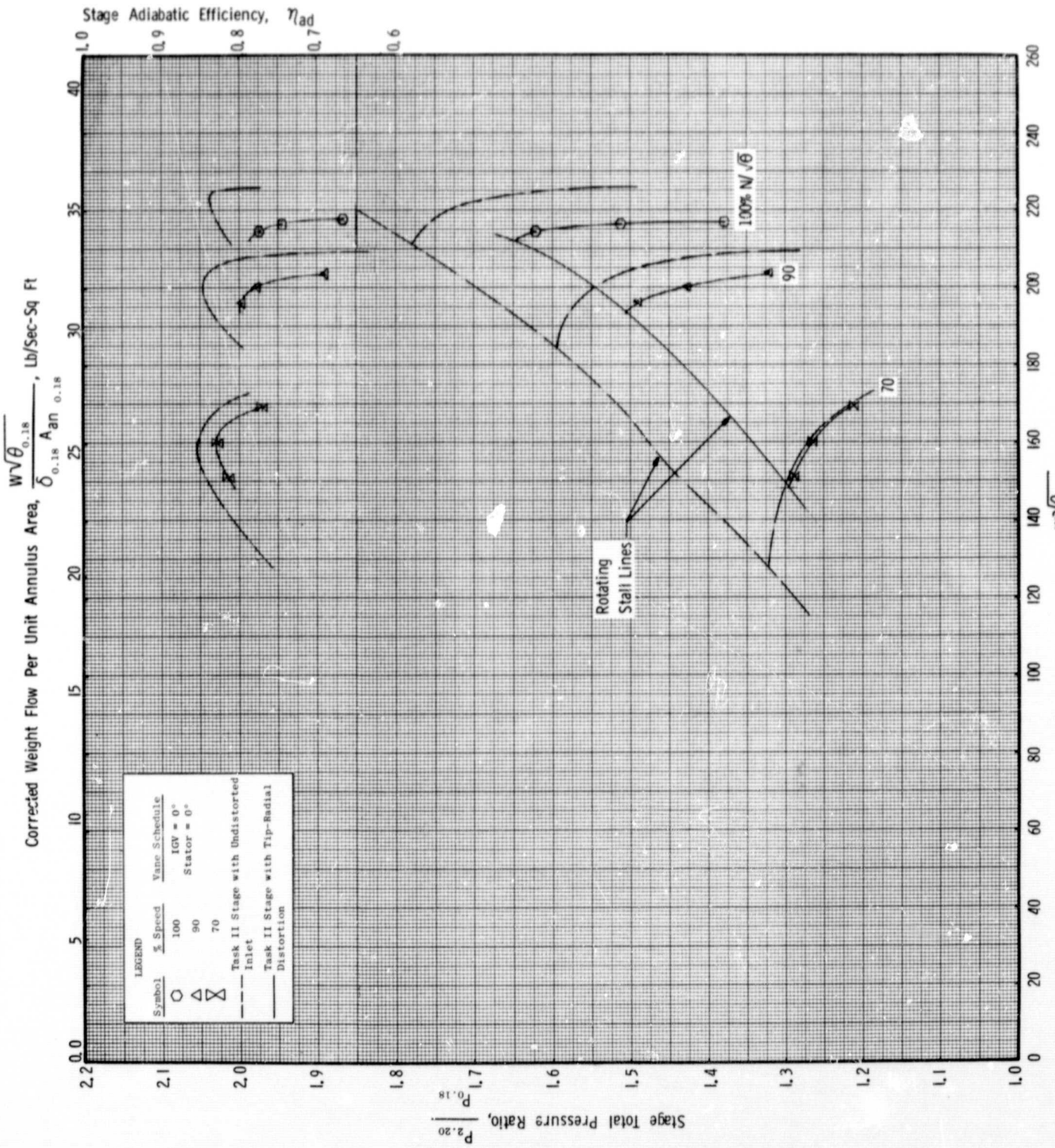

Figure 9. Task II Stage Performance Map with Tip-Radial Inlet Distortion for IGV/Stator Schedule of 0°/0°.

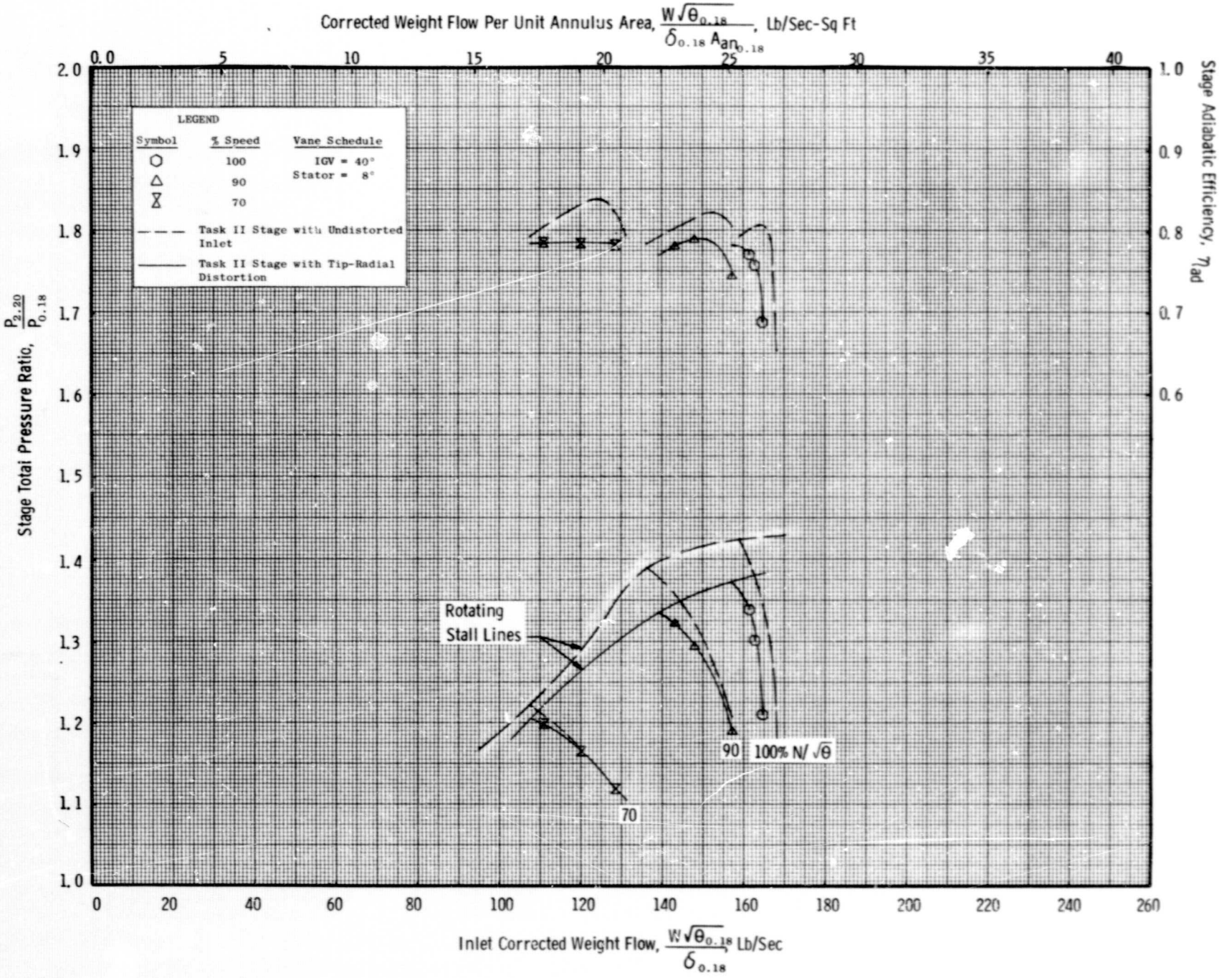

Figure 10. Task II Stage Performance Map with Tip-Radial Inlet Distortion for IGV/Stator Schedule of 40°/8°.

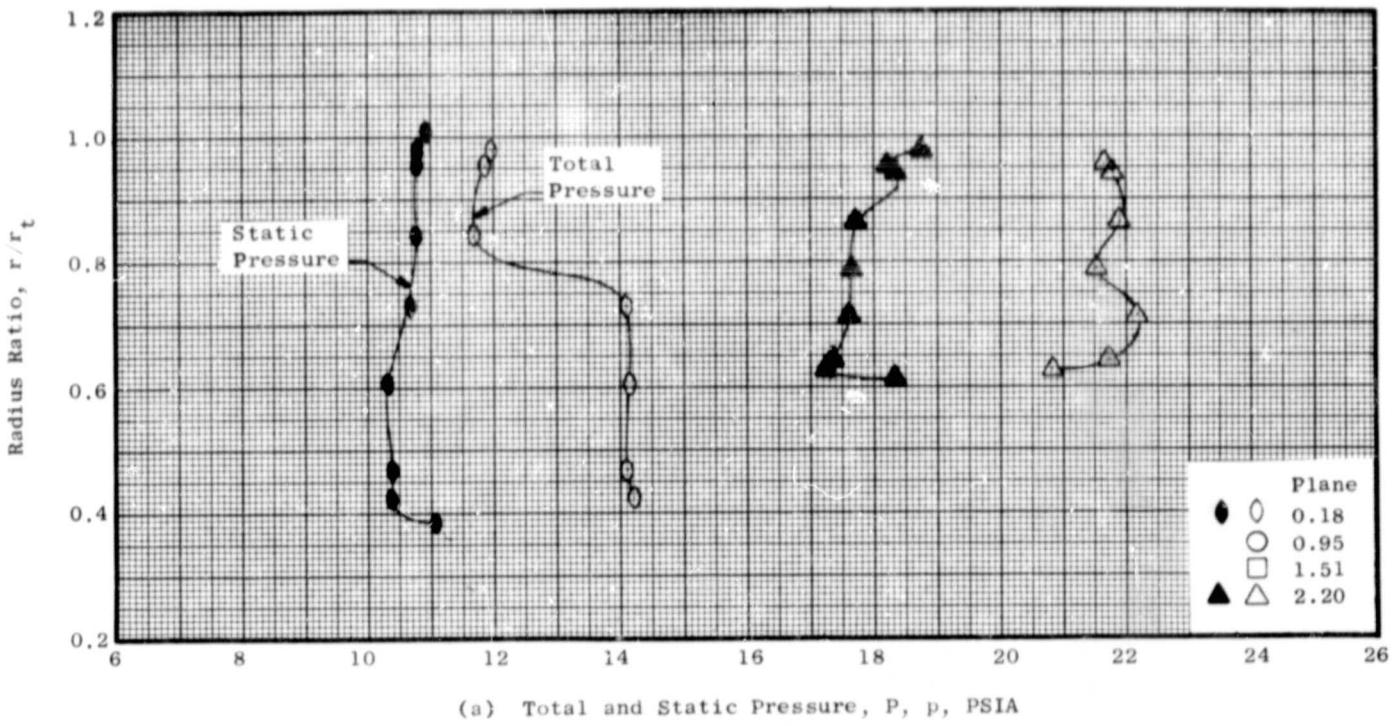

(a) Total and Static Pressure, P, p, PSIA

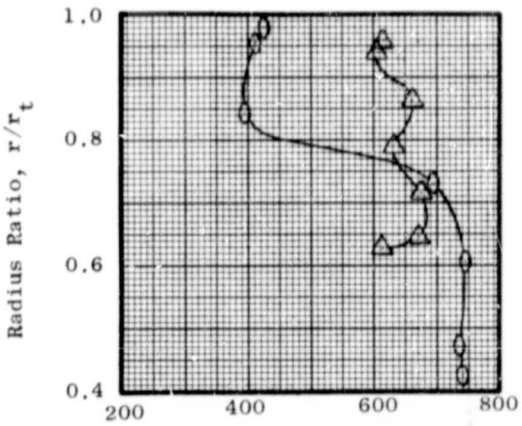

(b) Axial Velocity, V_z, Ft/Sec

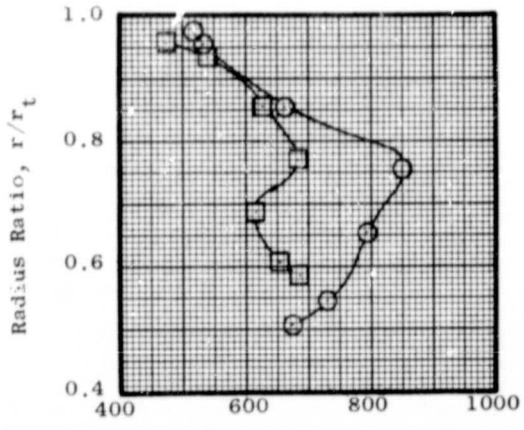

(b) Axial Velocity, V_z, Ft/Sec

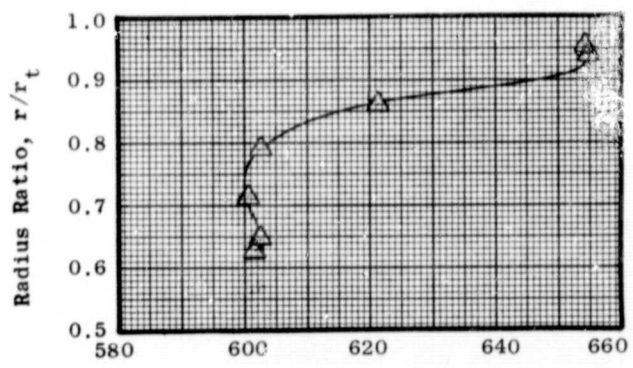

(c) Total Temperature, T, °R

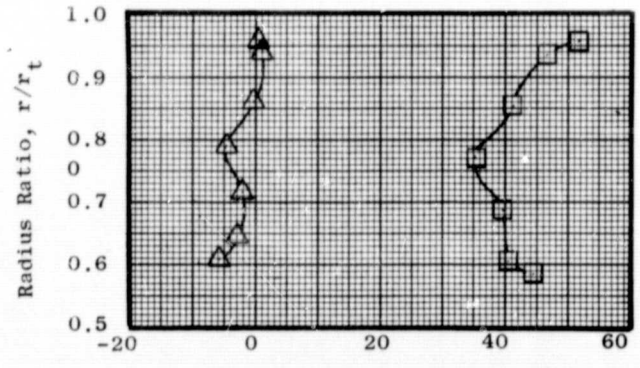

(d) Absolute Flow Angle, β, Degrees

Figure 11. Radial Distributions of Blade Element Parameters from Traverse Measurements at 100 Percent Speed Near Stall with 0°/0° IGV/Stator Schedule.

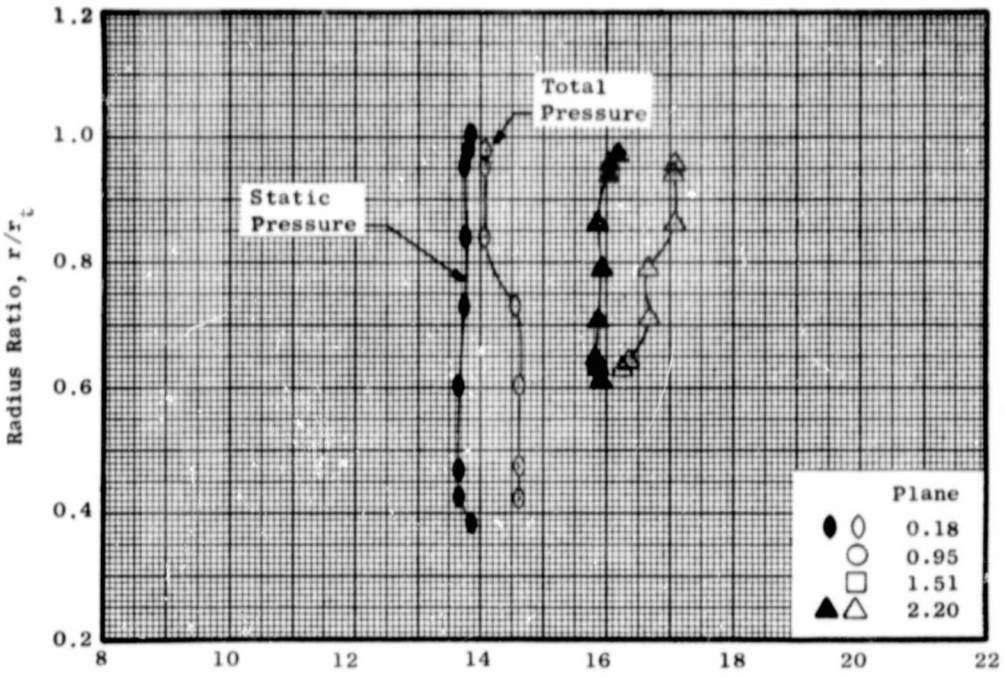

(a) Total and Static Pressure, P, p, PSIA

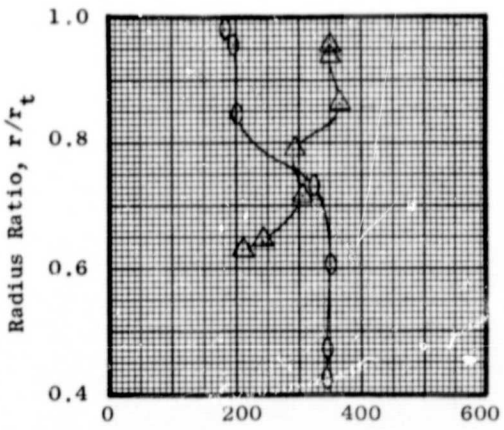

(b) Axial Velocity, V_z, Ft/Sec

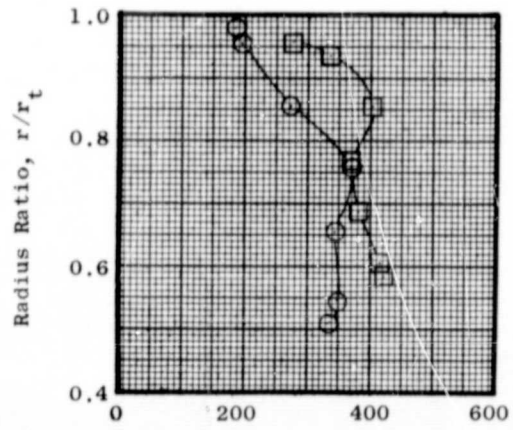

(b) Axial Velocity, V_z, Ft/Sec

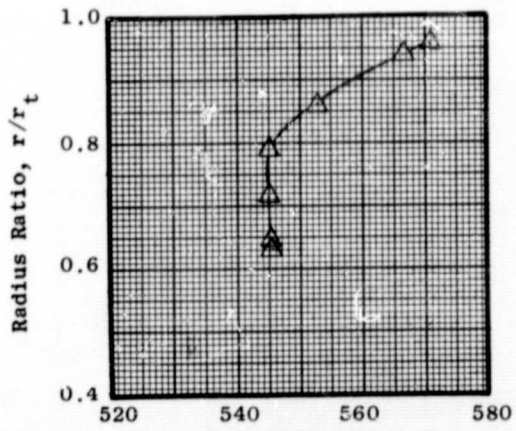

(c) Total Temperature, T, °R

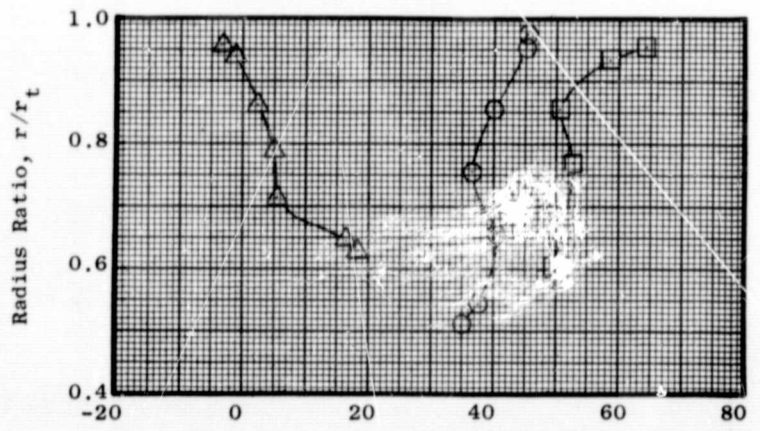

(d) Absolute Flow Angle, β, Degrees

Figure 12. Radial Distributions of Blade Element Parameters from Traverse Measurements at 70 Percent Speed Near Stall with 40°/8° IGV/Stator Schedule.

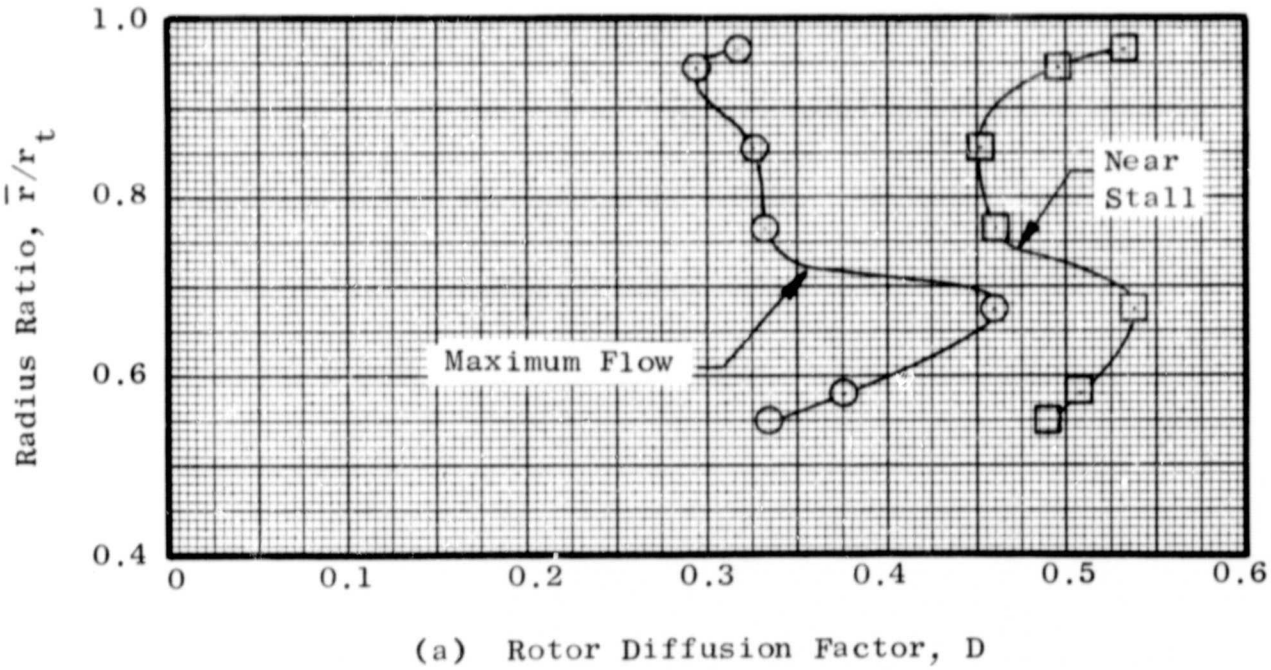

(a) Rotor Diffusion Factor, D

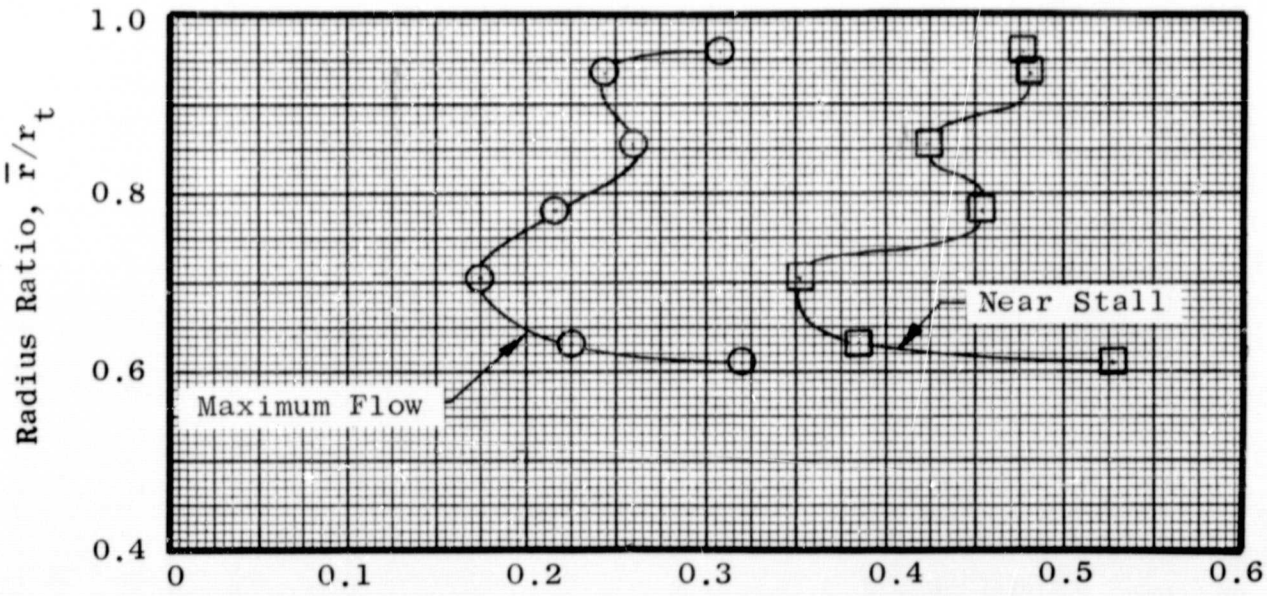

(b) Stator Diffusion Factor, D

Figure 13. Rotor and Stator Diffusion Factors at 100 Percent Speed Near Stall and at Maximum Flow with 0°/0° IGV/Stator Schedule.

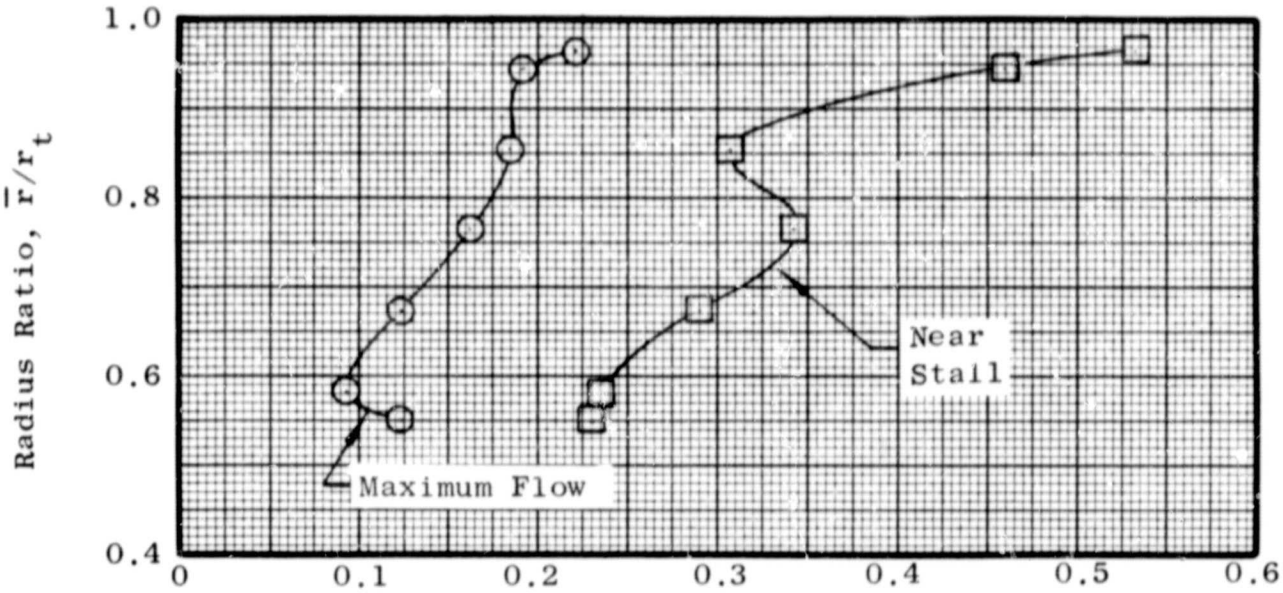

(a) Rotor Diffusion Factor, D

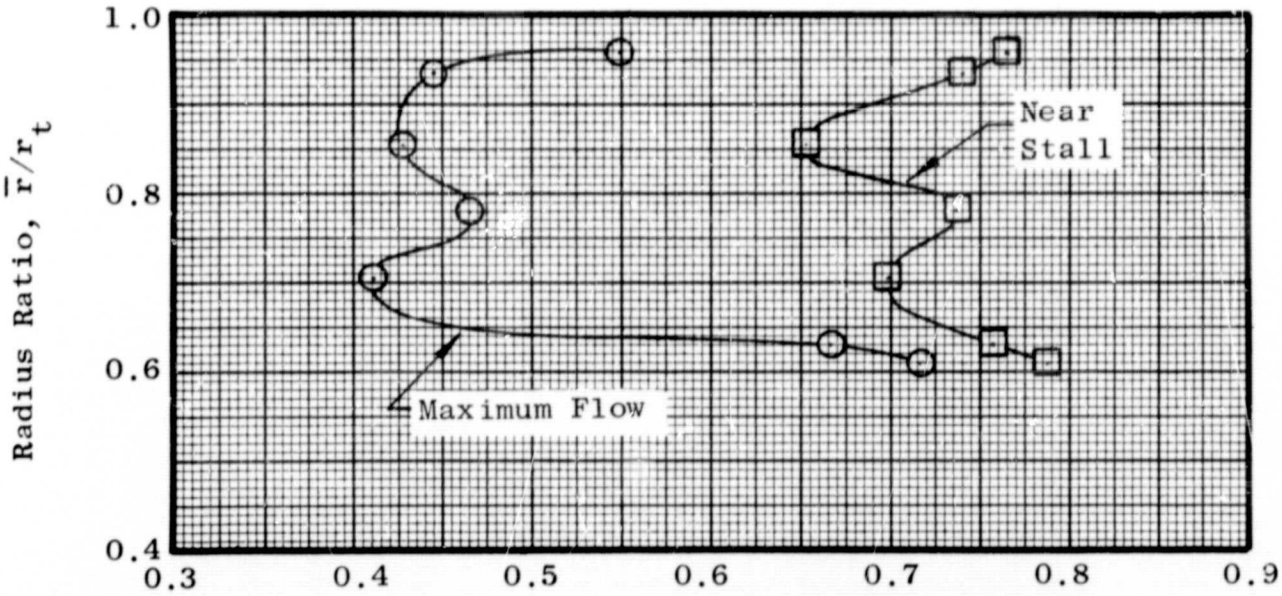

(b) Stator Diffusion Factor, D

Figure 14. Rotor and Stator Diffusion Factors at 70 Percent Speed Near Stall and at Maximum Flow with 40°/8° IGV/Stator Schedule.

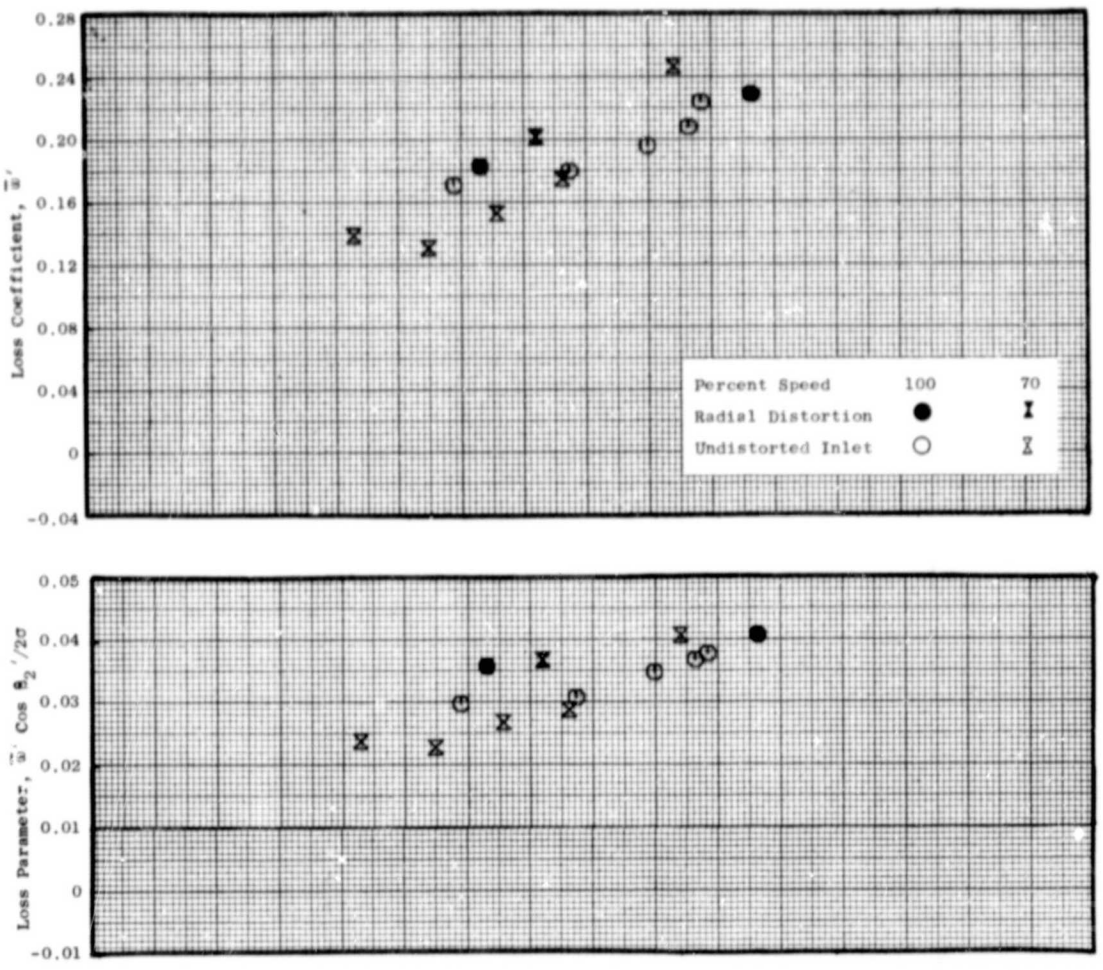

Figure 15(a). Rotor Blade Element Data for 0°/0° IGV/Stator Schedule Measured at 5% Immersion from Tip.

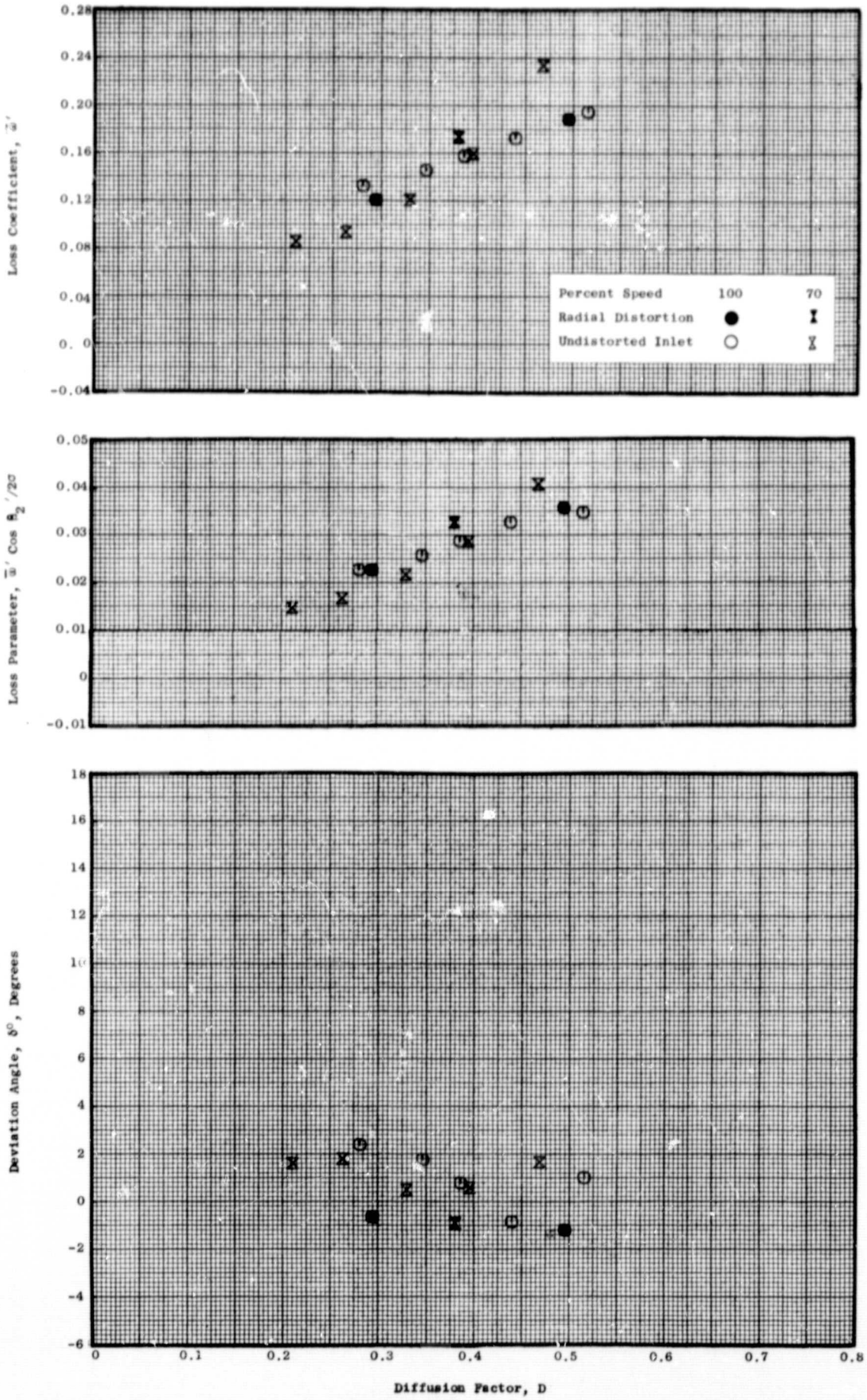

Figure 15(b). Rotor Blade Element Data for 0°/0° IGV/Stator Schedule Measured at 10% Immersion from Tip.

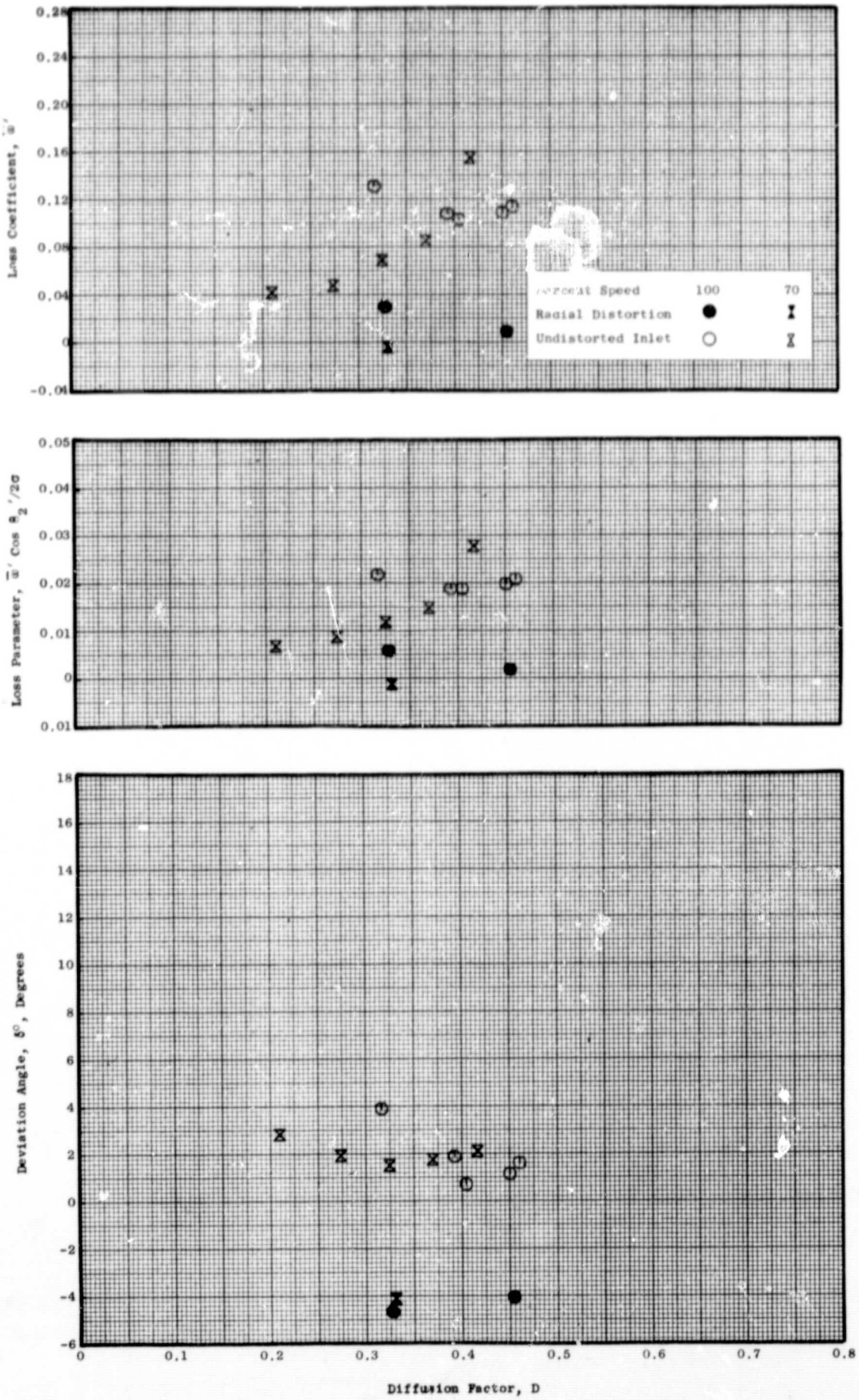

Figure 15(c). Rotor Blade Element Data for 0°/0° IGV/Stator Schedule Measured at 30% Immersion from Tip.

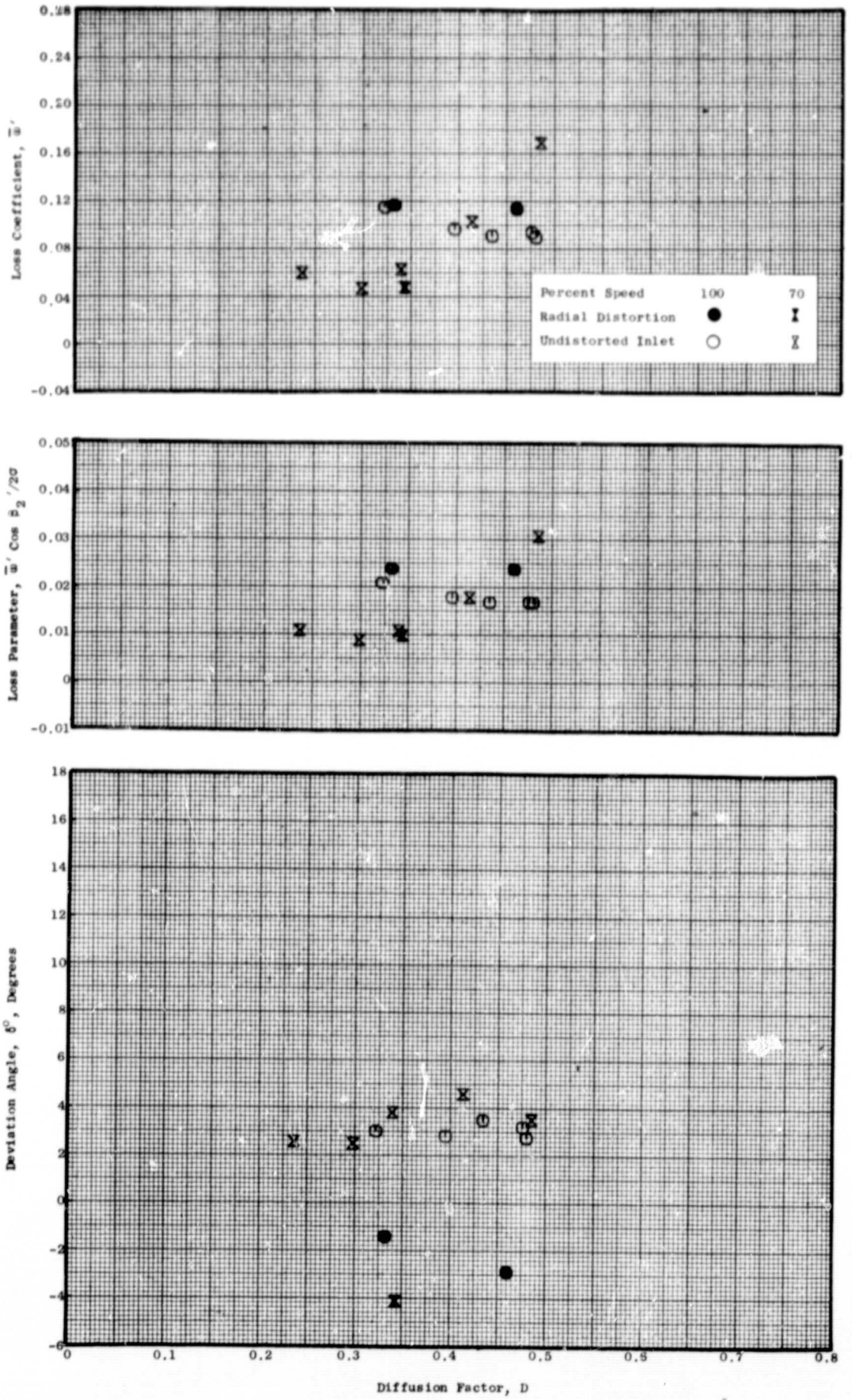

Figure 15(d). Rotor Blade Element Data for 0°/0° IGV Stator Schedule Measured at 50% Immersion from Tip.

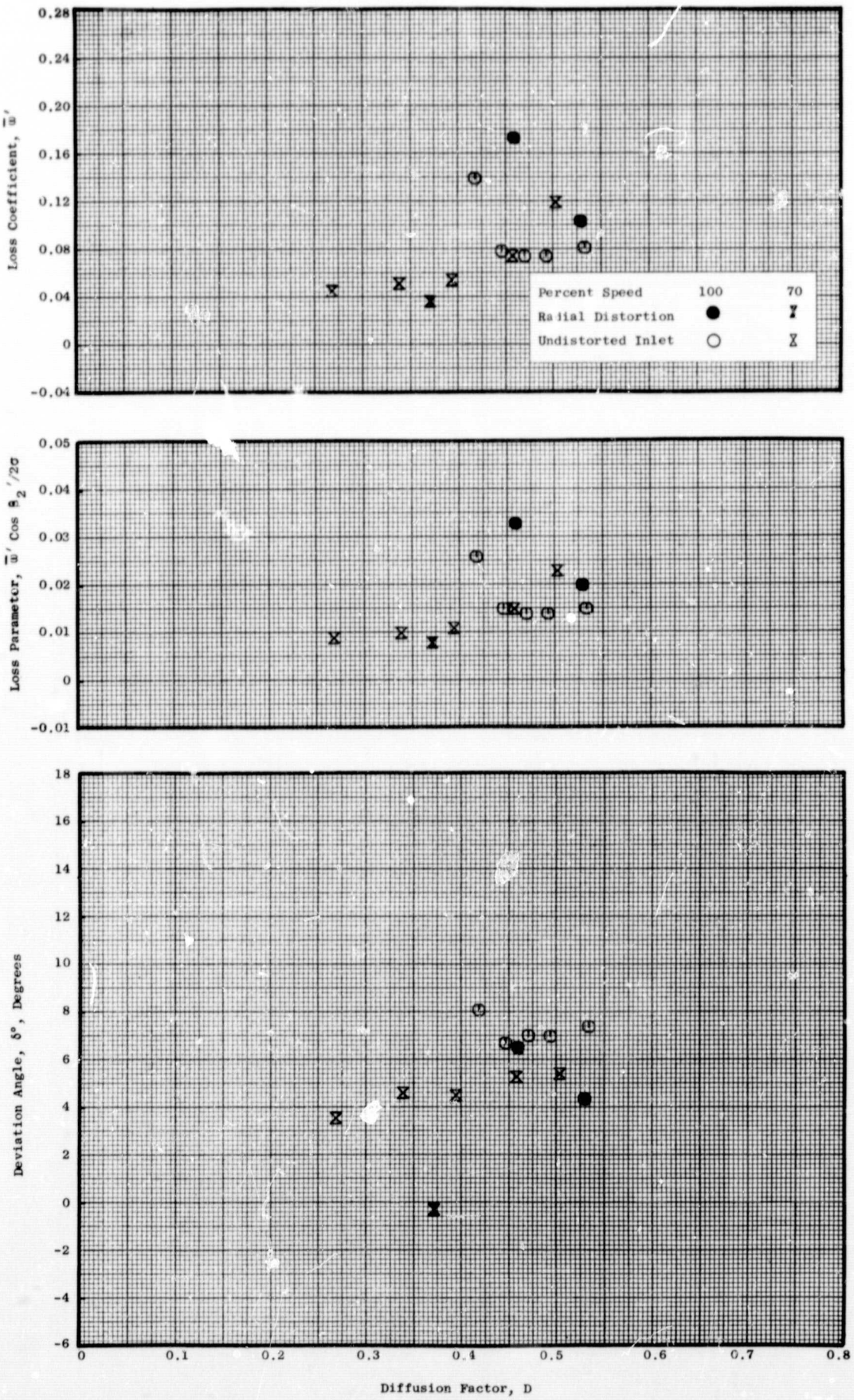

Figure 15(e). Rotor Blade Element Data for 0°/0° IGV/Stator Schedule Measured at 70% Immersion from Tip.

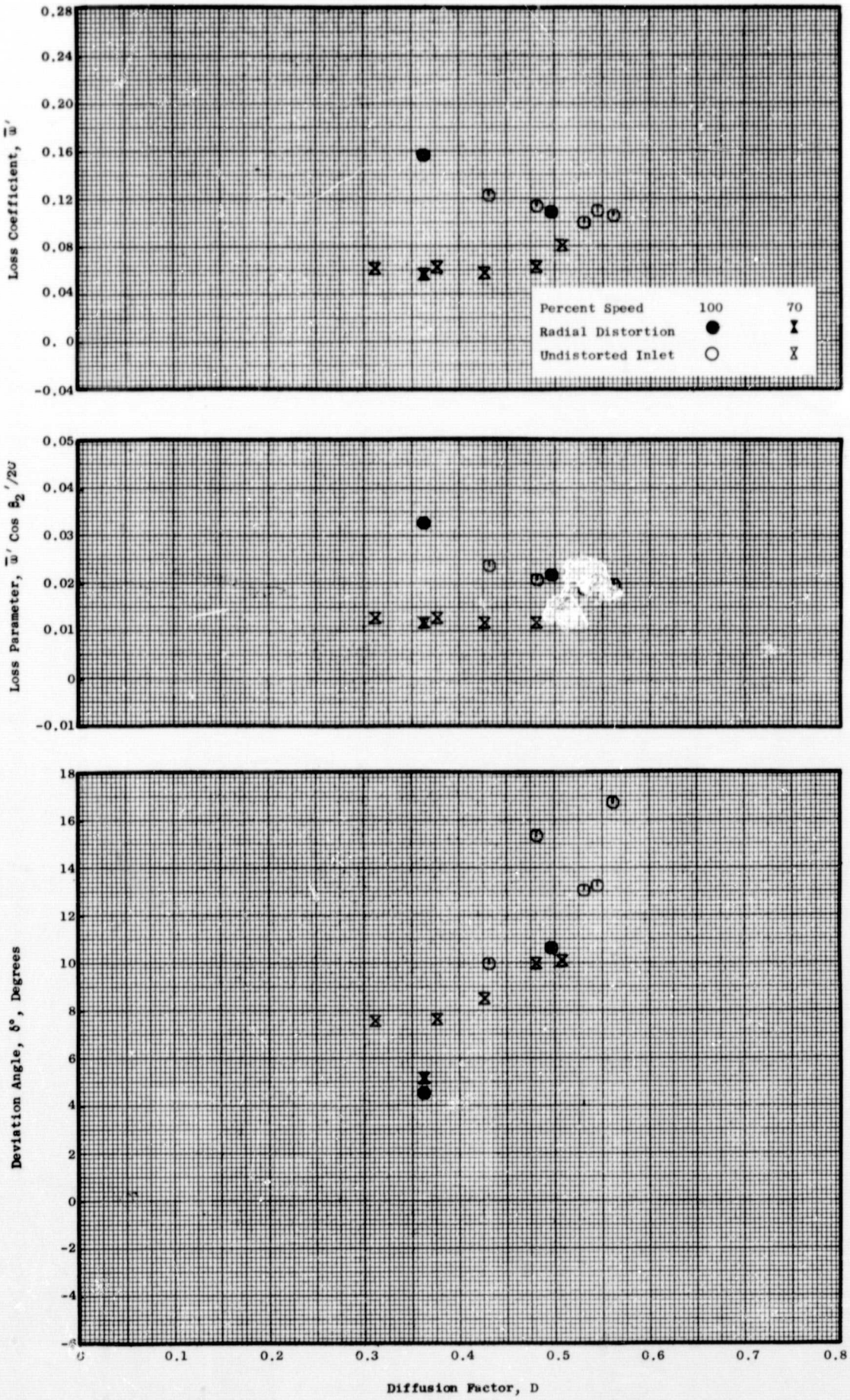

Figure 15(f). Rotor Blade Element Data for 0°/0° IGV/Stator Schedule Measured at 90% Immersion from Tip.

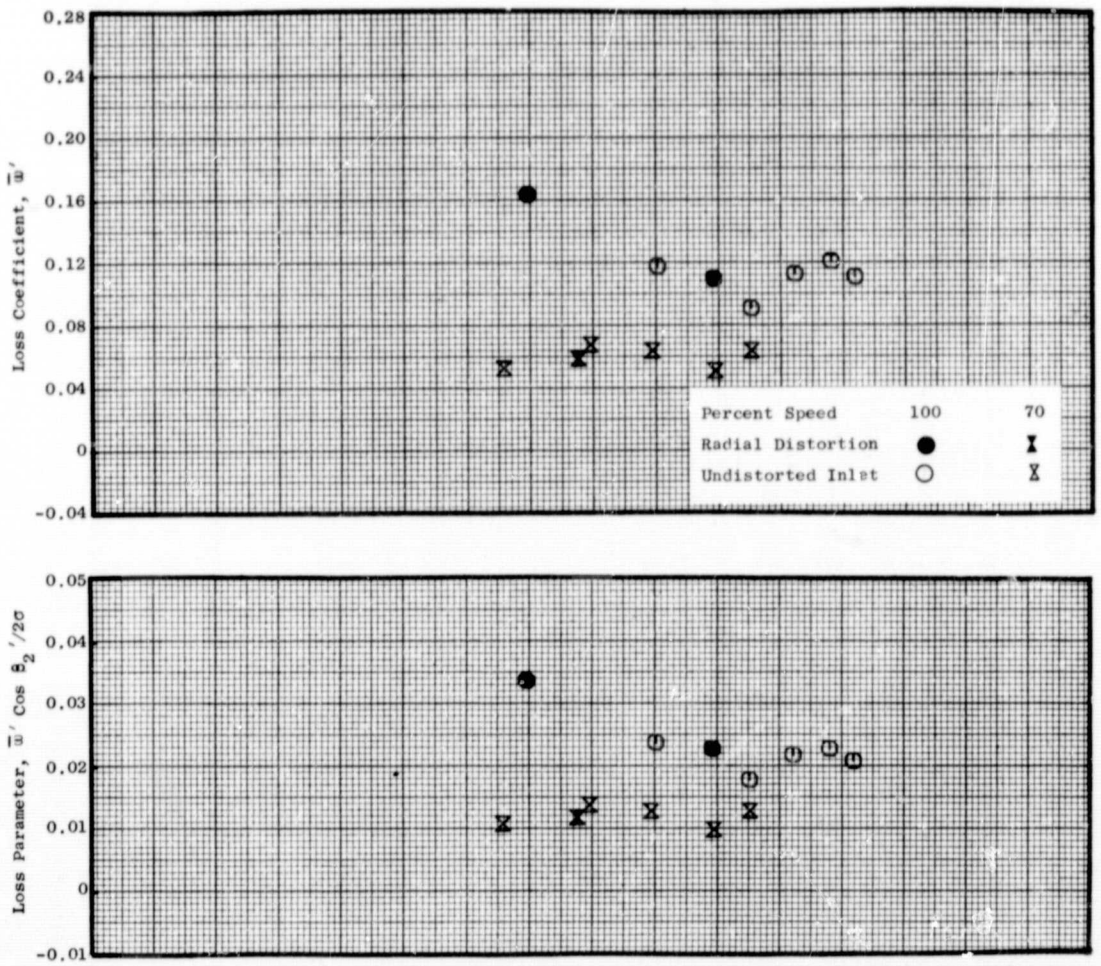

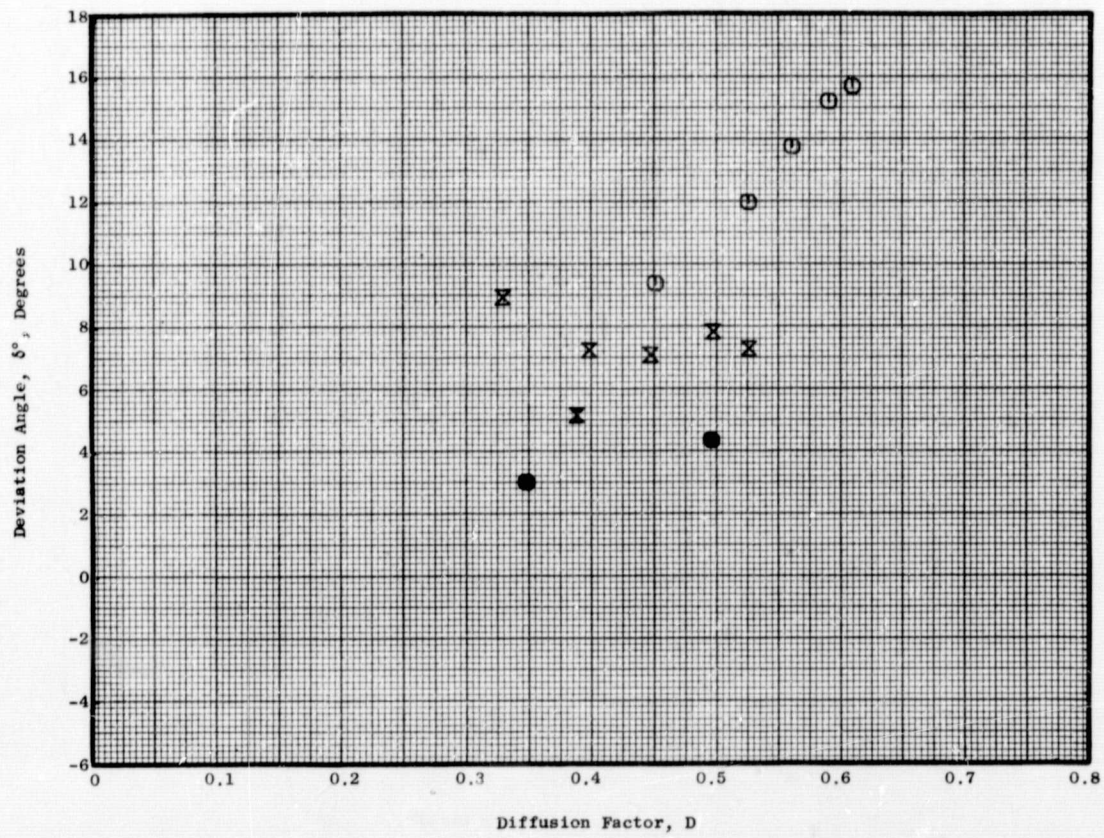

Figure 15(g). Rotor Blade Element Data for 0°/0° IGV/Stator Schedule Measured at 95% Immersion from Tip.

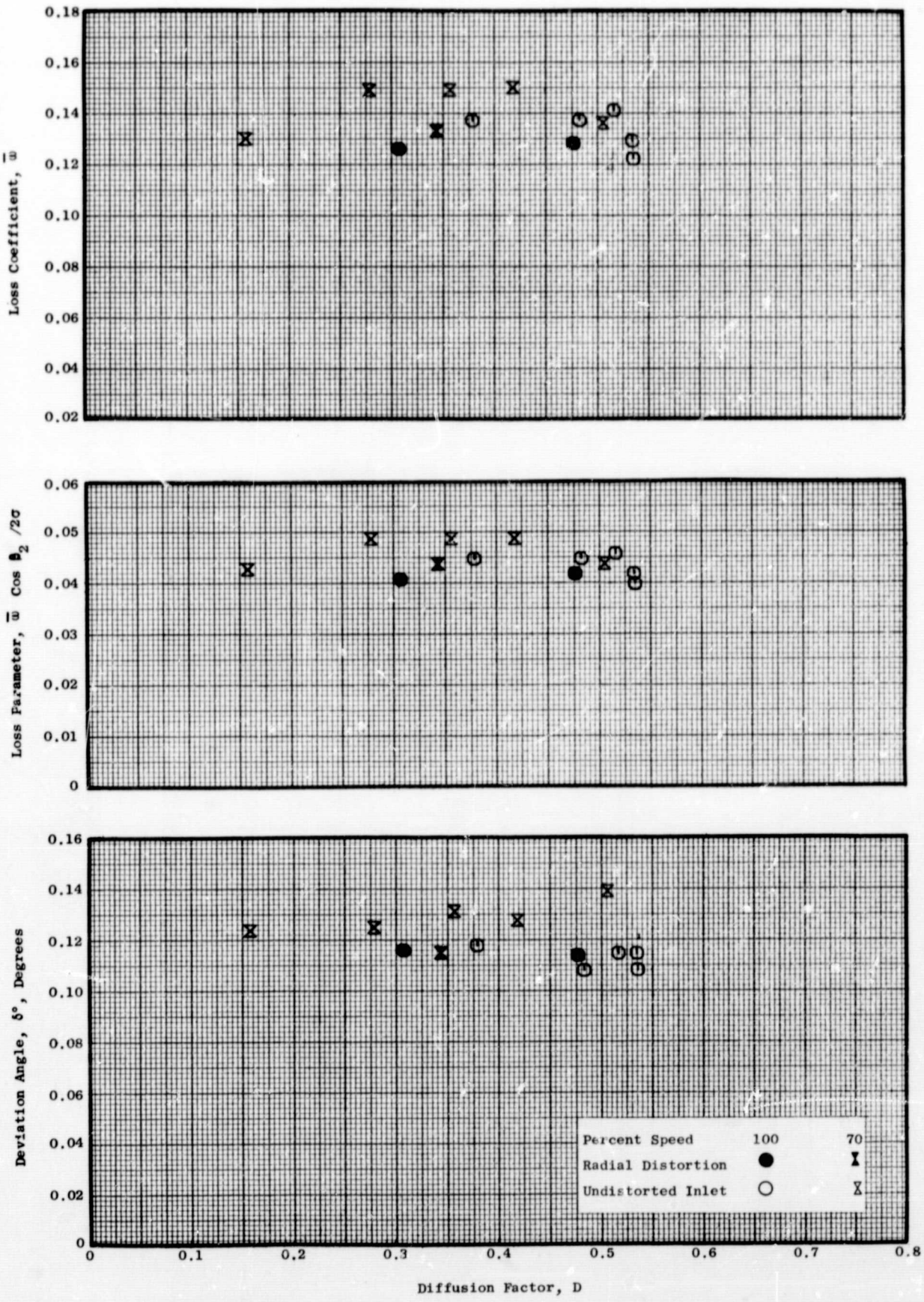

Figure 16(a). Stator Blade Element Data for 0°/0° IGV/Stator Schedule Measured at 5% Immersion from Tip.

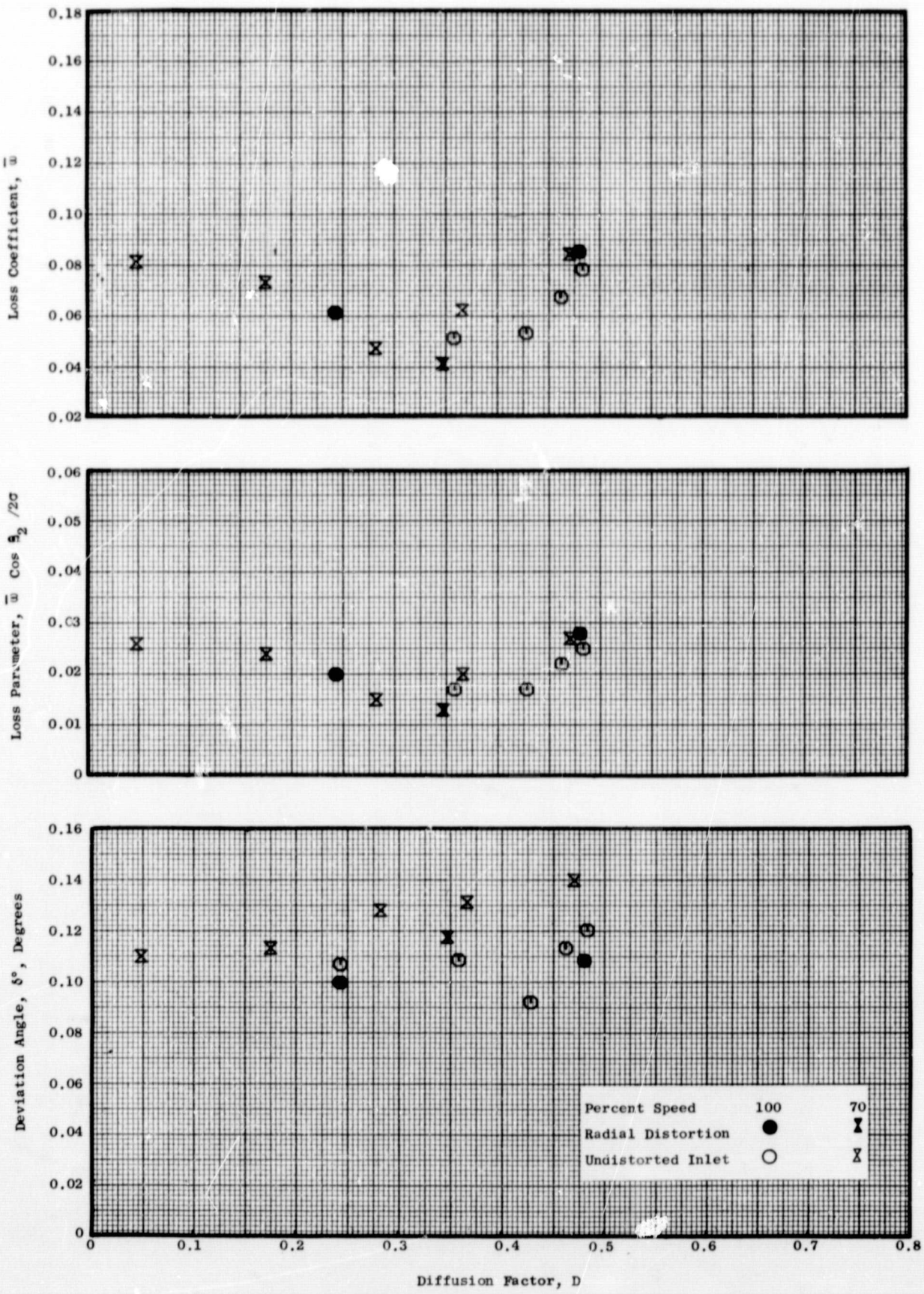

Figure 16(b). Stator Blade Element Data for 0°/0° IGV/Stator Schedule Measured at 10% Immersion from Tip.

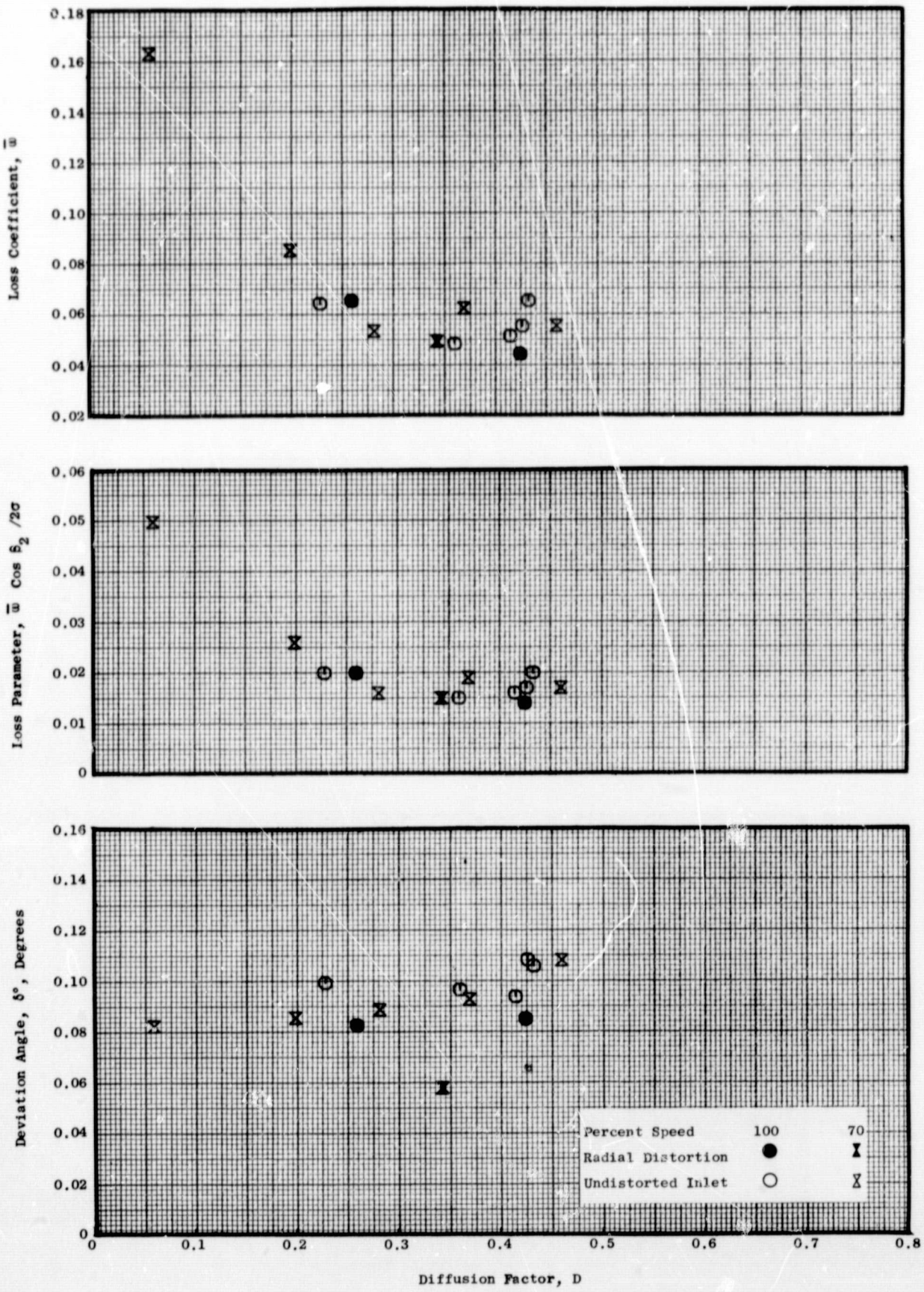

Figure 16(c). Stator Blade Element Data for 0°/0° IGV/Stator Schedule Measured at 30% Immersion from Tip.

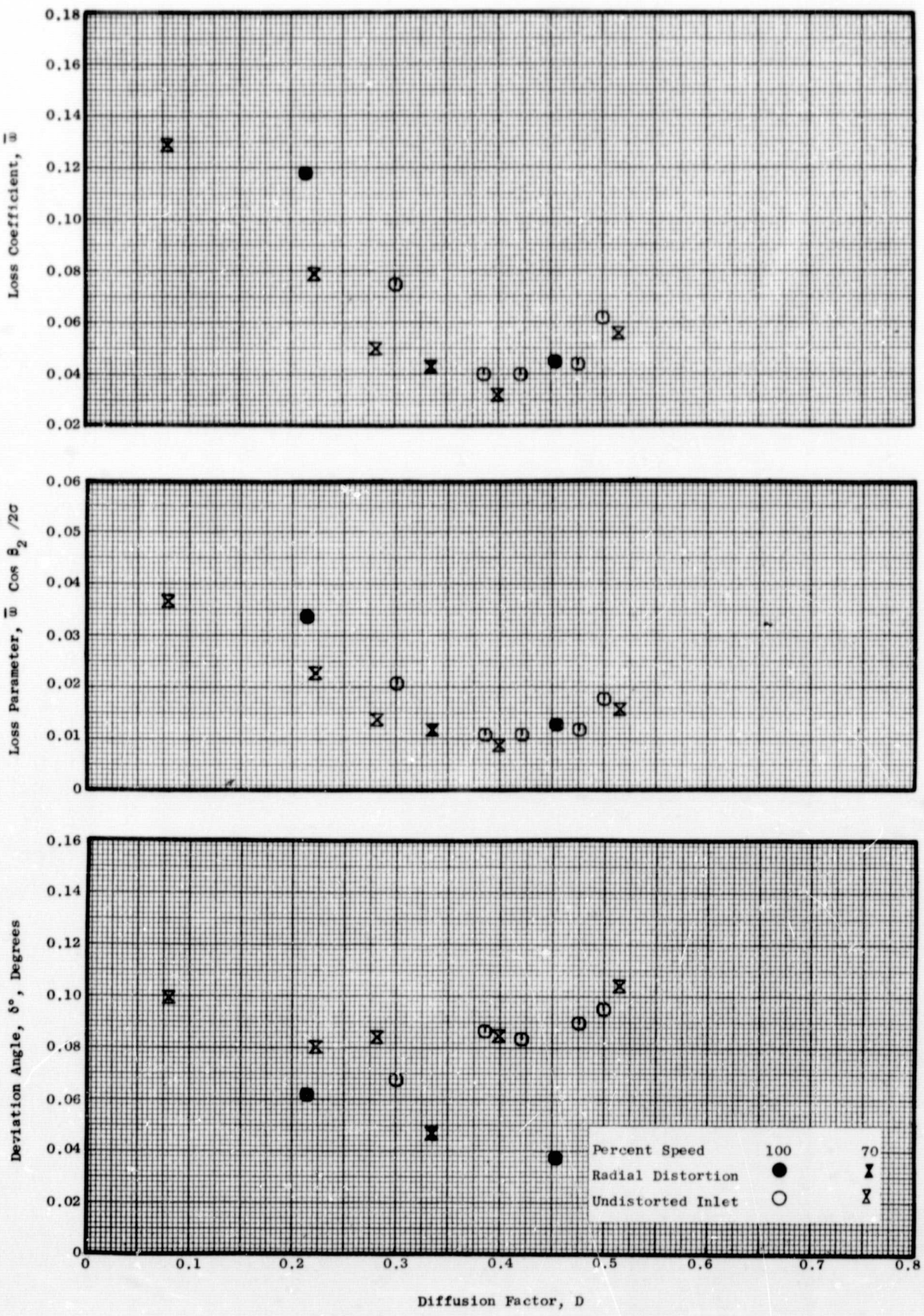

Figure 16(d). Stator Blade Element Data for 0°/0° IGV/Stator Schedule Measured at 50% Immersion from Tip.

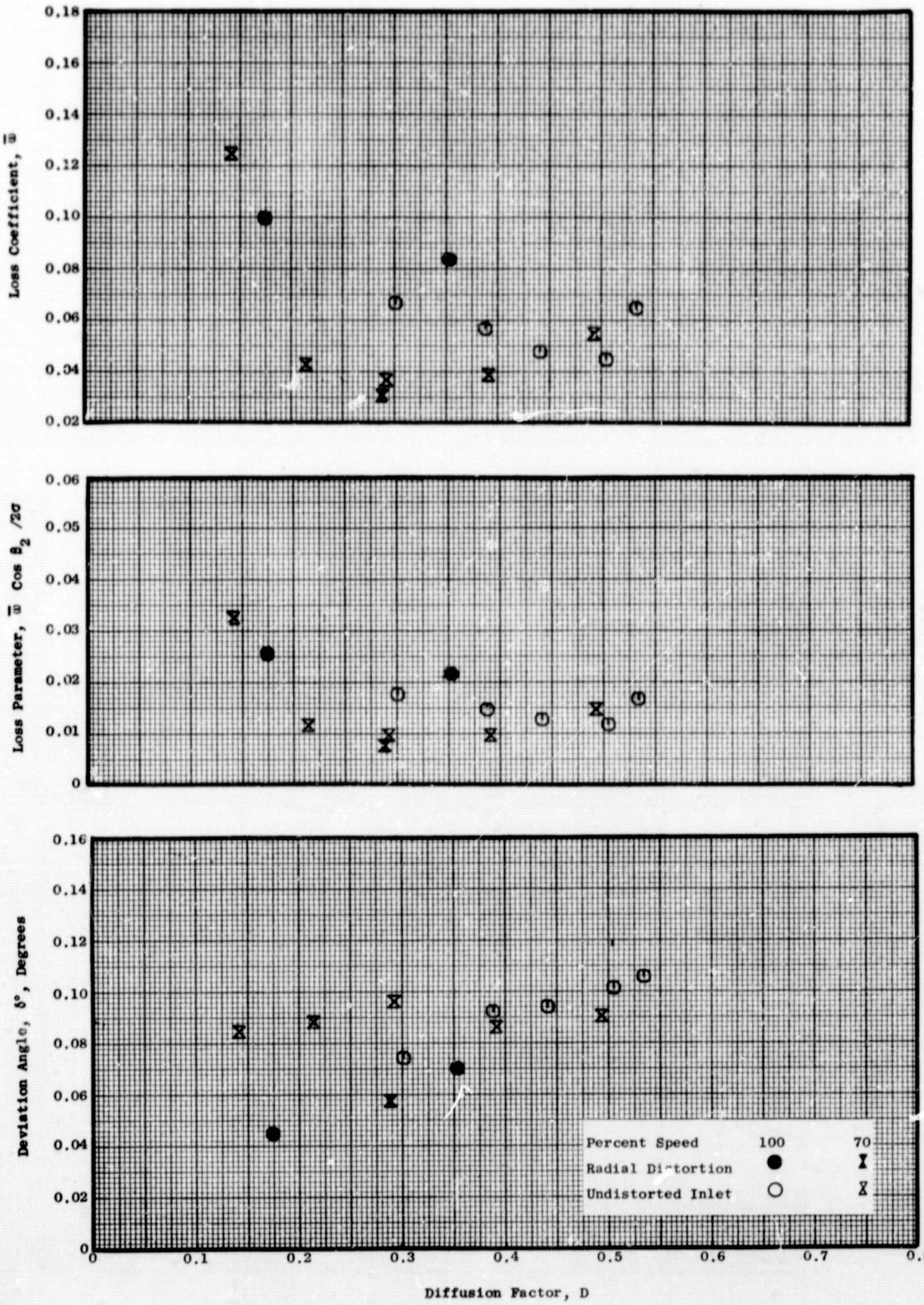

Figure 16(e). Stator Blade Element Data for 0°/0° IGV/Stator Schedule Measured at 70% Immersion from Tip.

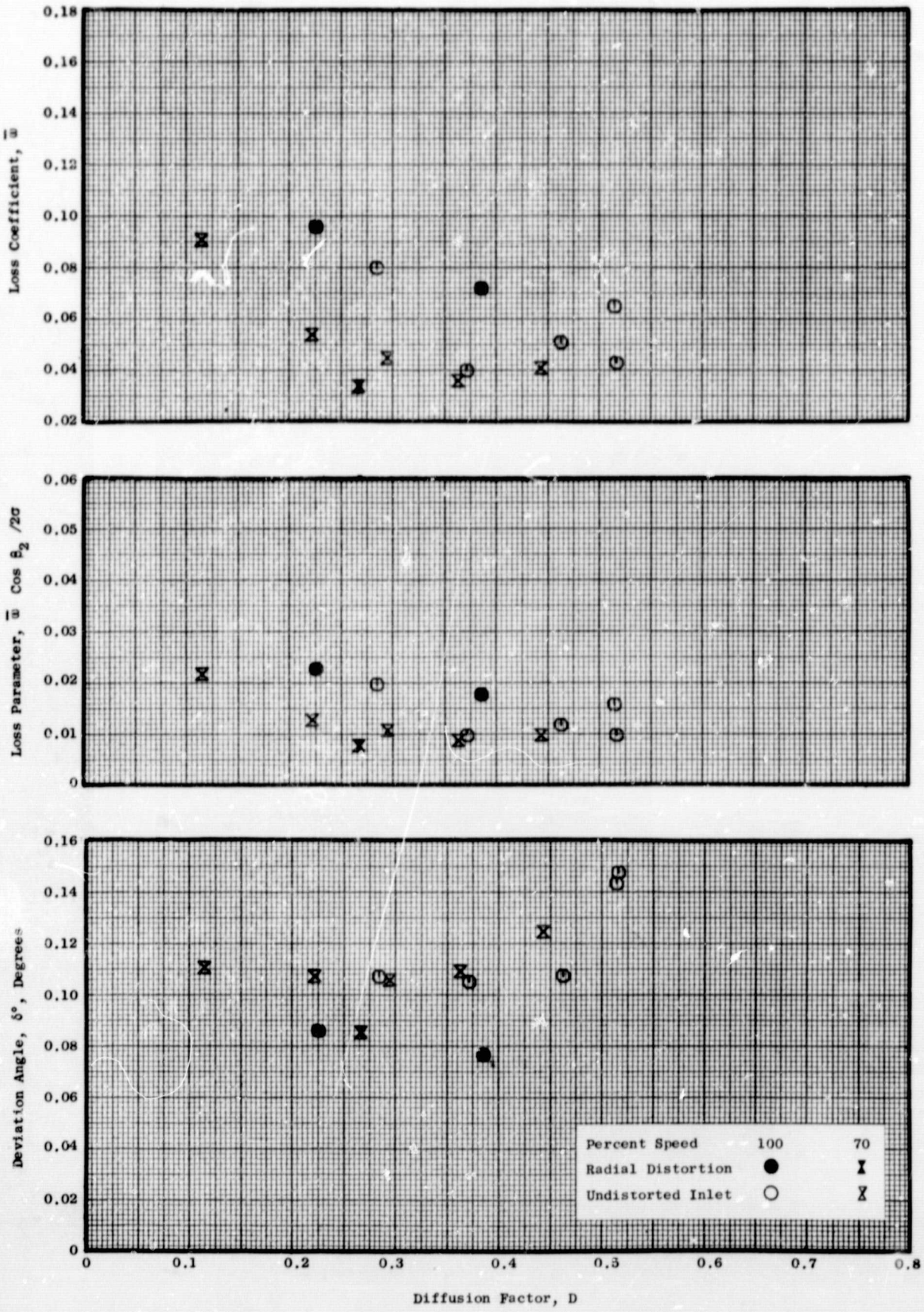

Figure 16(f). Stator Blade Element Data for 0°/0° IGV/Stator Schedule Measured at 90% Immersion from Tip.

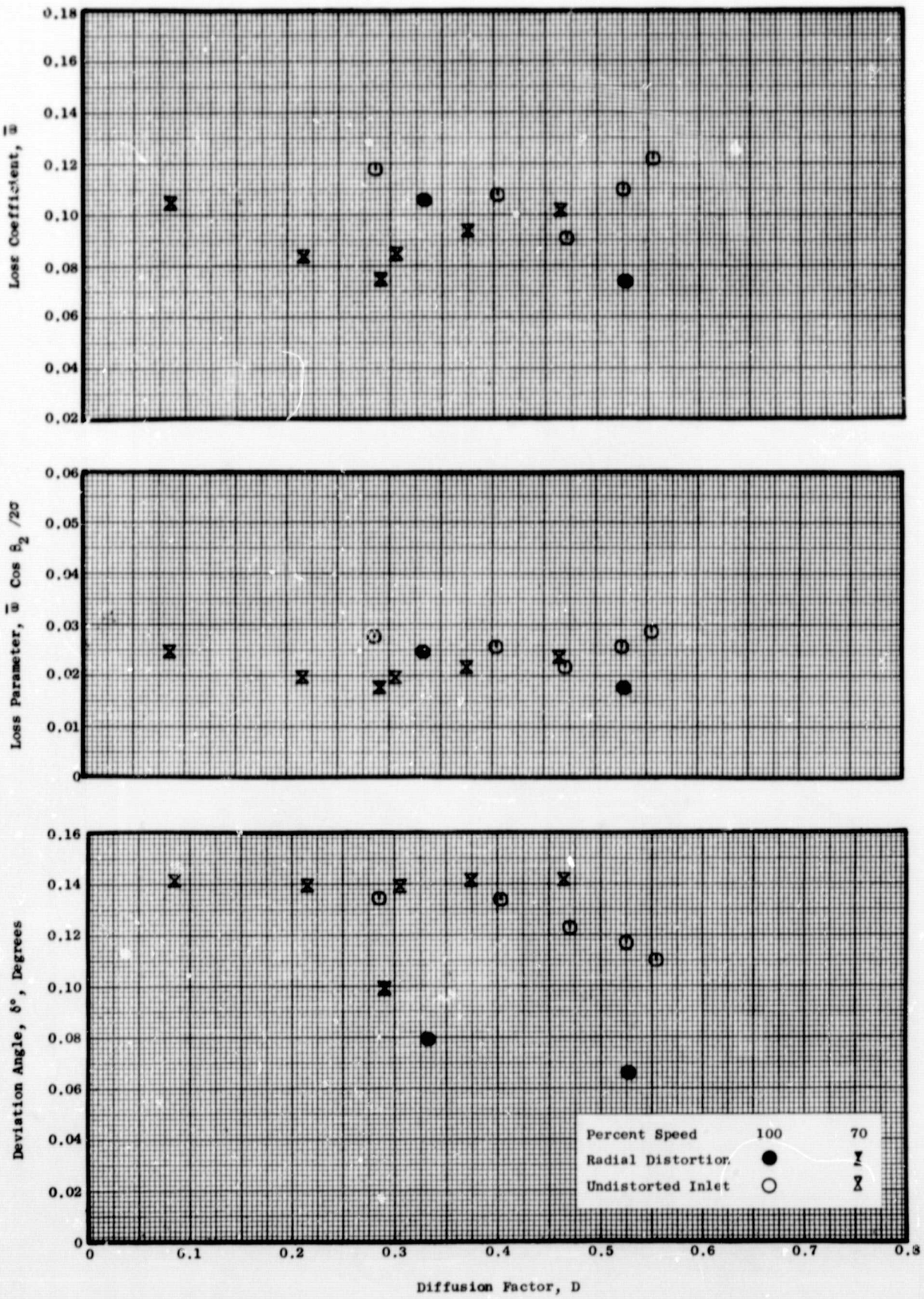

Figure 16(g). Stator Blade Element Data for 0°/0° IGV/Stator Schedule Measured at 95% Immersion from Tip.

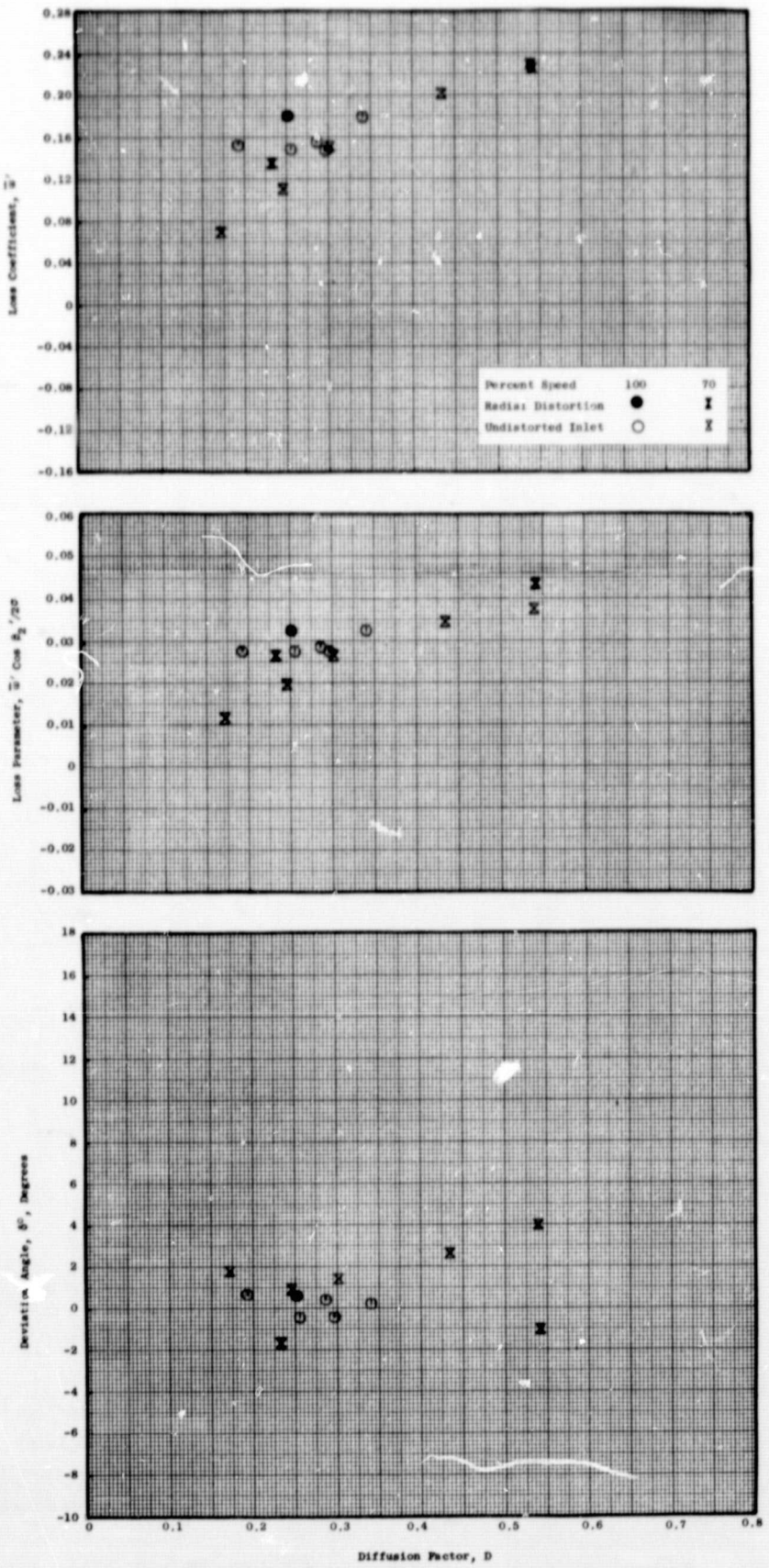

Figure 17(a). Rotor Blade Element Data for 40°/8° IGV/Stator Schedule Measured at 5% Immersion from Tip.

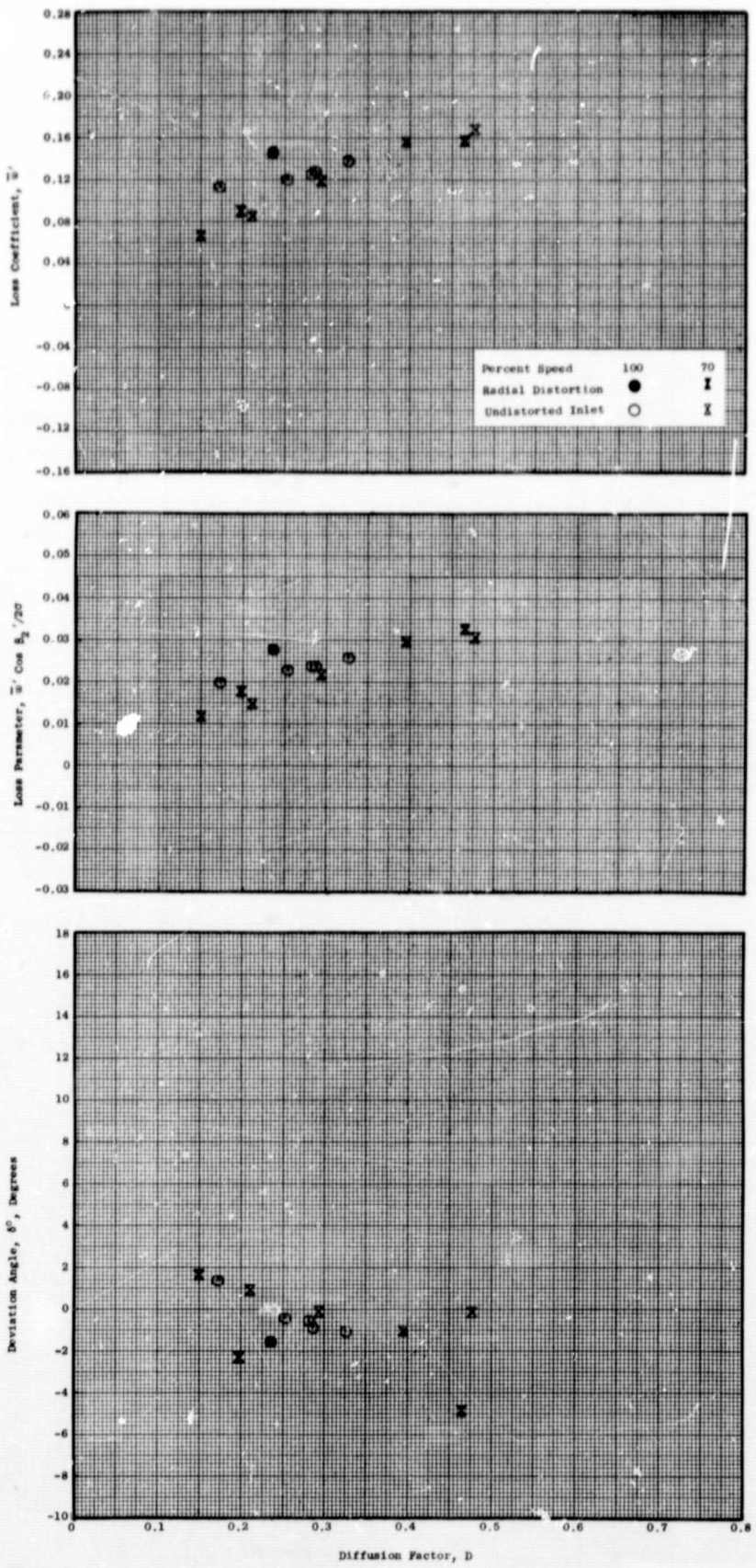

Figure 17(b). Rotor Blade Element Data for 40°/8° IGV/Stator Schedule Measured at 10% Immersion from Tip.

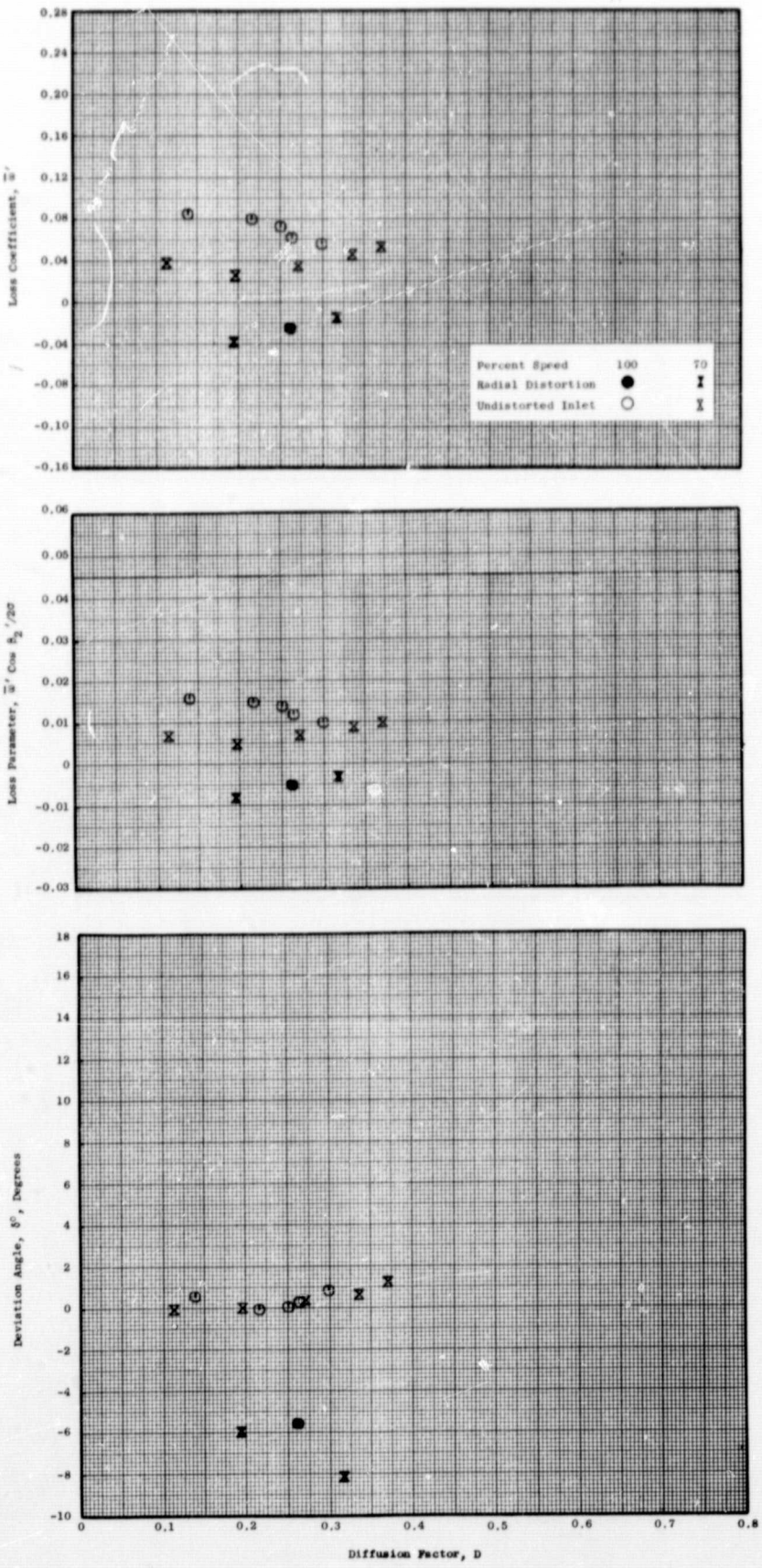

Figure 17(c). Rotor Blade Element Data for 40°/8° IGV/Stator Schedule Measured at 30% Immersion from Tip.

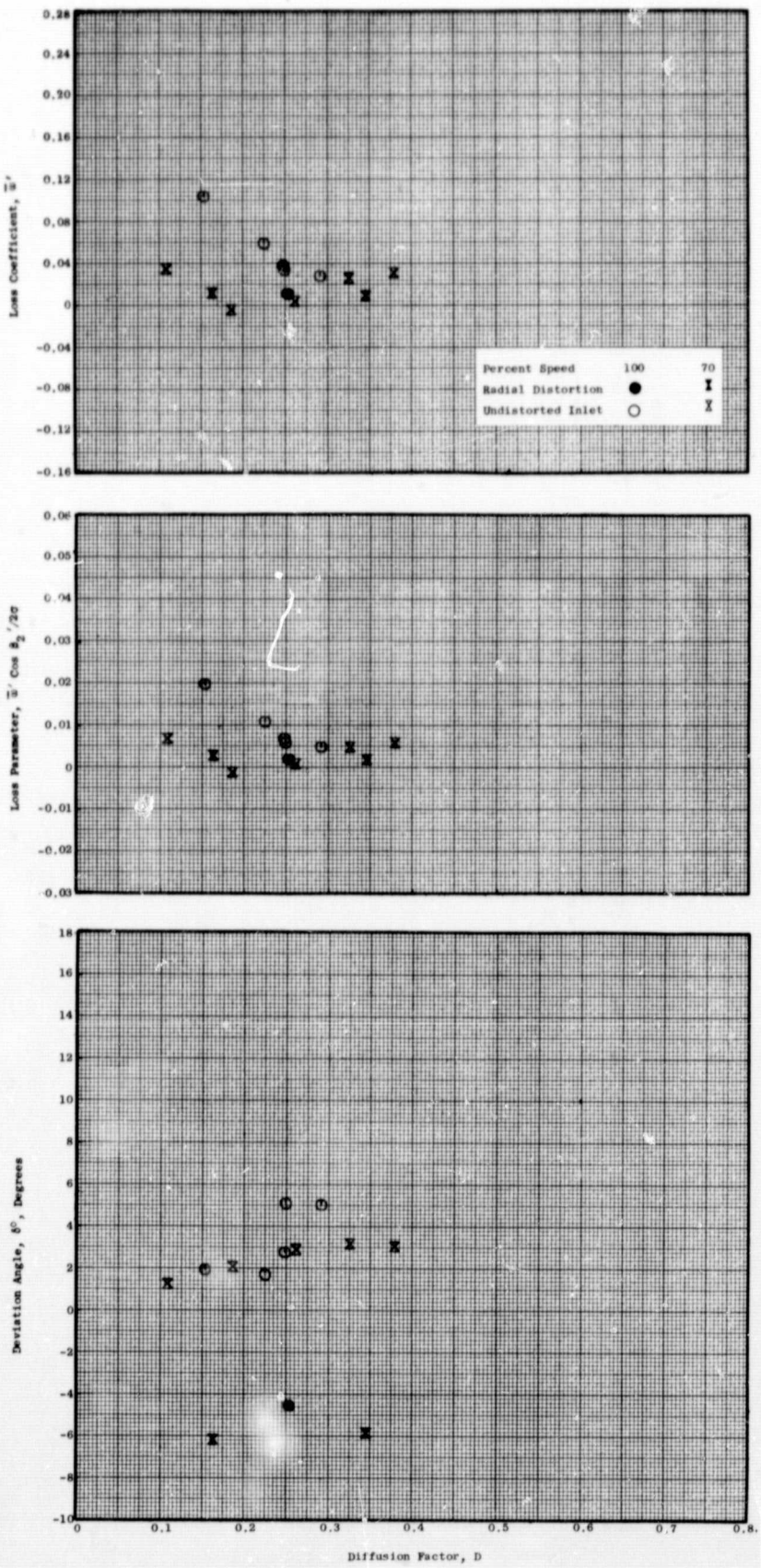

Figure 17(d). Rotor Blade Element Data for 40°/8° IGV/Stator Schedule Measured at 50% Immersion from Tip.

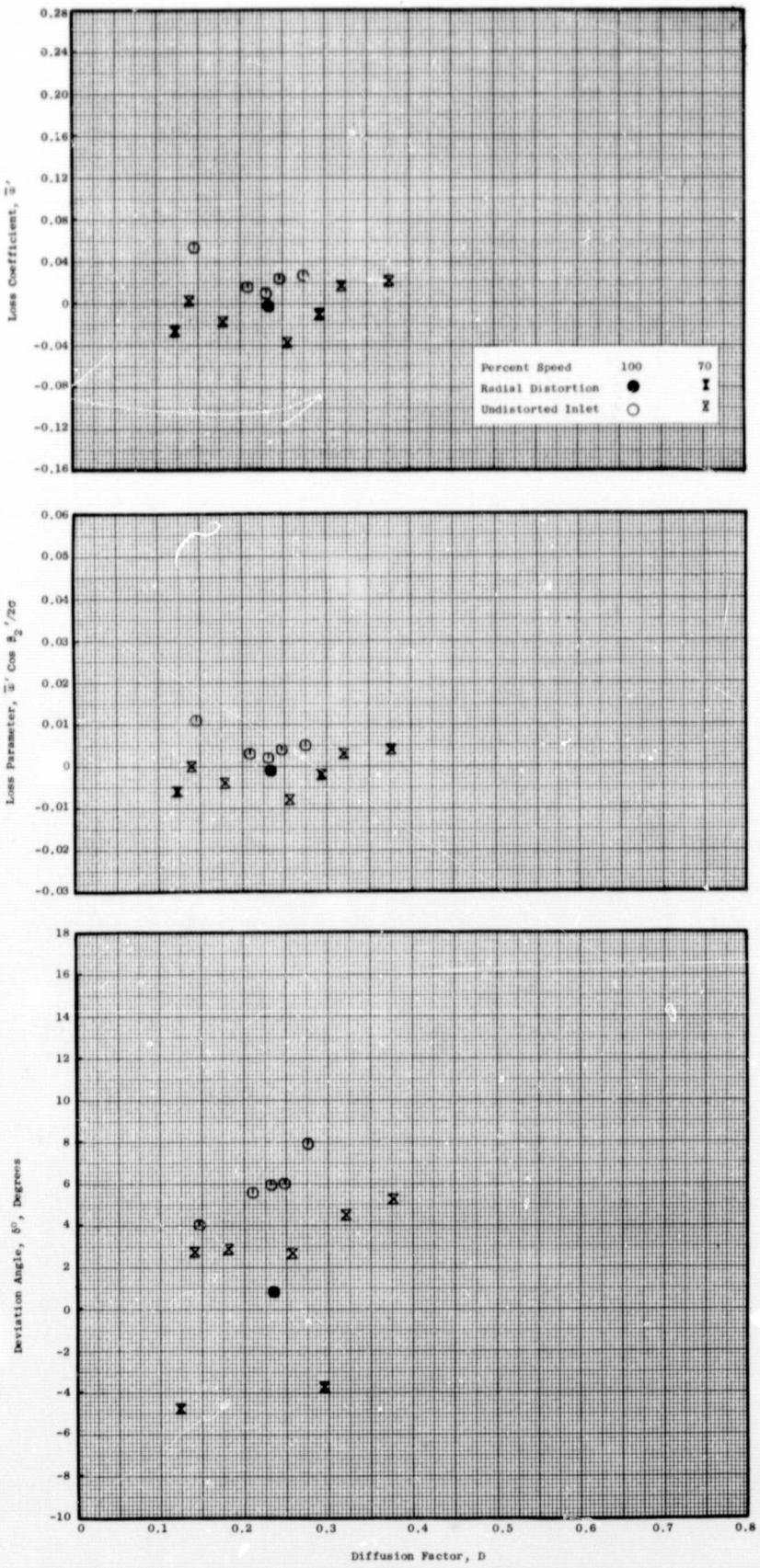

Figure 17(e). Rotor Blade Element Data for 40°/8° IGV/Stator Schedule Measured at 70% Immersion from Tip.

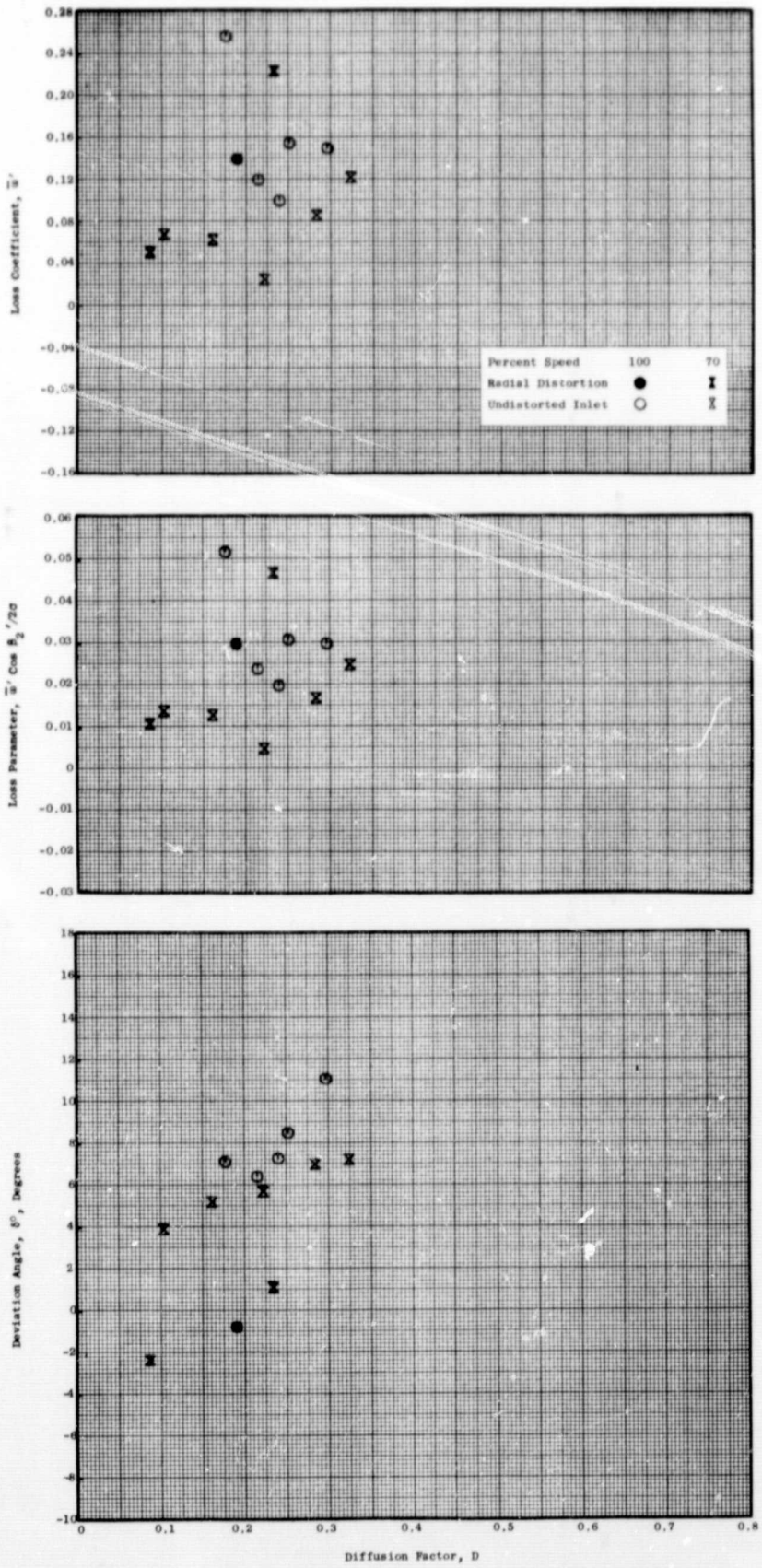

Figure 17(f). Rotor Blade Element Data for 40°/8° IGV/Stator Schedule Measured at 90% Immersion from Tip.

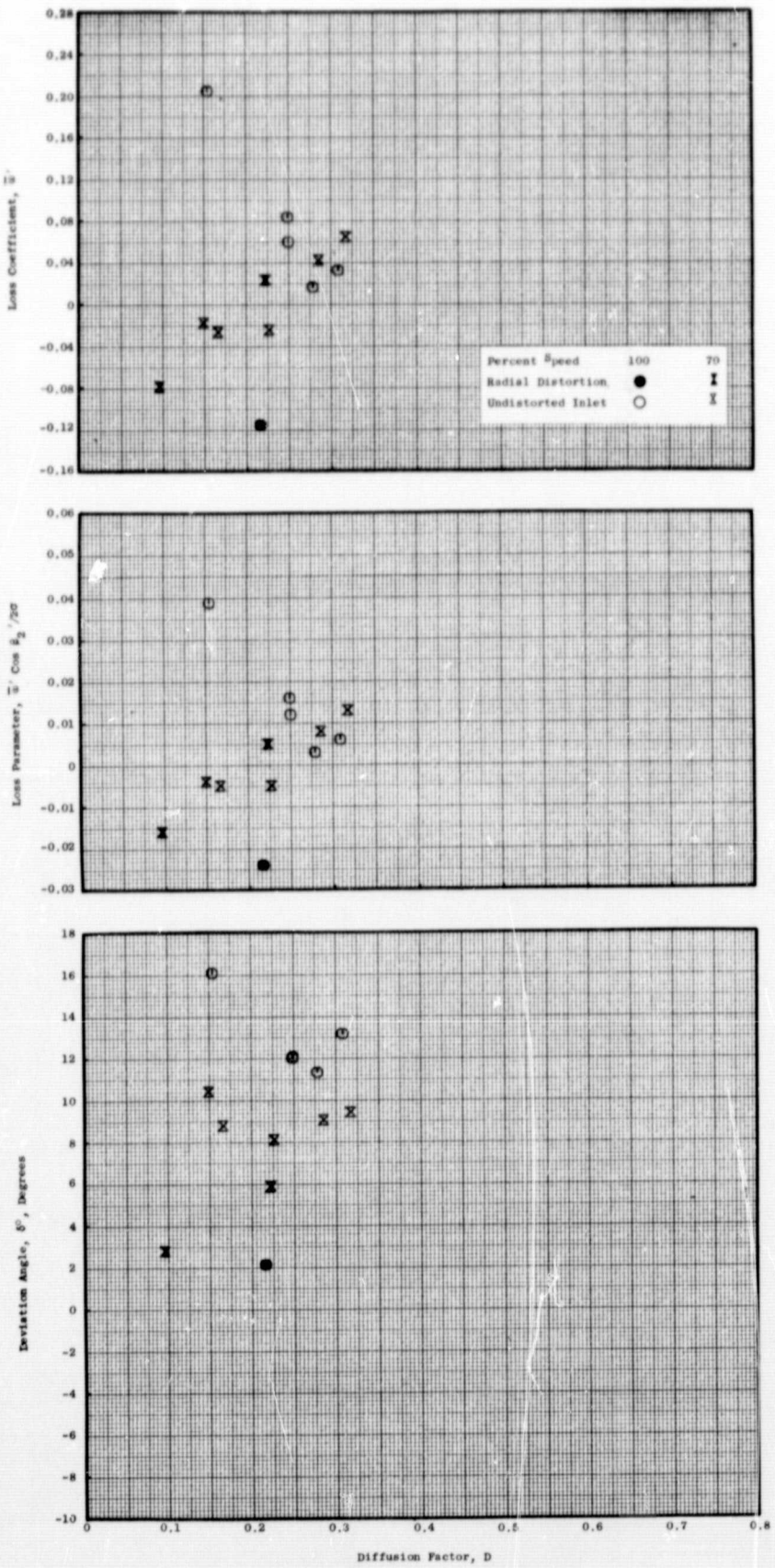

Figure 17(g). Rotor Blade Element Data for 40°/8° IGV/Stator Schedule Measured at 95% Immersion from Tip.

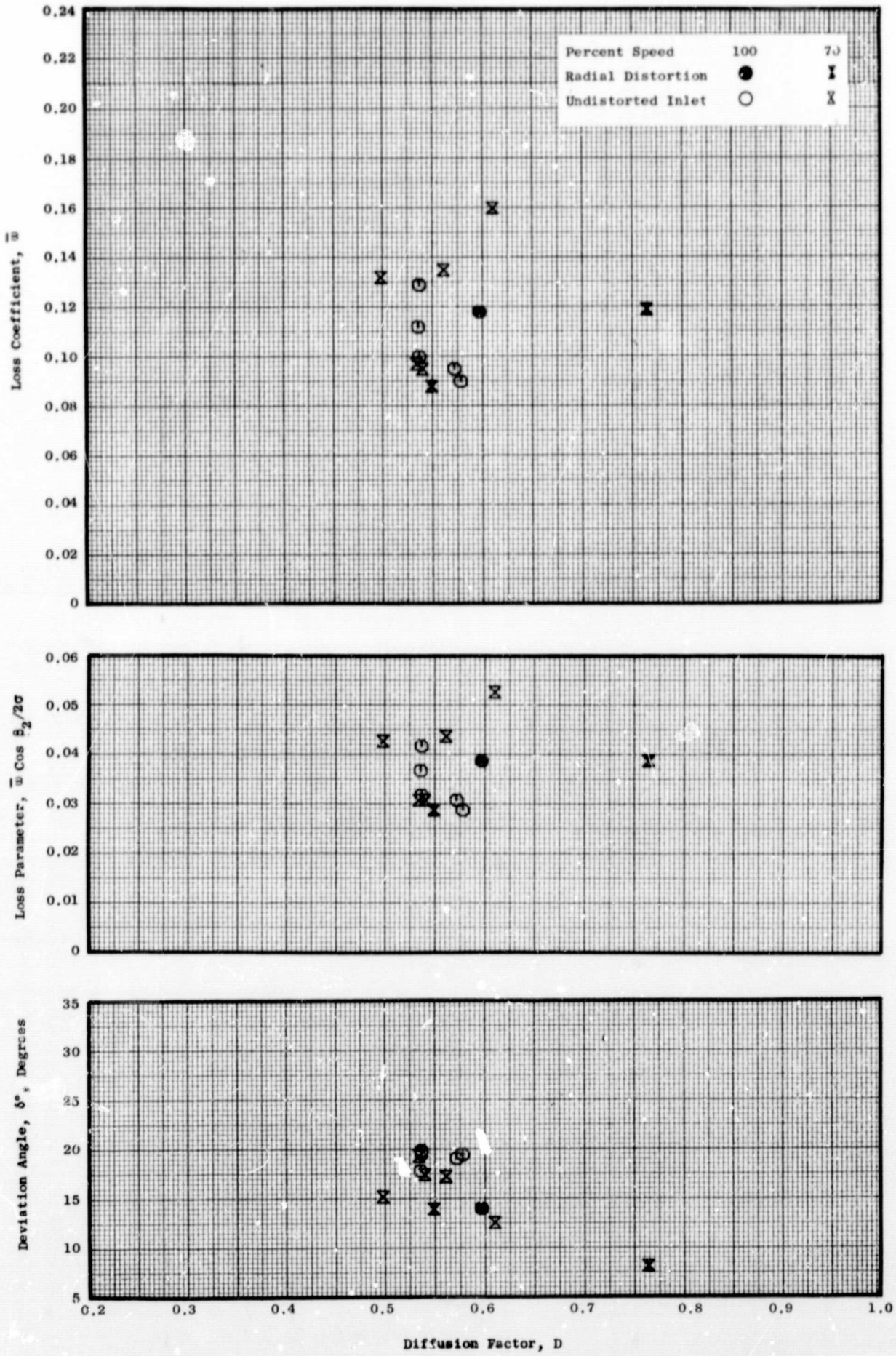

Figure 18(a). Stator Blade Element Data for 40°/8° IGV/Stator Schedule Measured at 5% Immersion from Tip.

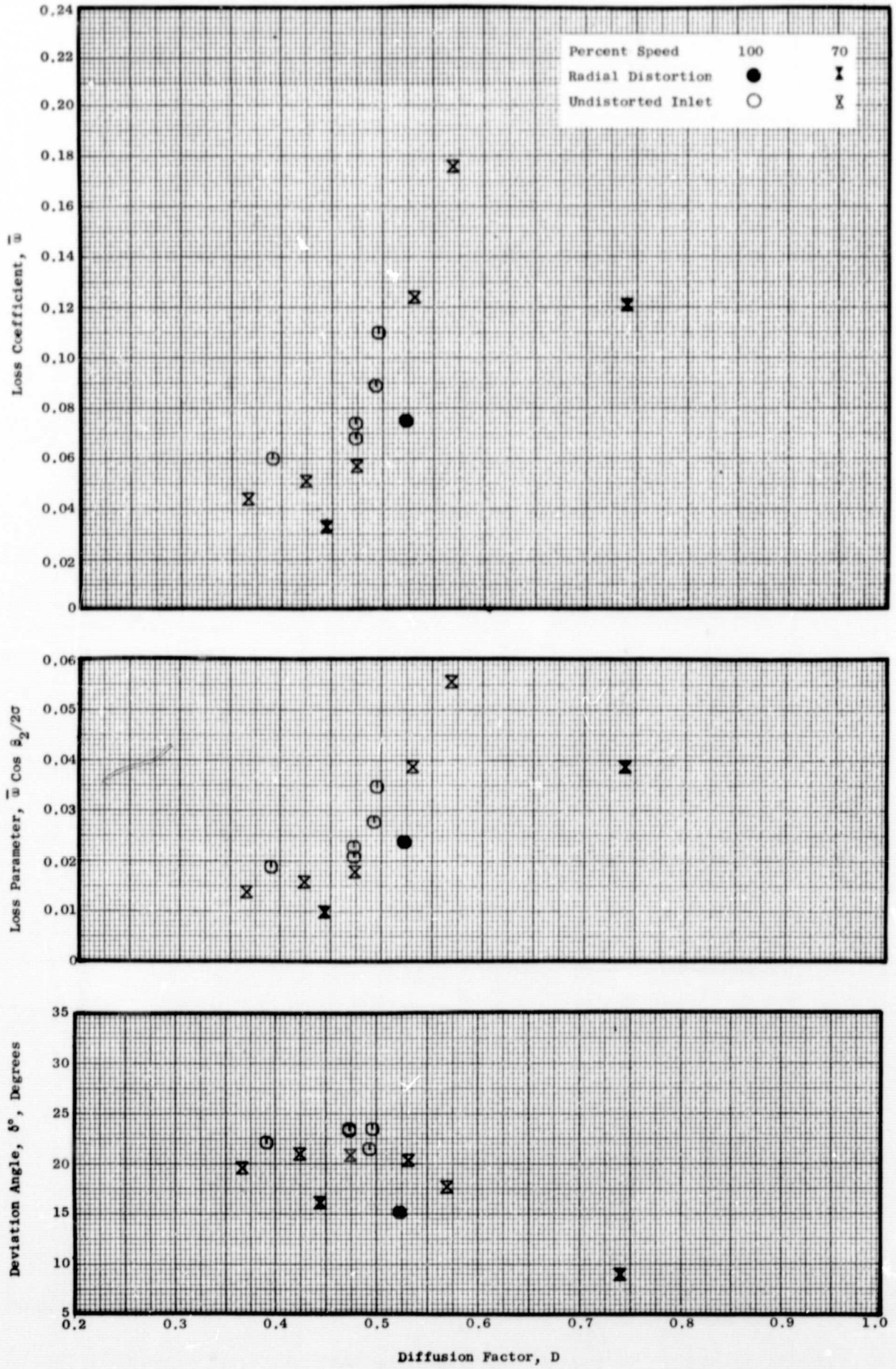

Figure 18(b). Stator Blade Element Data for 40°/8° IGV/Stator Schedule Measured at 10% Immersion from Tip.

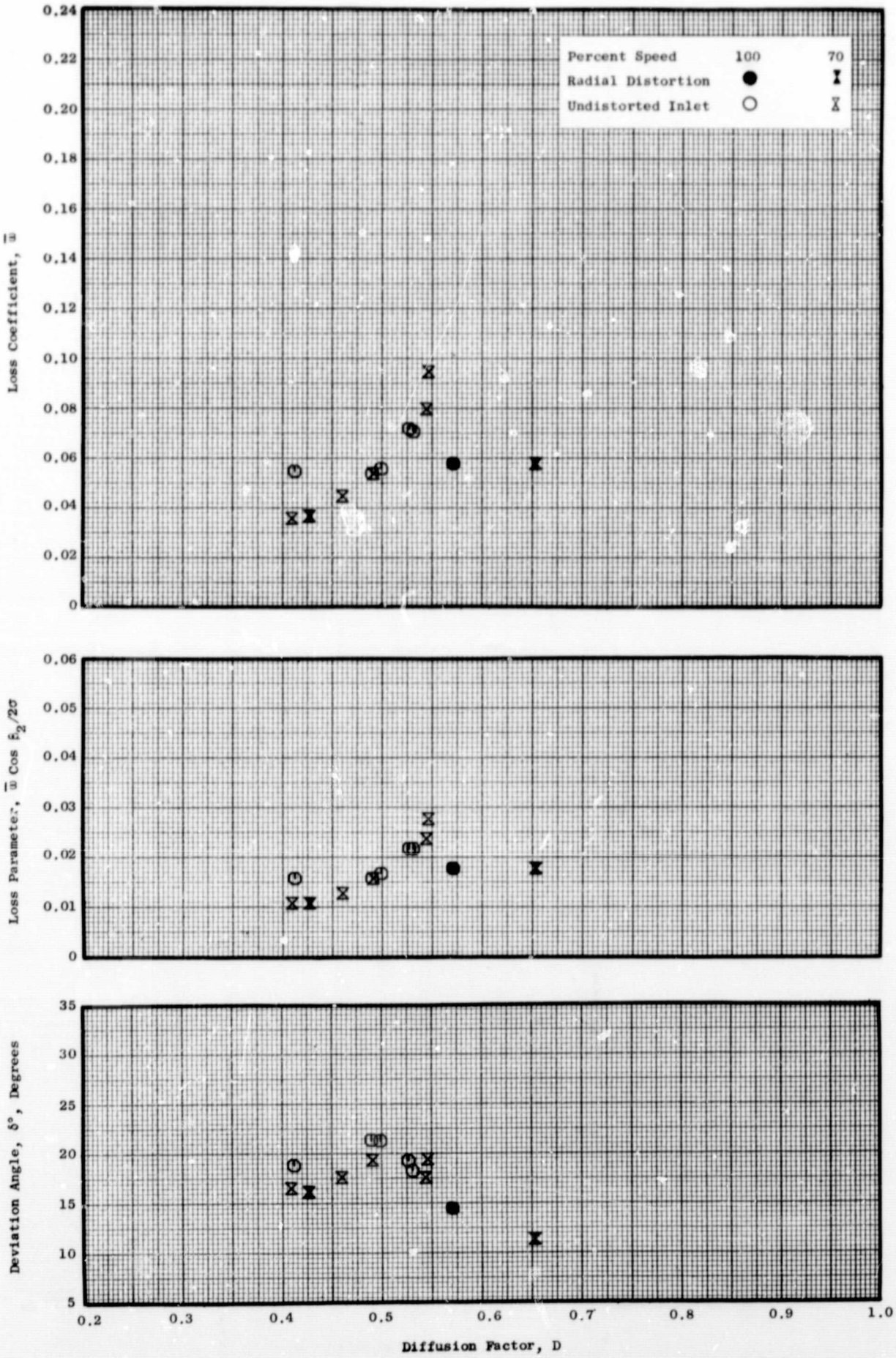

Figure 18(c). Stator Blade Element Data for 40°/8° IGV/Stator Schedule Measured at 30% Immersion from Tip.

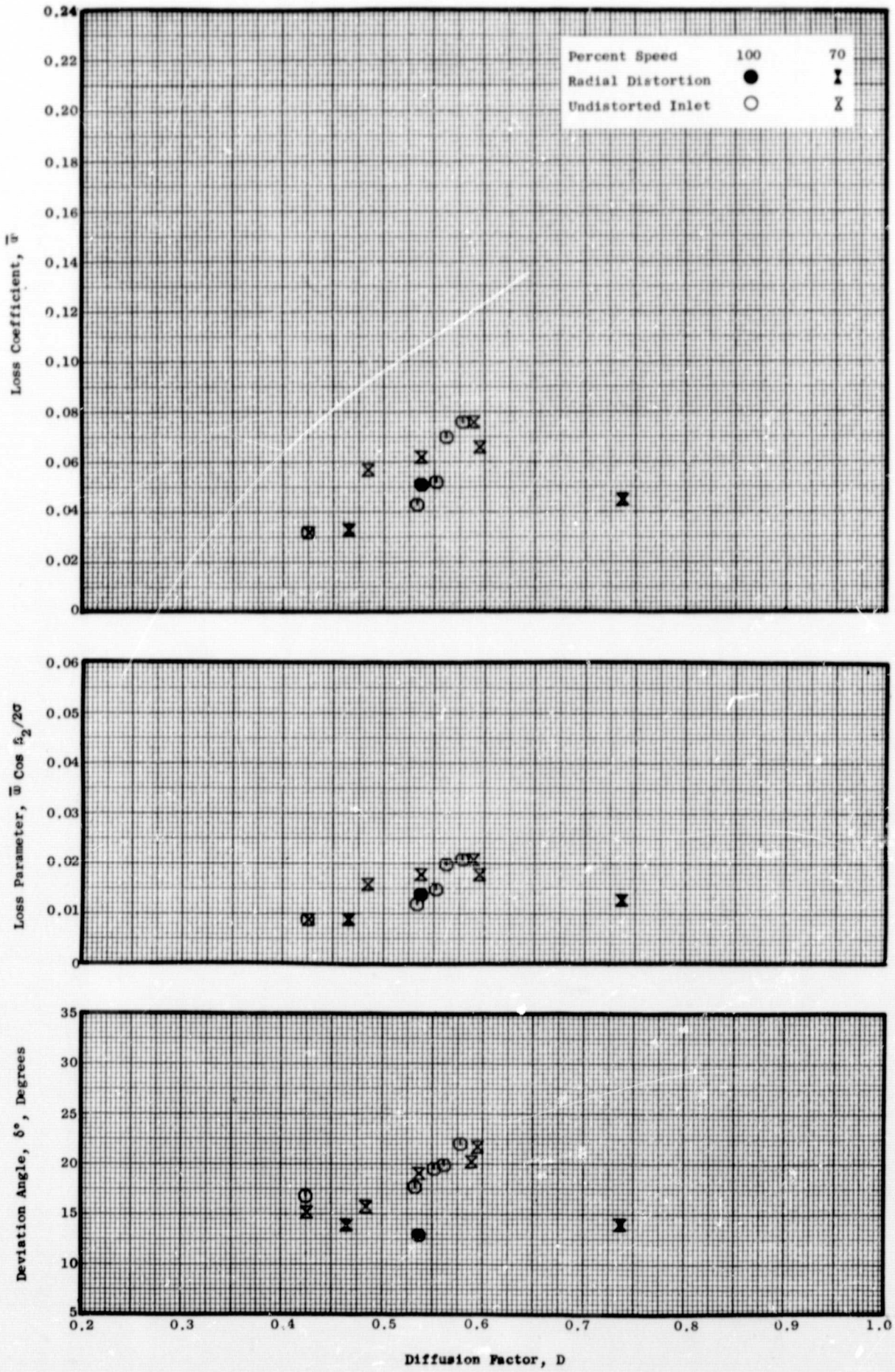

Figure 18(d). Stator Blade Element Data for 40°/8° IGV/Stator Schedule Measured at 50% Immersion from Tip.

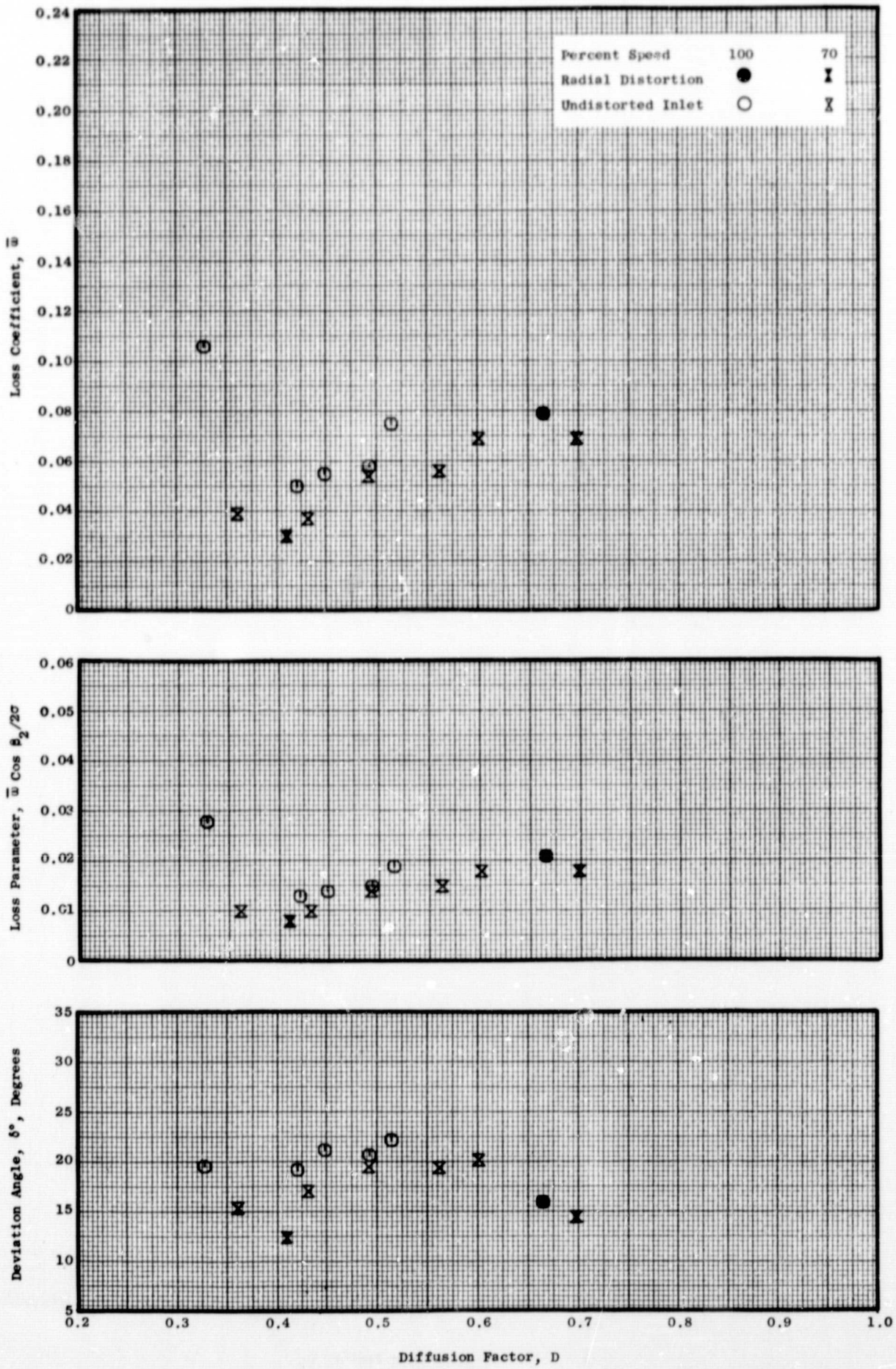

Figure 18(e). Stator Blade Element Data for 40°/8° IGV/Stator Schedule Measured at 70% Immersion from Tip.

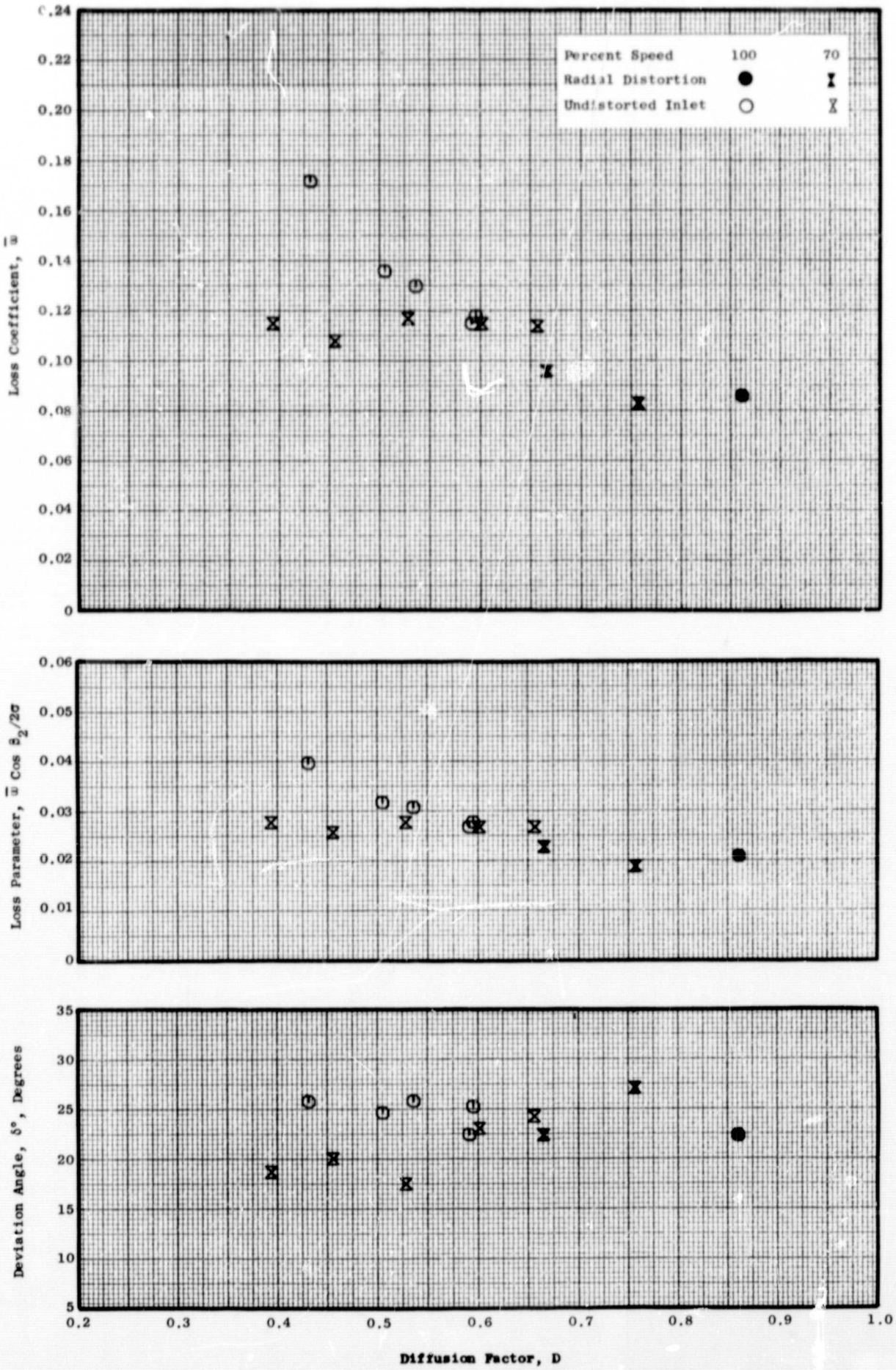

Figure 18(f). Stator Blade Element Data for 40°/8° IGV/Stator Schedule Measured at 90% Immersion from Tip.

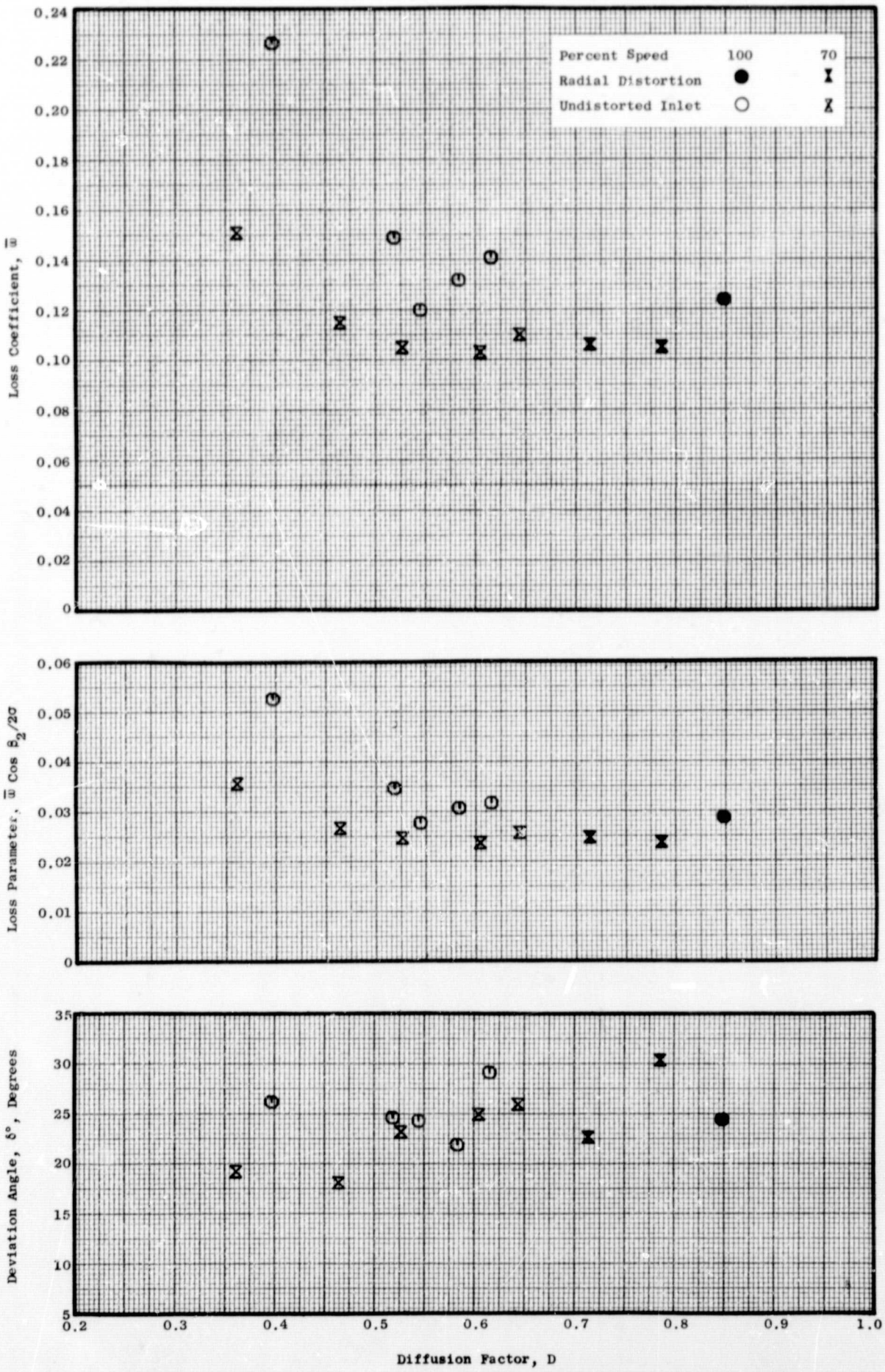

Figure 18(g). Stator Blade Element Data for 40°/8° IGV/Stator Schedule Measured at 95% Immersion from Tip.

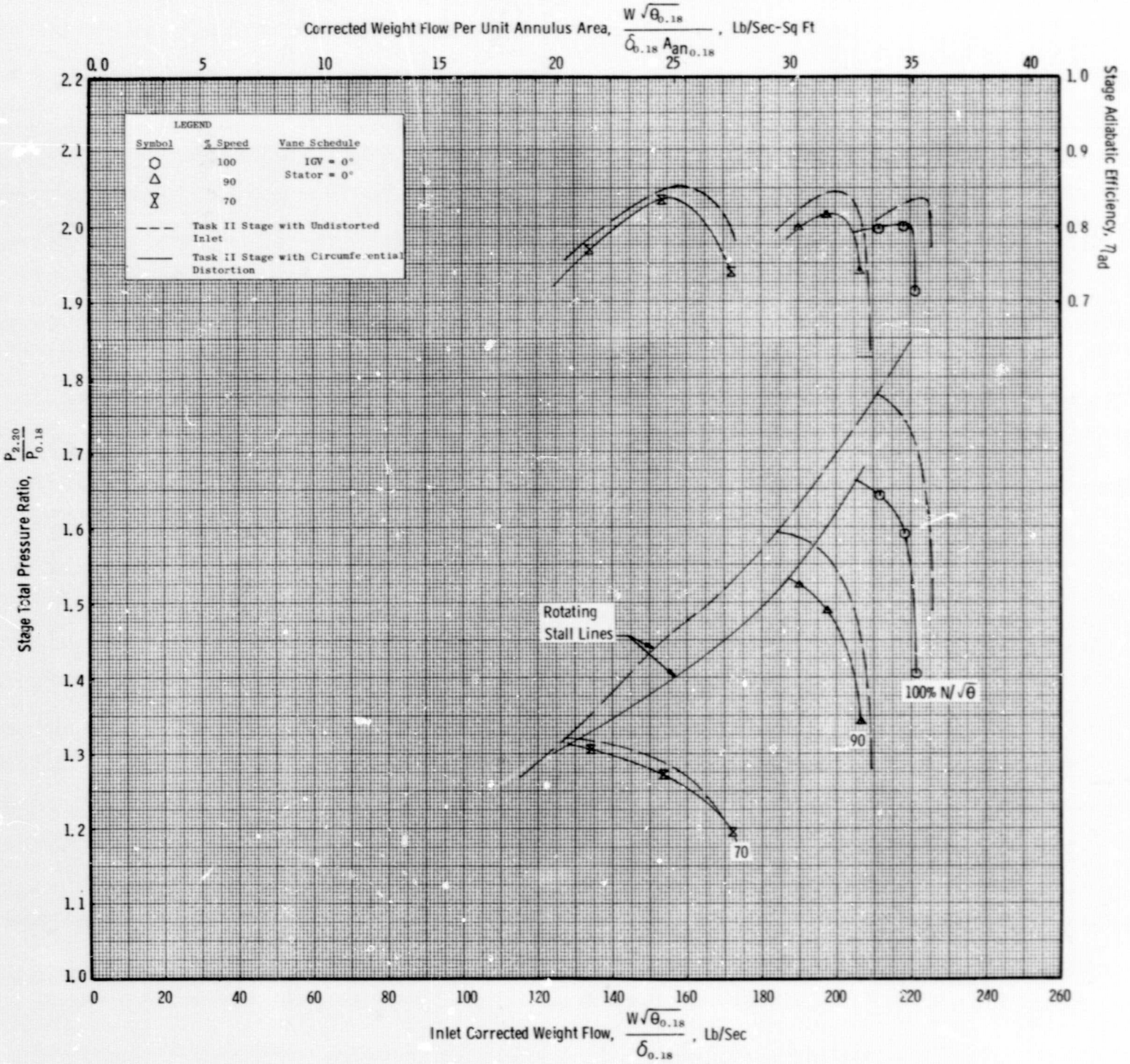

Figure 19. Task II Stage Performance Map with Circumferential Inlet Distortion for IGV/Stator Schedule of 0°/0°.

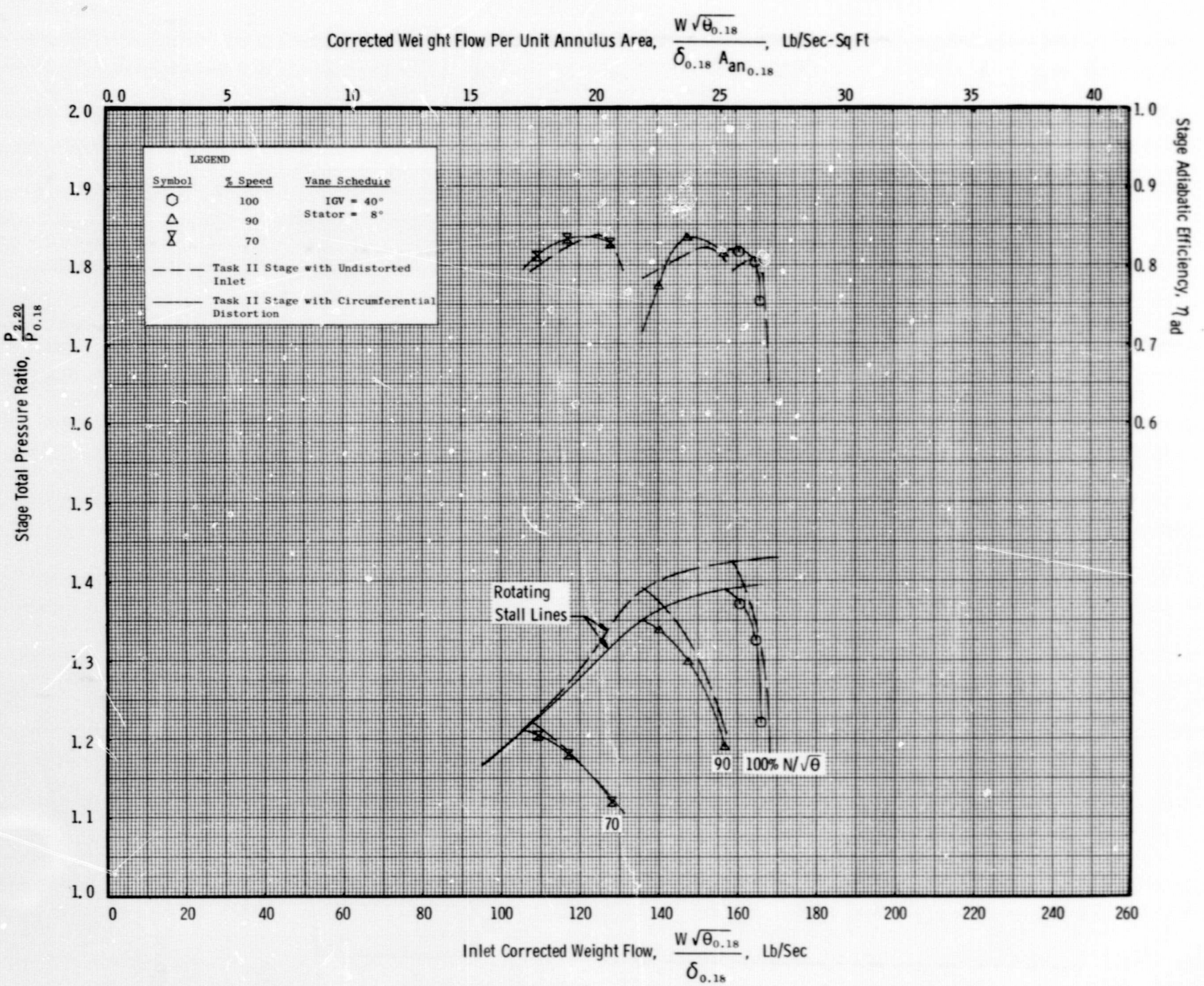

Figure 20. Task II Stage Performance Map with Circumferential Inlet Distortion for IGV/Stator Schedule of 40°/8°.

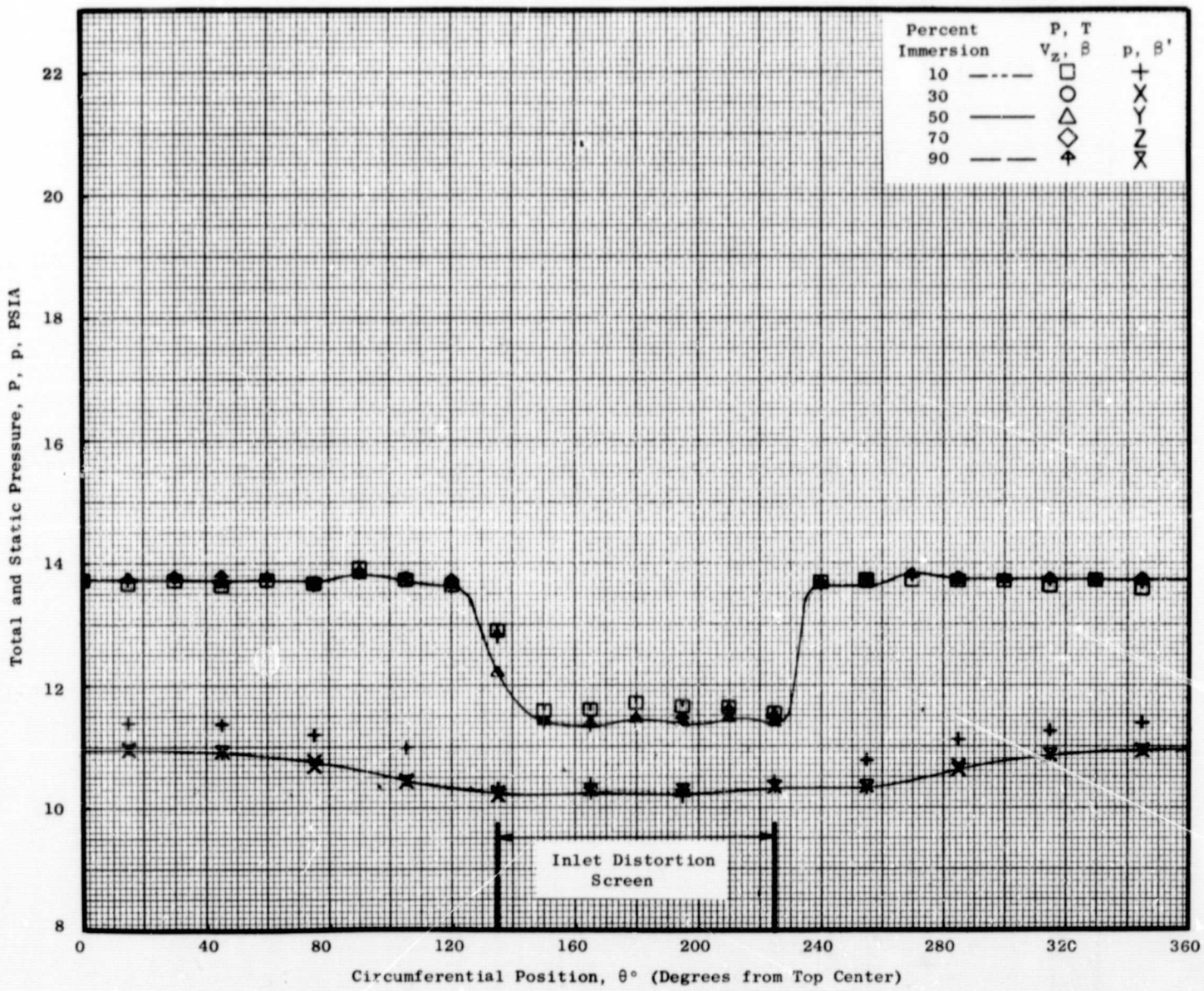

Figure 21(a). Circumferential Variation of Flow Conditions at 100 Percent Speed Maximum Flow with 0°/0° IGV/Stator Schedule at Plane 0.18.

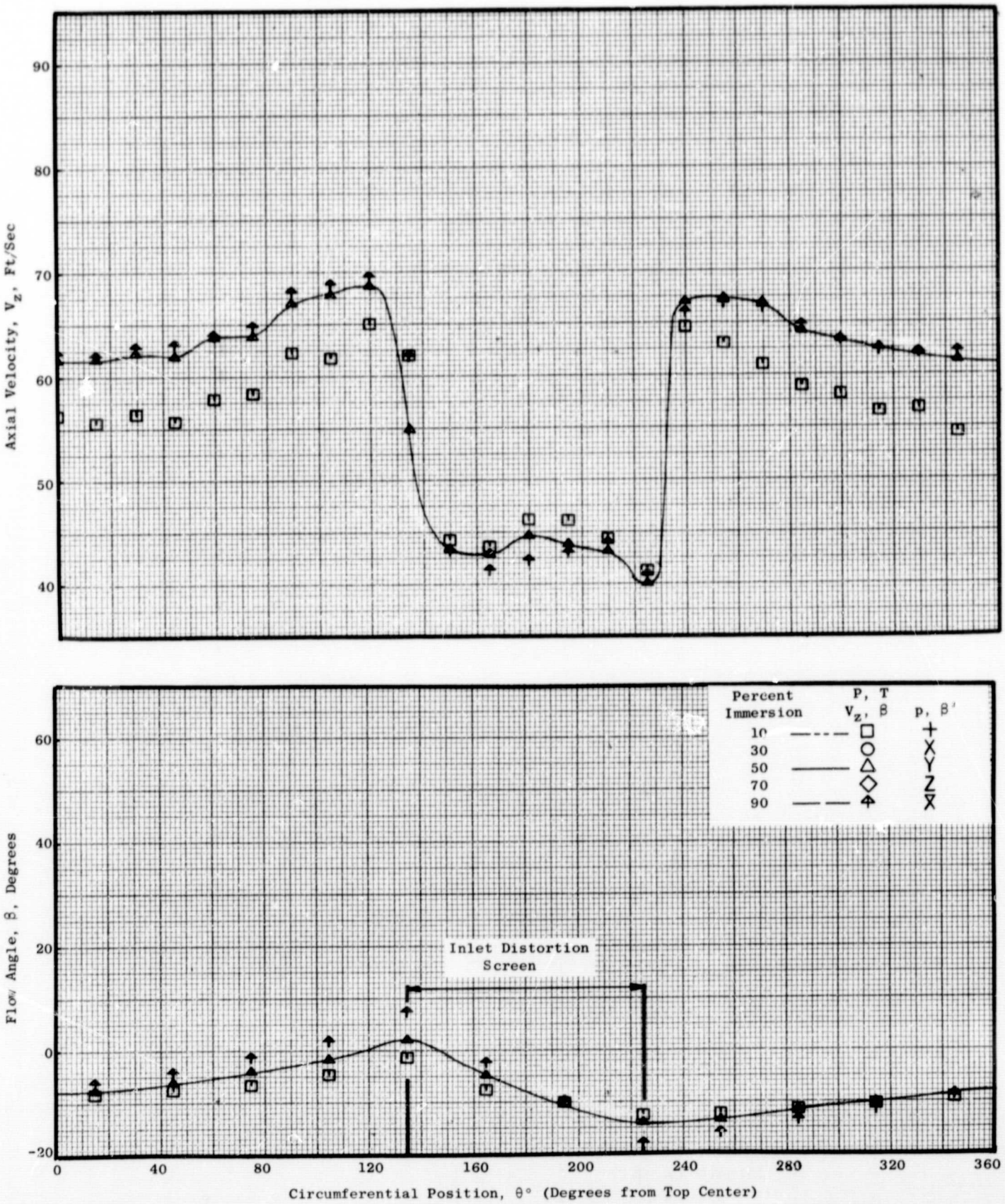

Figure 21(a). Circumferential Variation of Flow Conditions at 100 Percent Speed Maximum Flow with 0°/0° IGV/Stator Schedule at Plane 0.18 (Concluded).

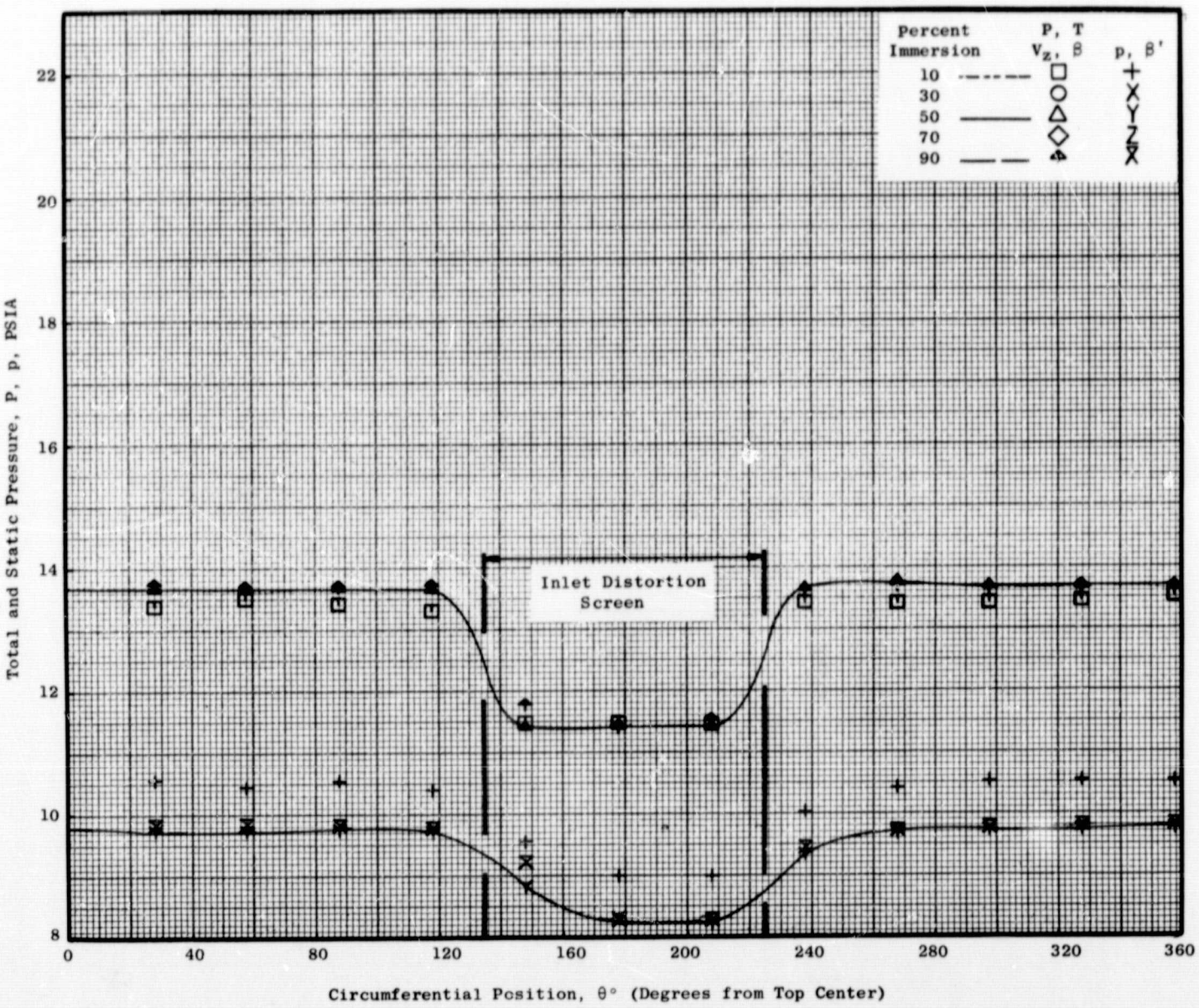

Figure 21(b). Circumferential Variation of Flow Conditions at 100 Percent Speed Maximum Flow with 0°/0° IGV/Stator Schedule at Plane 0.95.

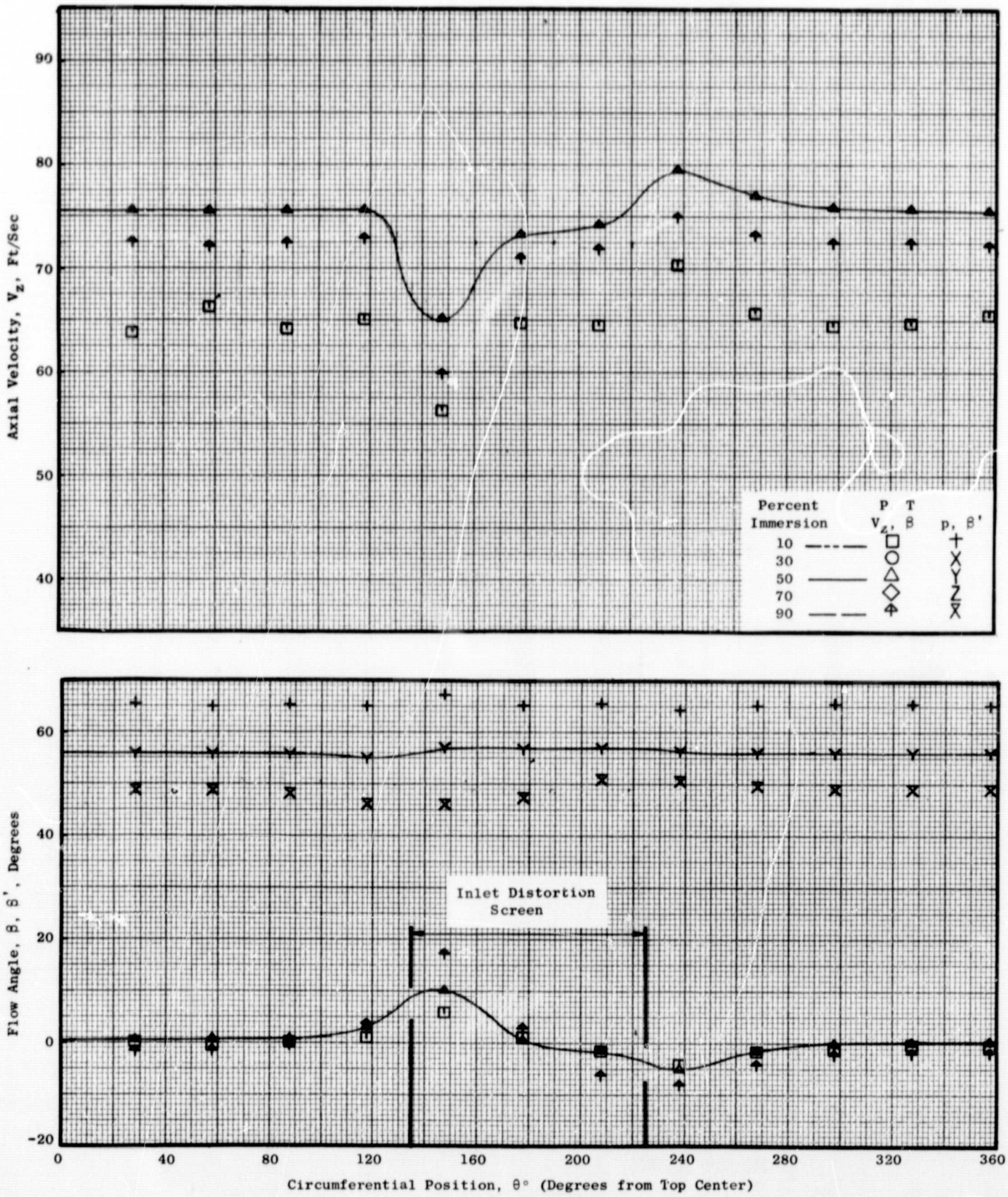

Figure 21(b). Circumferential Variation of Flow Conditions at 100 Percent Speed Maximum Flow with 0°/0° IGV/Stator Schedule at Plane 0.95 (Concluded).

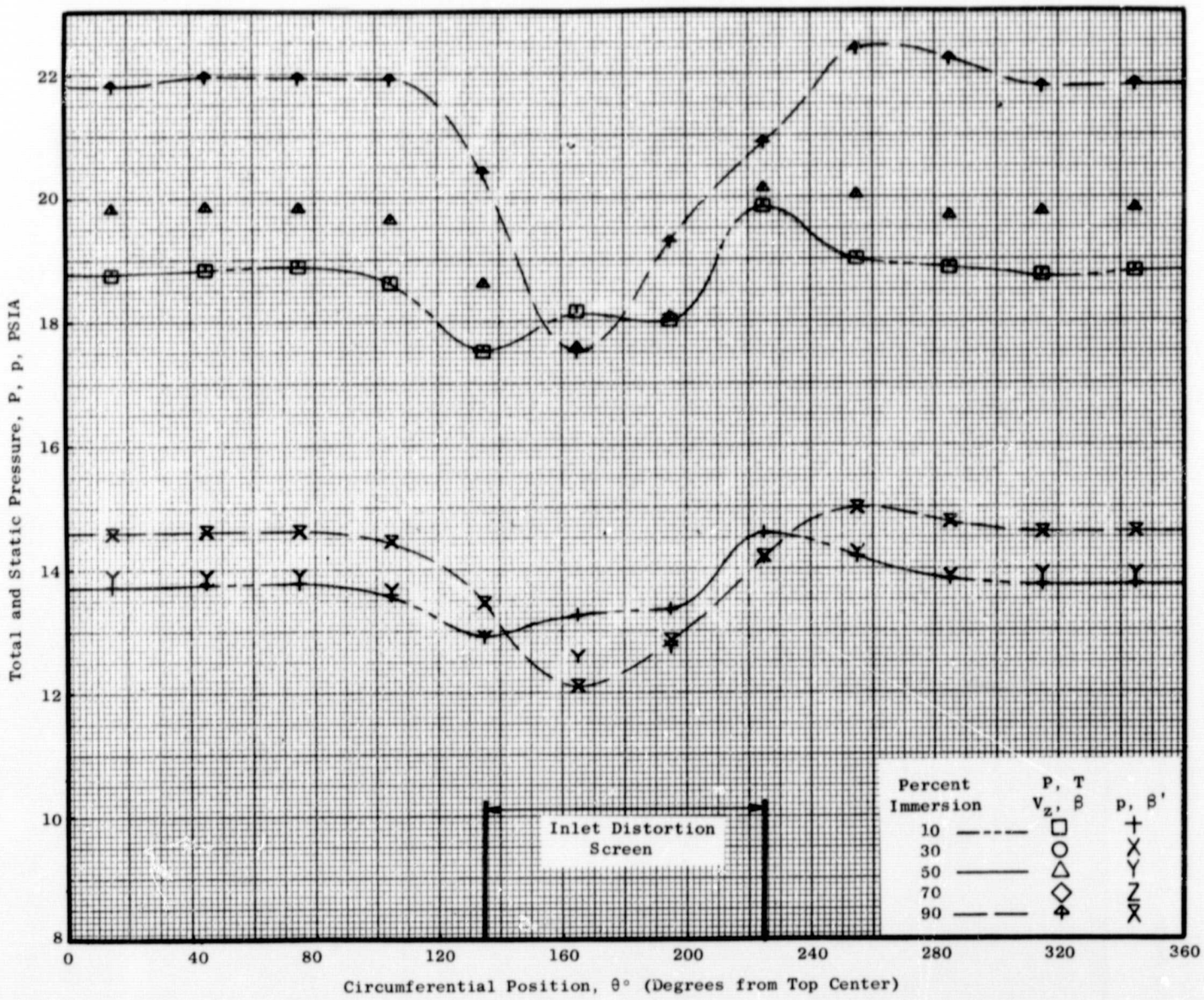

Figure 21(c). Circumferential Variation of Flow Conditions at 100 Percent Speed Maximum Flow with 0°/0° IGV/Stator Schedule at Plane 1.51.

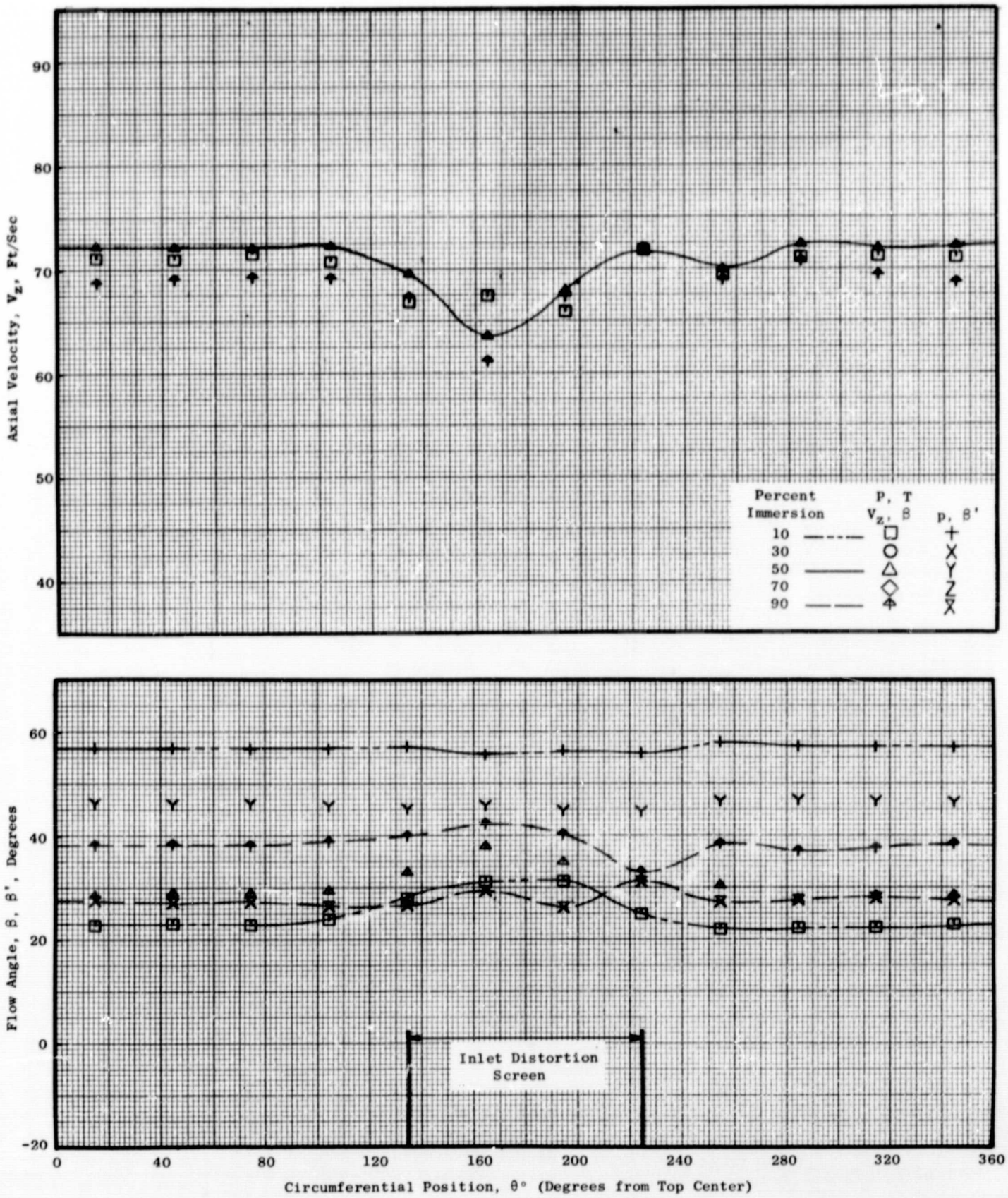

Figure 21(c). Circumferential Variation of Flow Conditions at 100 Percent Speed Maximum Flow with 0°/0° IGV/Stator Schedule at Plane 1.51 (Concluded).

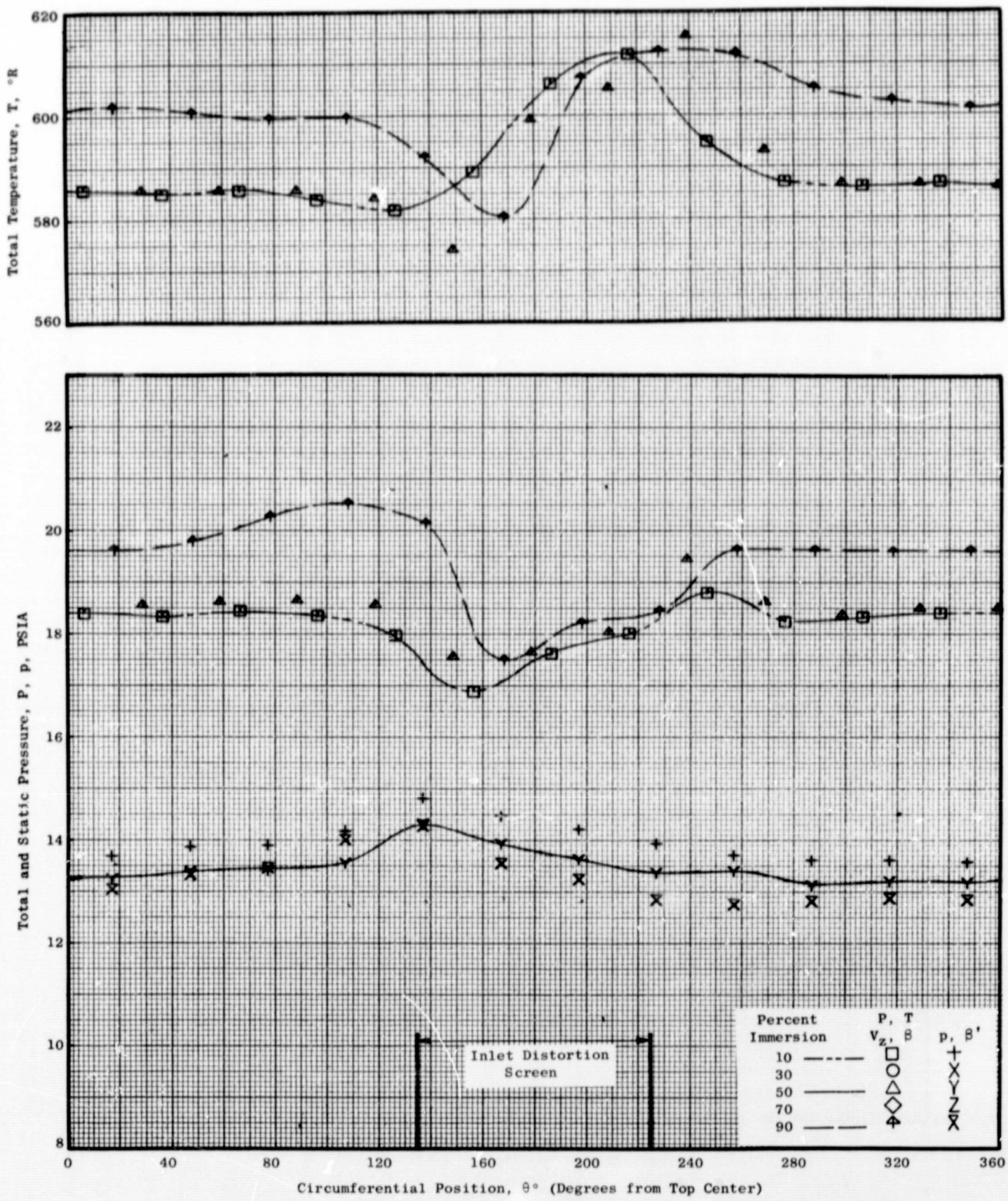

Figure 21(d). Circumferential Variation of Flow Conditions at 100 Percent Speed Maximum Flow with 0°/0° IGV/Stator Schedule at Plane 2.20.

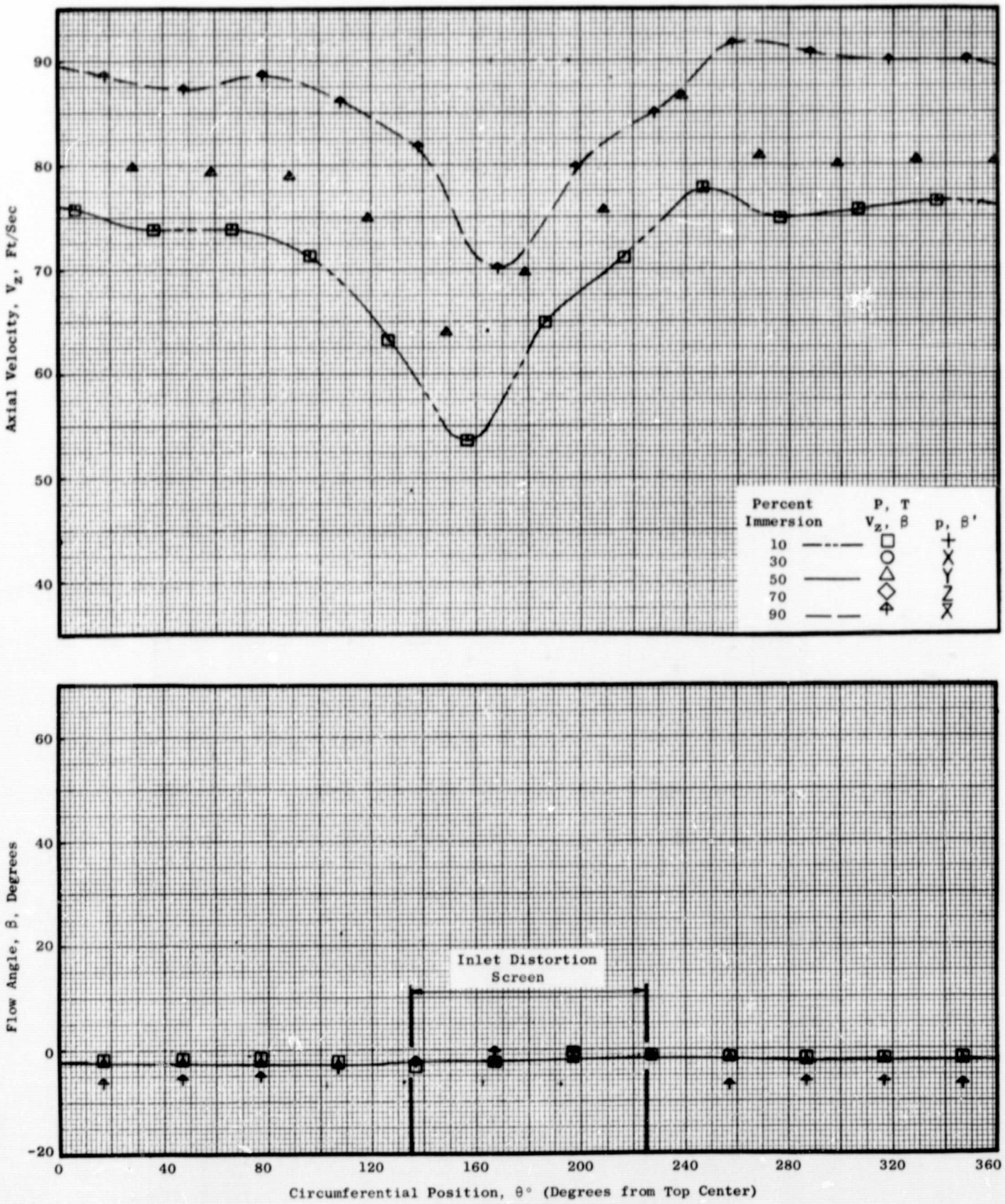

Figure 21(d). Circumferential Variation of Flow Conditions at 100 Percent Speed Maximum Flow with 0°/0° IGV/Stator Schedule at Plane 2.20 (Concluded).

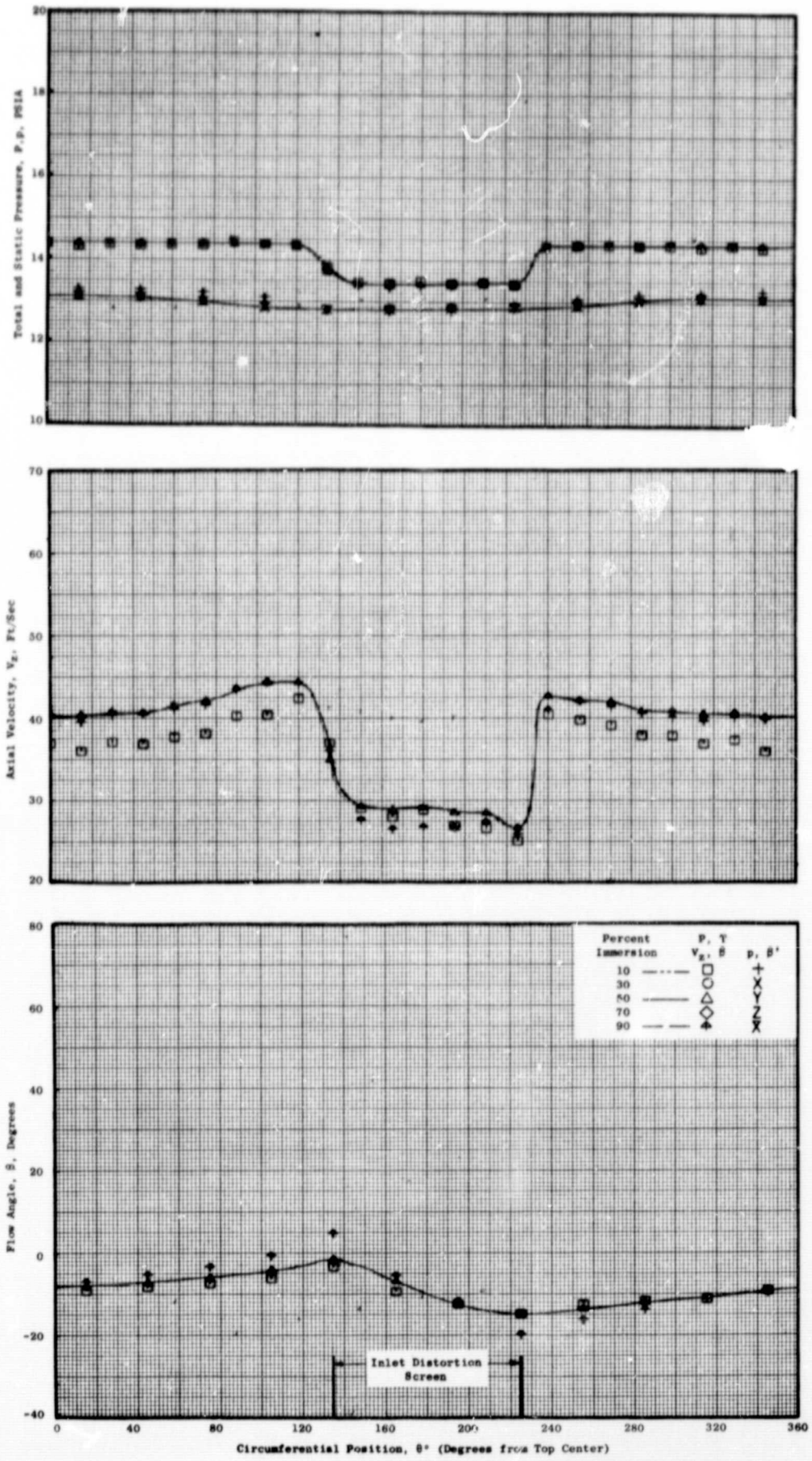

Figure 22 (a). Circumferential Distortion Profiles of Flow Conditions at 70 Percent Speed Intermediate Flow with 0°/0° IGV/Stator Schedule at Plane 0.18.

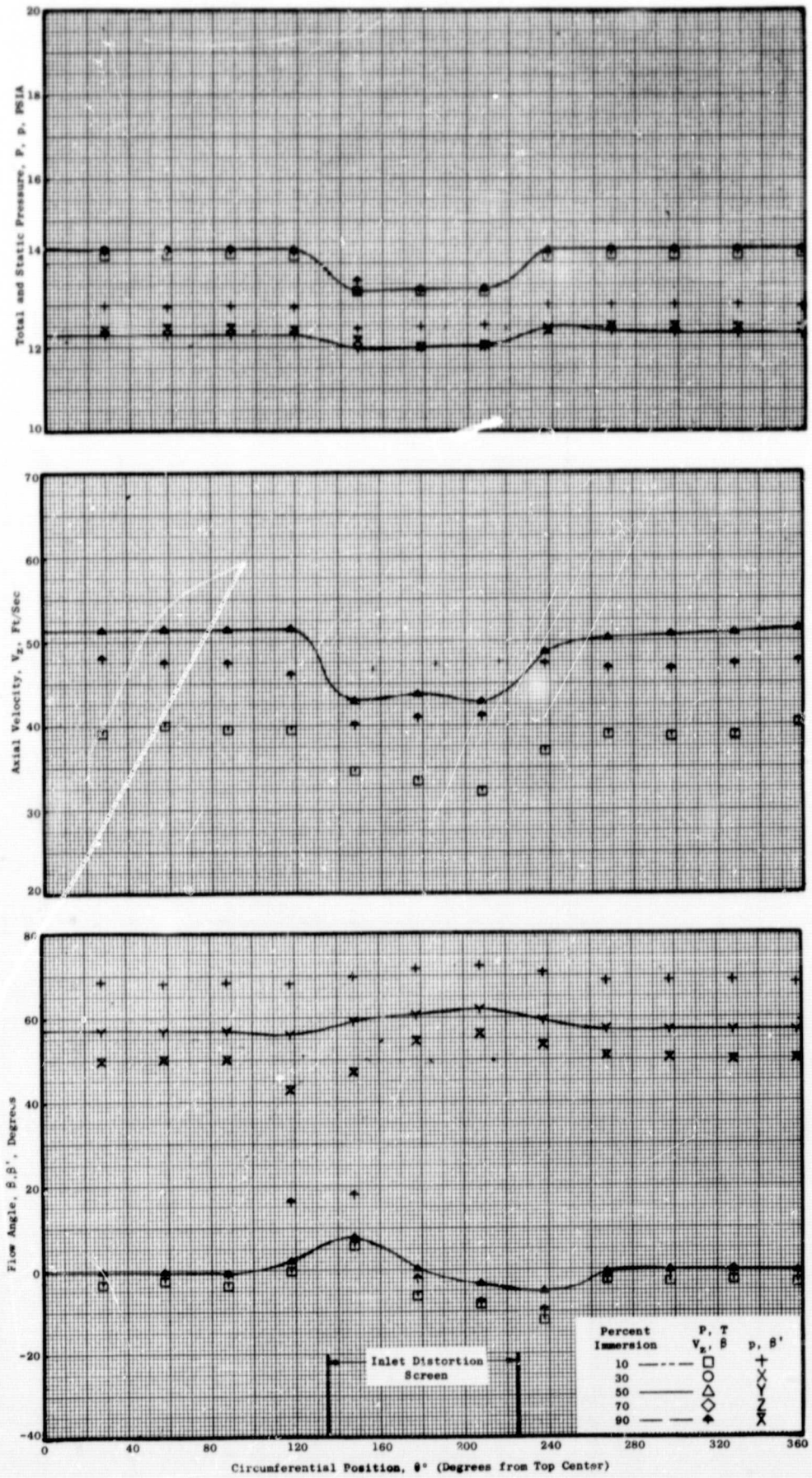

Figure 22 (b). Circumferential Distortion Profiles of Flow Conditions at 70 Percent Speed Intermediate Flow with 0°/0° IGV/Stator Schedule at Plane 0.95.

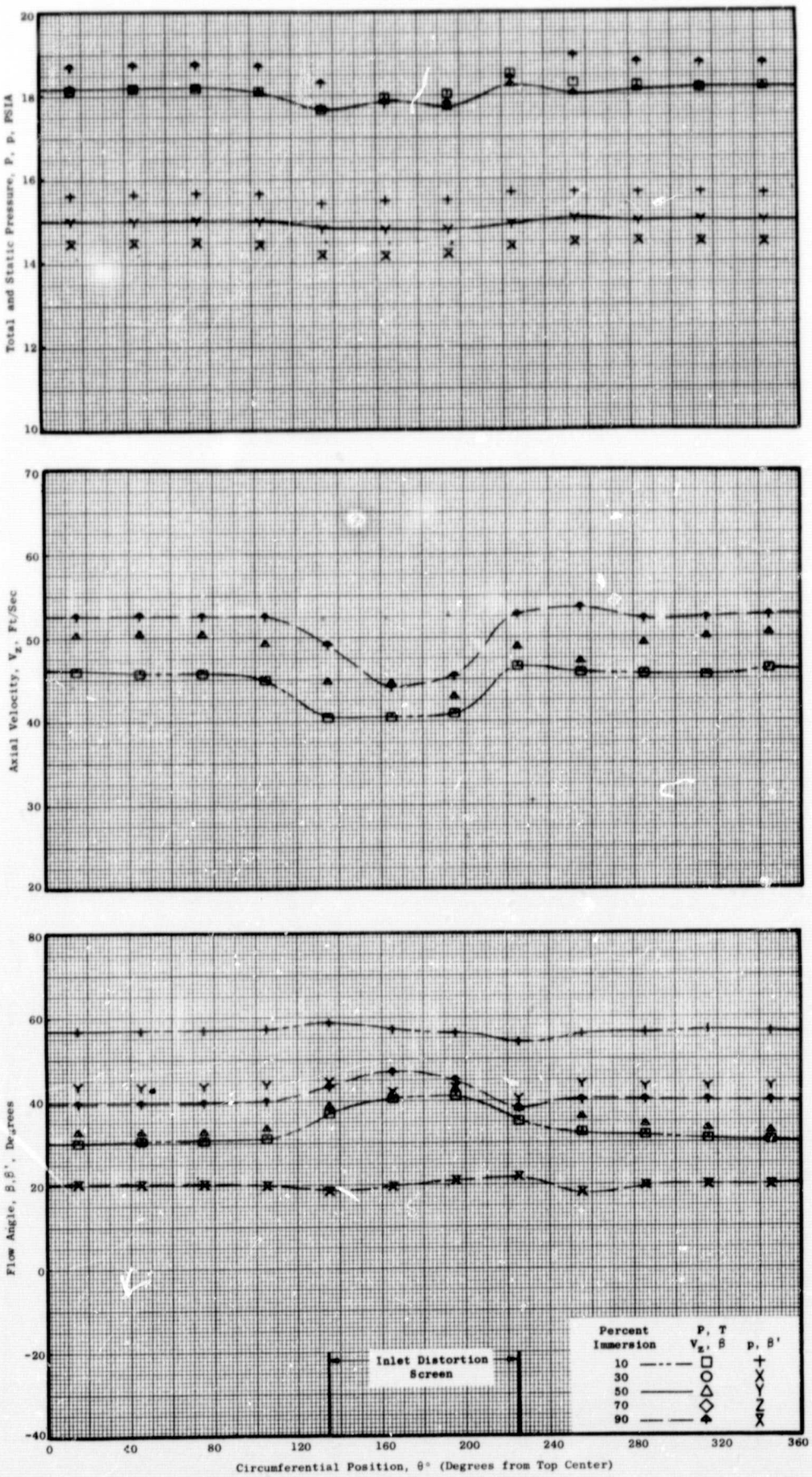

Figure 22 (c). Circumferential Distortion Profiles of Flow Conditions at 70 Percent Speed Intermediate Flow with 0°/0° IGV/Stator Schedule at Plane 1.51.

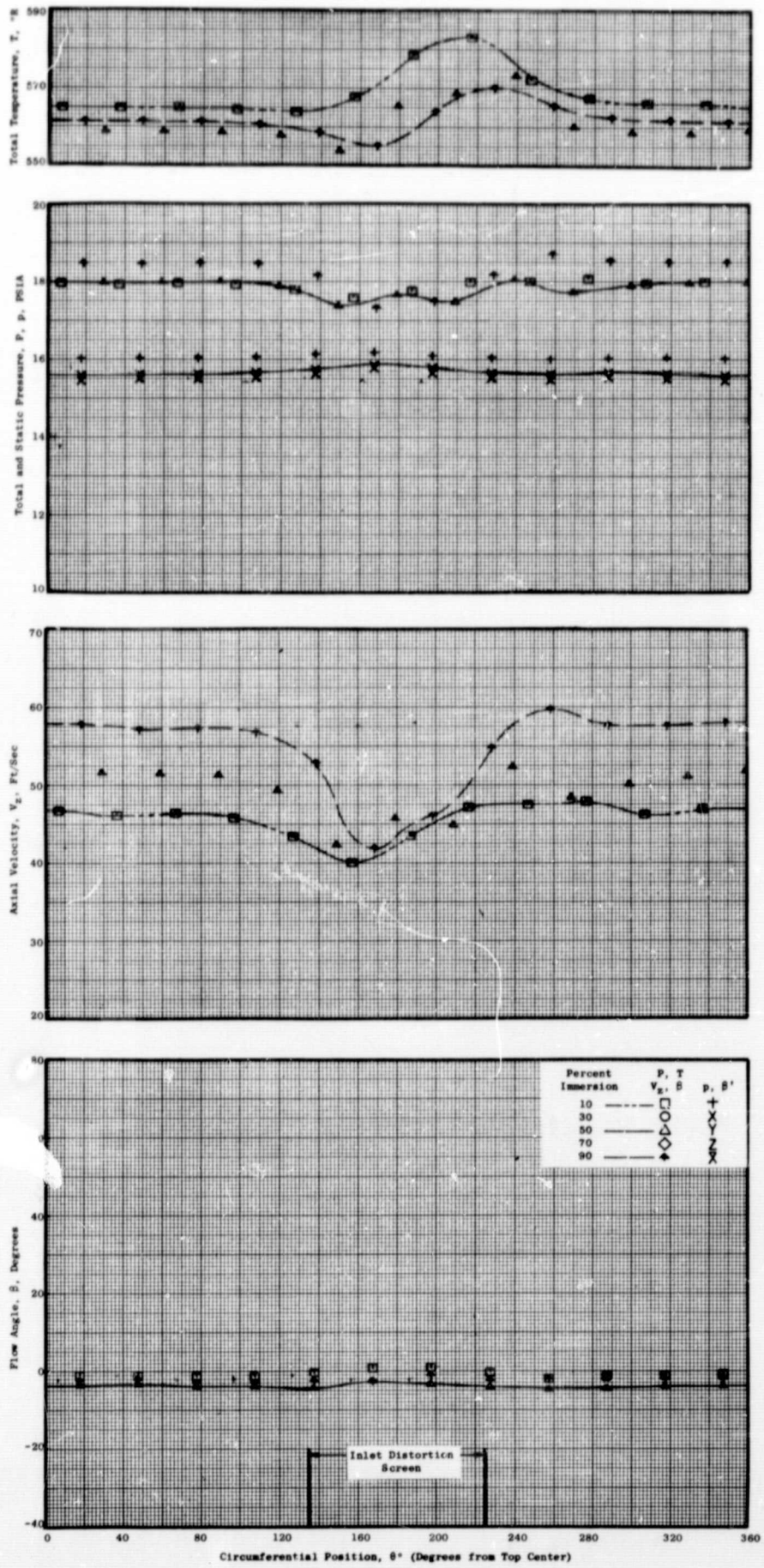

Figure 22 (d). Circumferential Distortion Profiles of Flow Conditions at 70 Percent Speed Intermediate Flow with 0°/0° IGV/Stator Schedule at Plane 2.20.

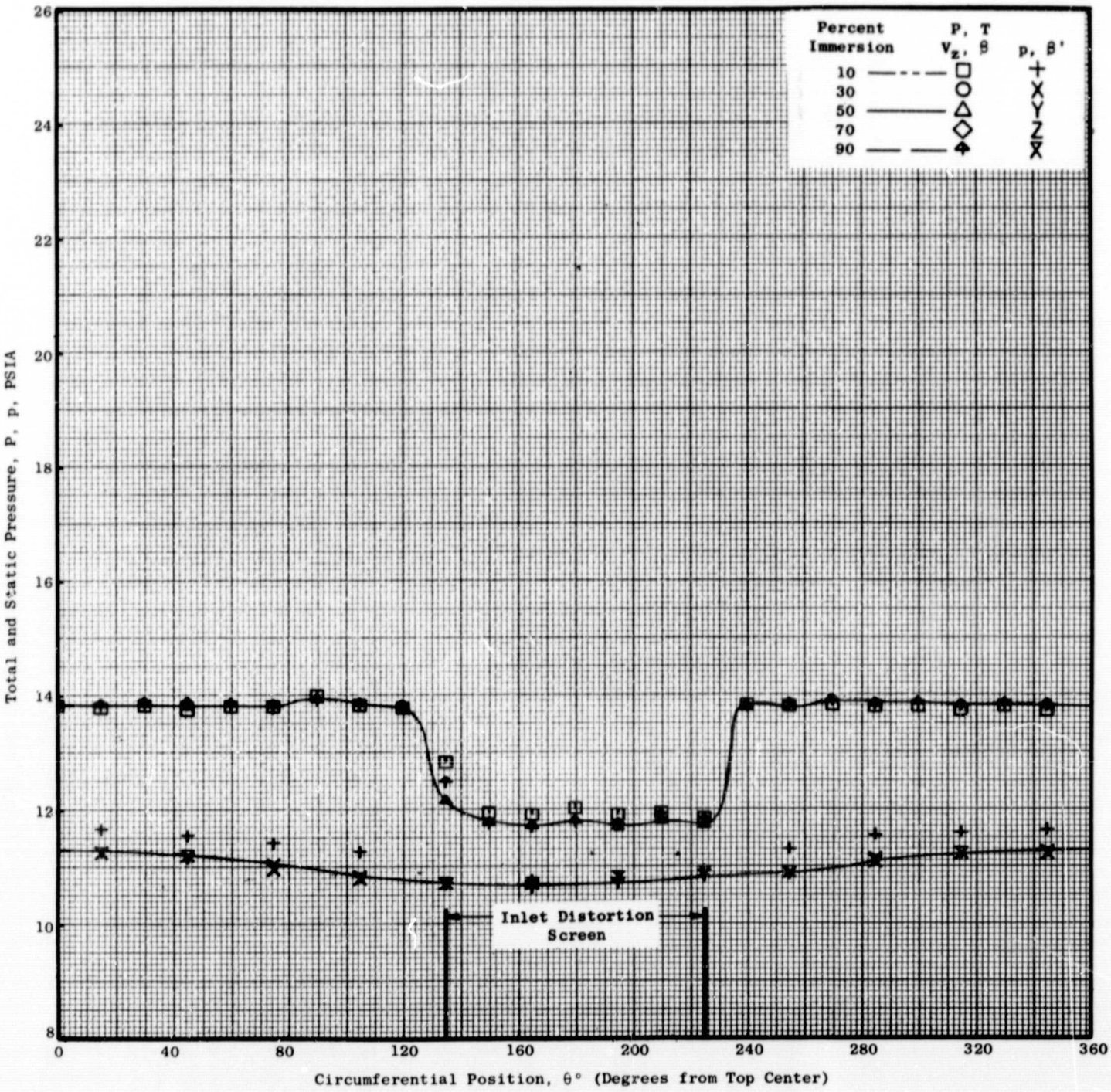

Figure 23(a). Circumferential Distortion Profiles of Flow Conditions at 100 Percent Speed Near Stall with 0°/0° IGV/Stator Schedule at Plane 0.18.

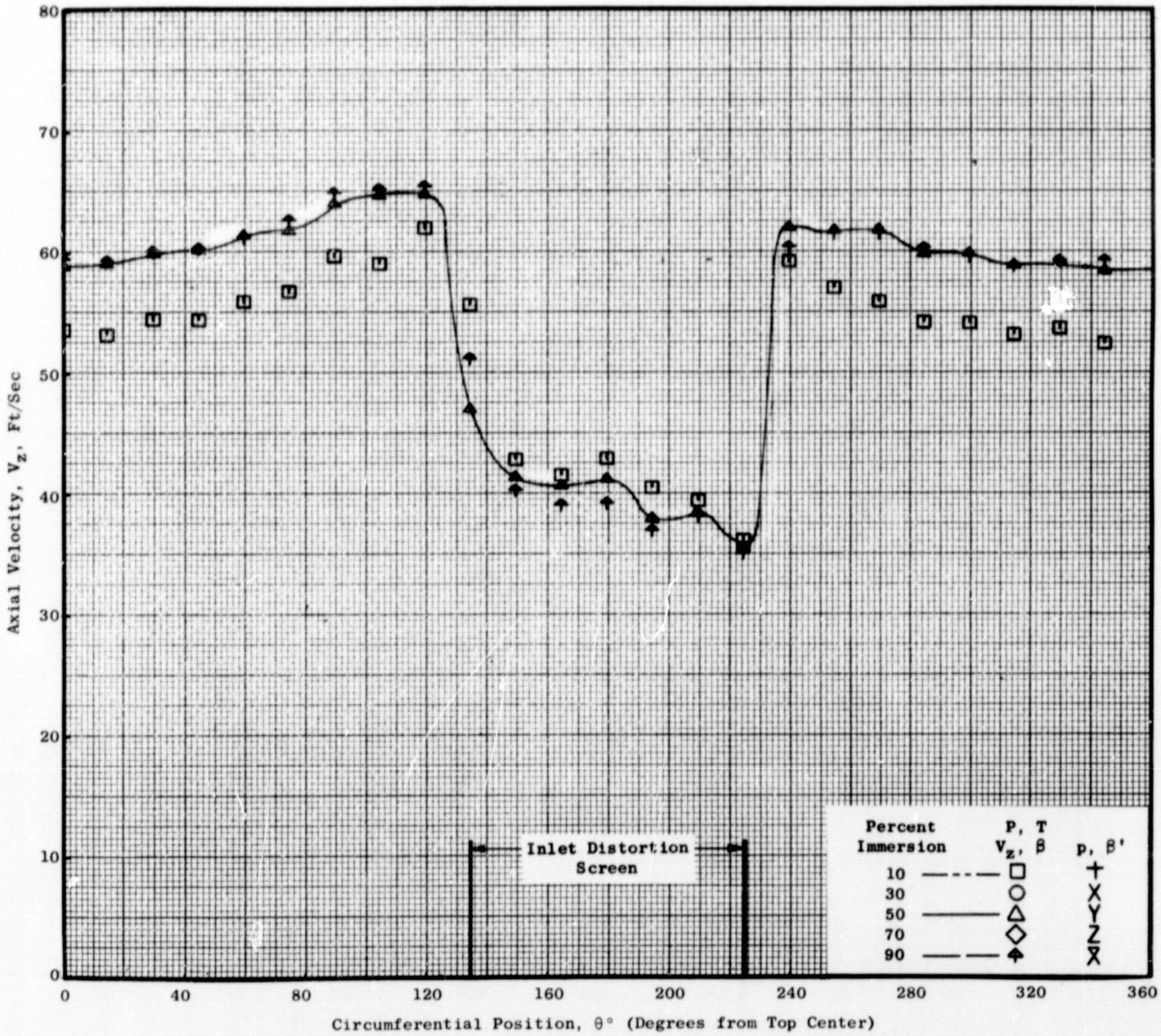

Figure 23(a). Circumferential Distortion Profiles of Flow Conditions at 100 Percent Speed Near Stall with 0°/0° IGV/Stator Schedule at Plane 0.18 (Continued).

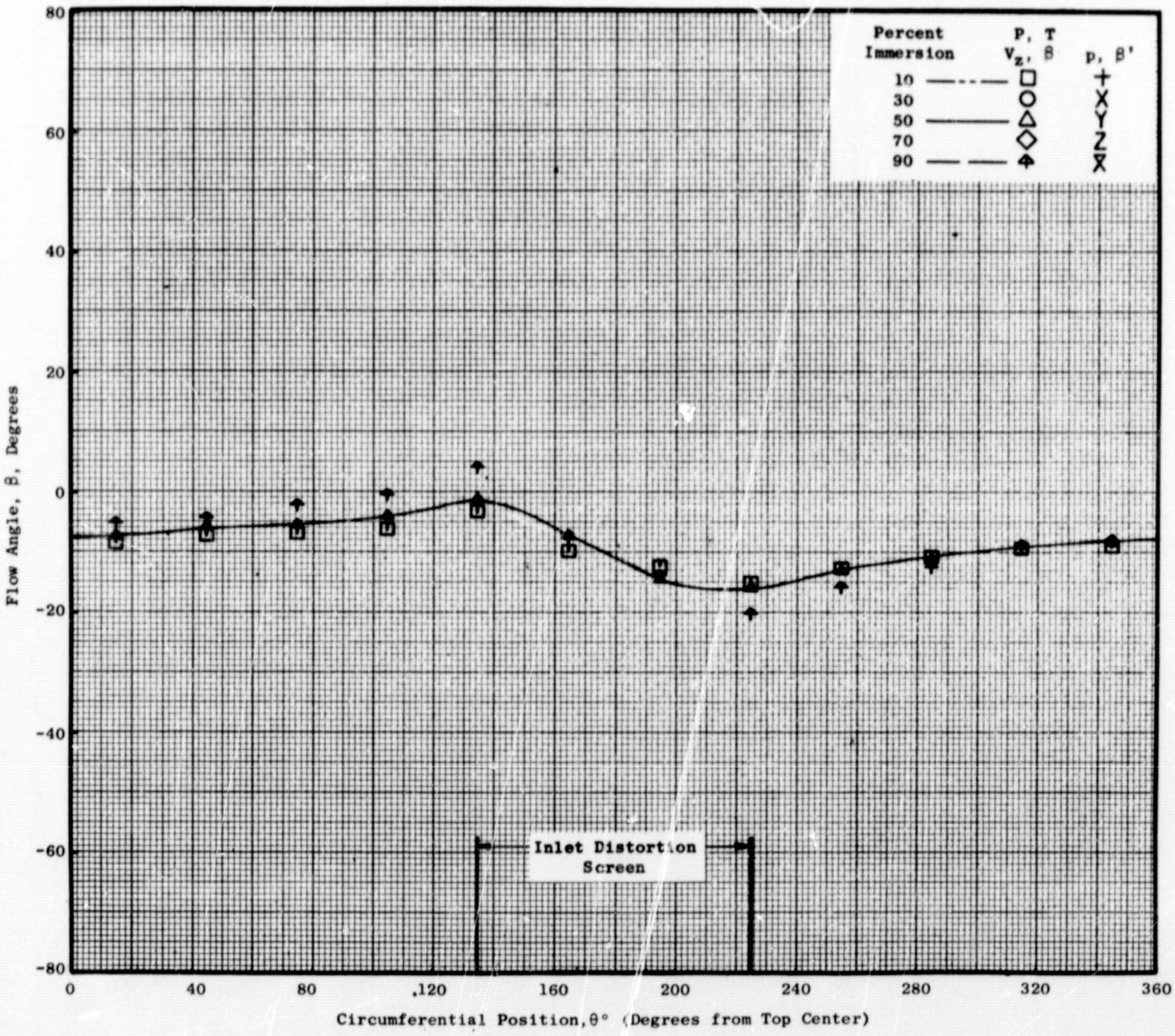

Figure 23(a). Circumferential Distortion Profiles of Flow Conditions at 100 Percent Speed Near Stall with 0°/0° IGV/Stator Schedule at Plane 0.18 (Concluded).

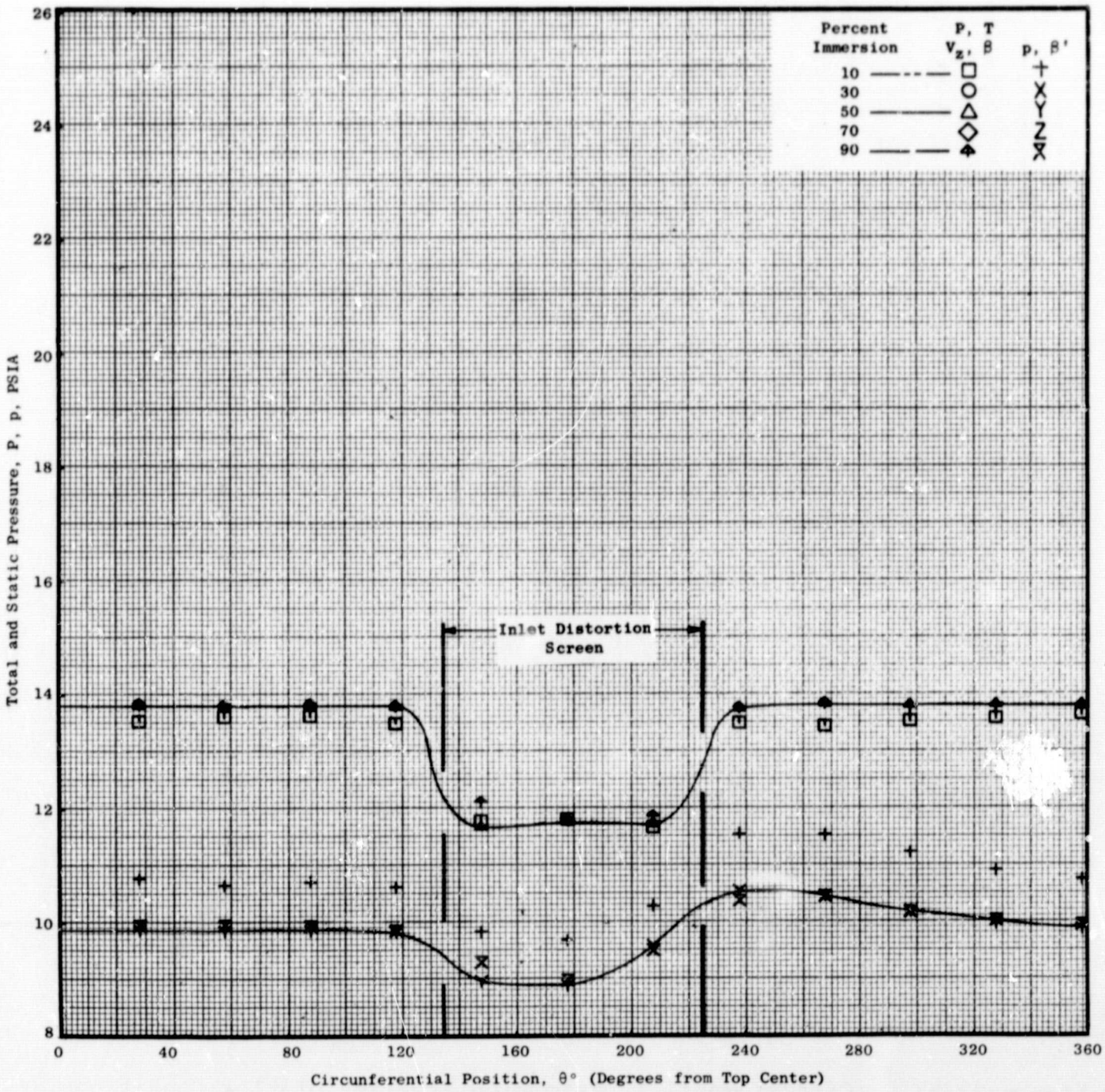

Figure 23(b). Circumferential Distortion Profiles of Flow Conditions at 100 Percent Speed Near Stall with 0°/0° IGV/Stator Schedule at Plane 0.95.

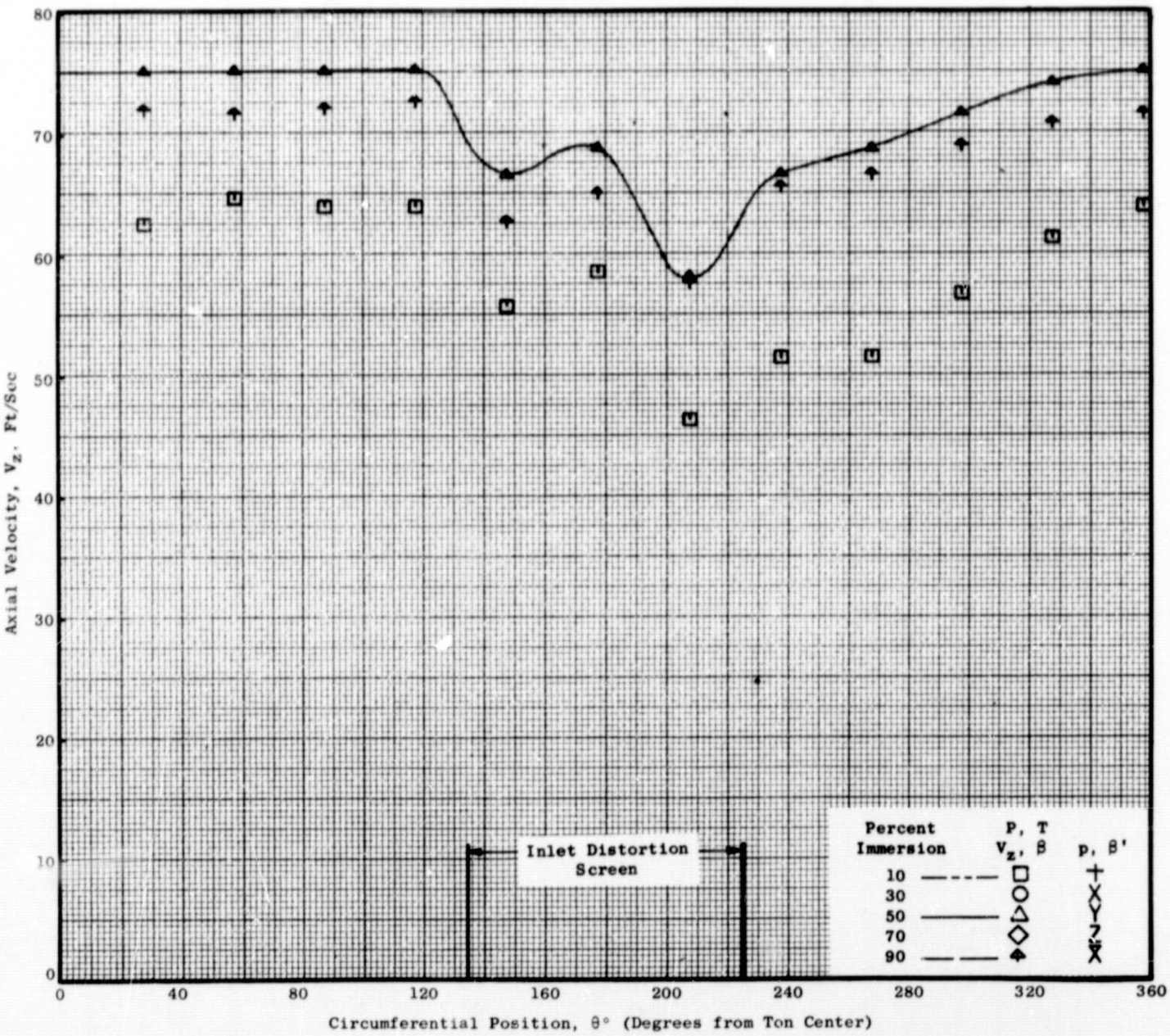

Figure 23(b). Circumferential Distortion Profiles of Flow Conditions at 100 Percent Speed Near Stall with 0°/0° IGV/Stator Schedule at Plane 0.95 (Continued).

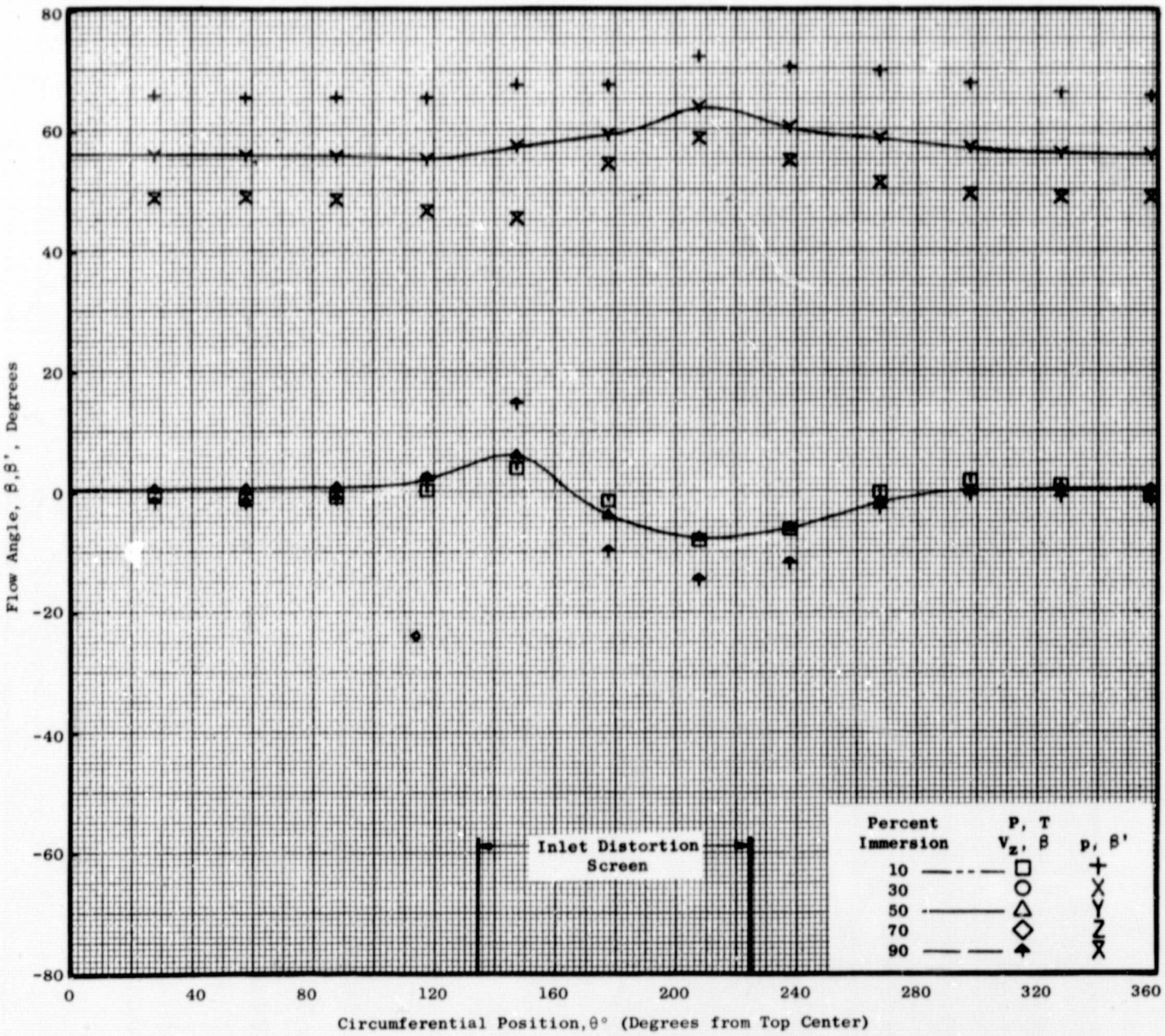

Figure 23(b). Circumferential Distortion Profiles of Flow Conditions at 100 Percent Speed Near Stall with 0°/0° IGV/Stator Schedule at Plane 0.95 (Concluded).

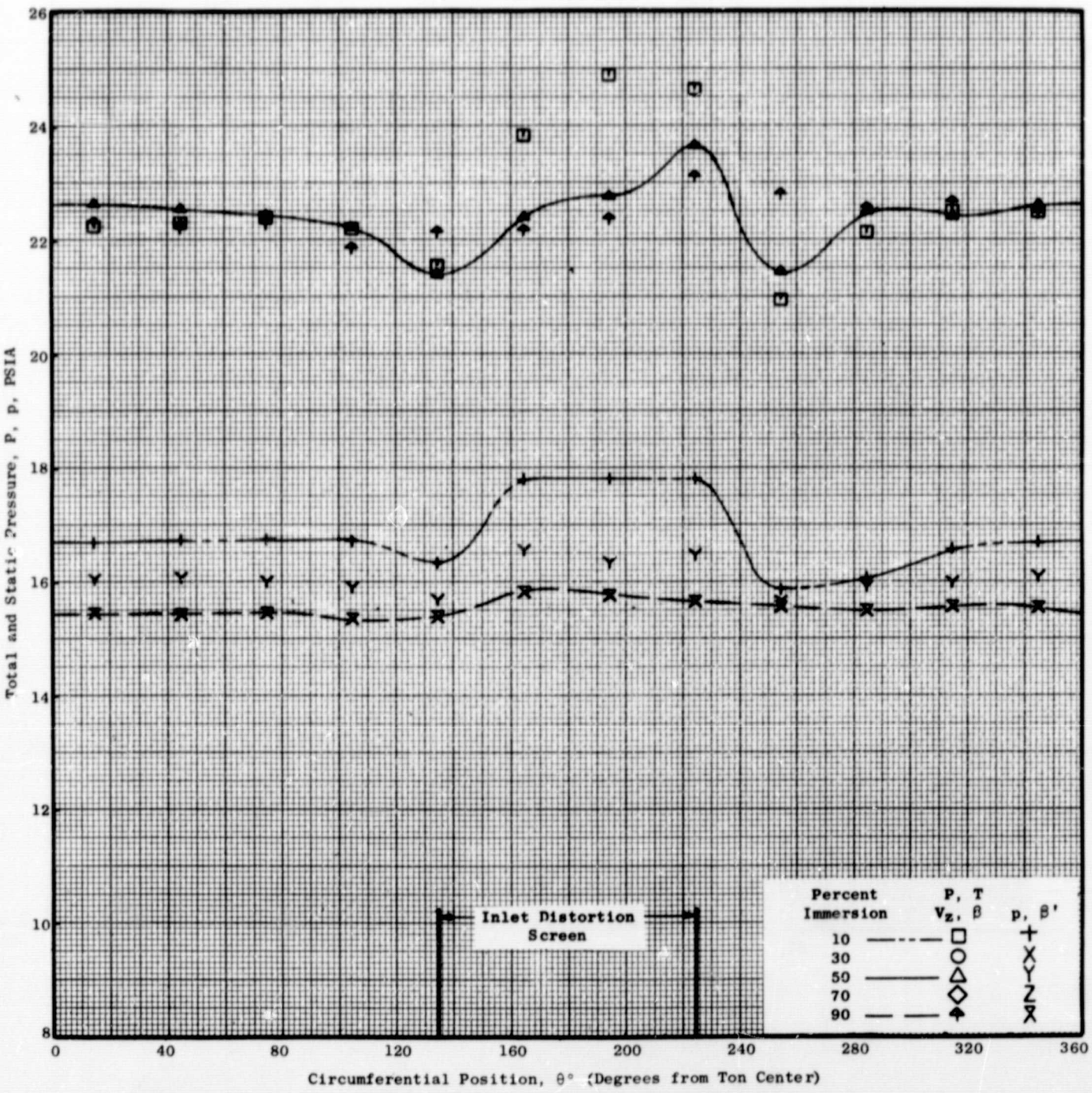

Figure 23(c). Circumferential Distortion Profiles of Flow Conditions at 100 Percent Speed Near Stall with 0°/0° IGV/Stator Schedule at Plane 1.51.

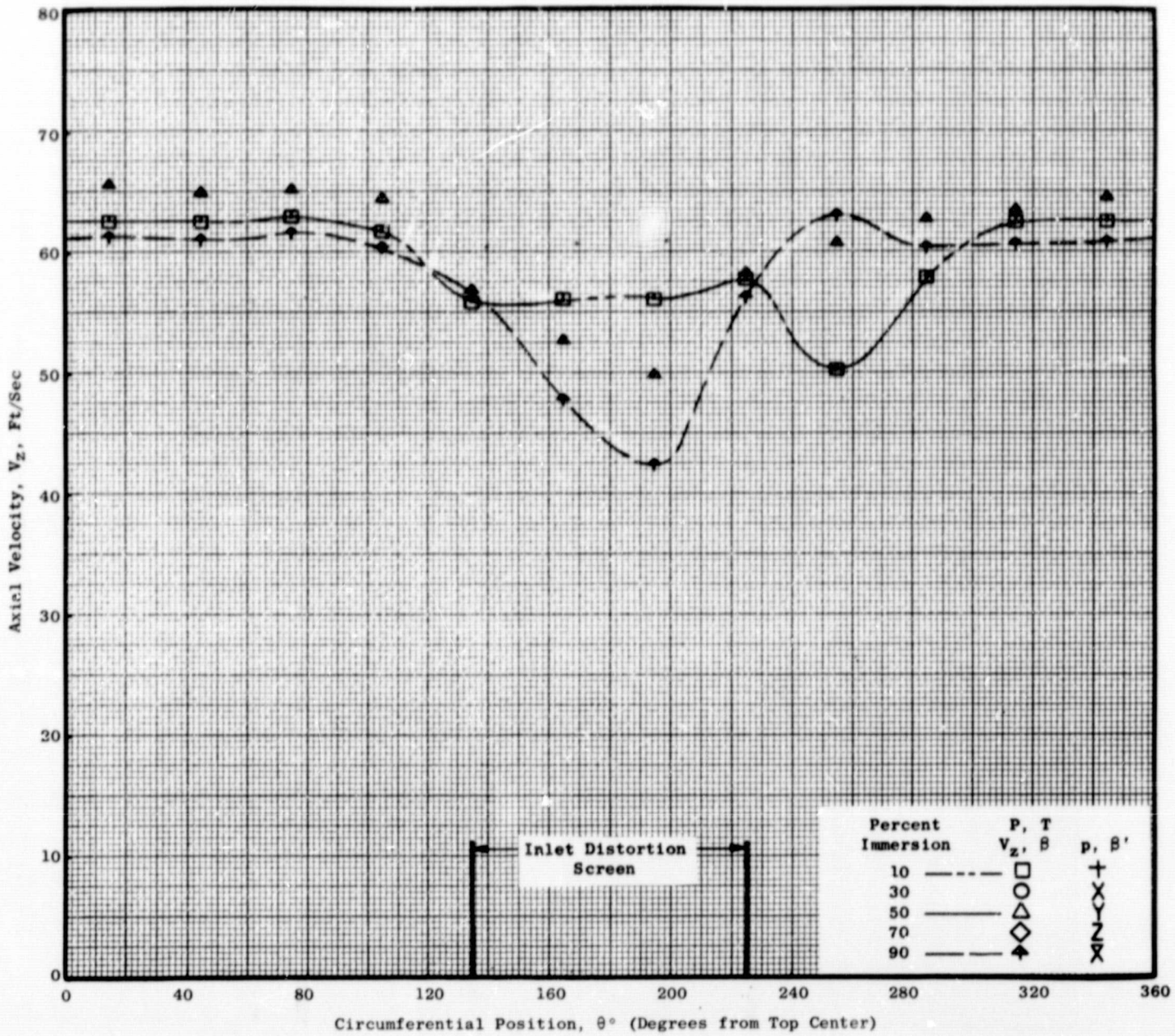

Figure 23(c). Circumferential Distortion Profiles of Flow Conditions at 100 Percent Speed Near Stall with 0°/0° IGV/Stator Schedule at Plane 1.51 (Continued).

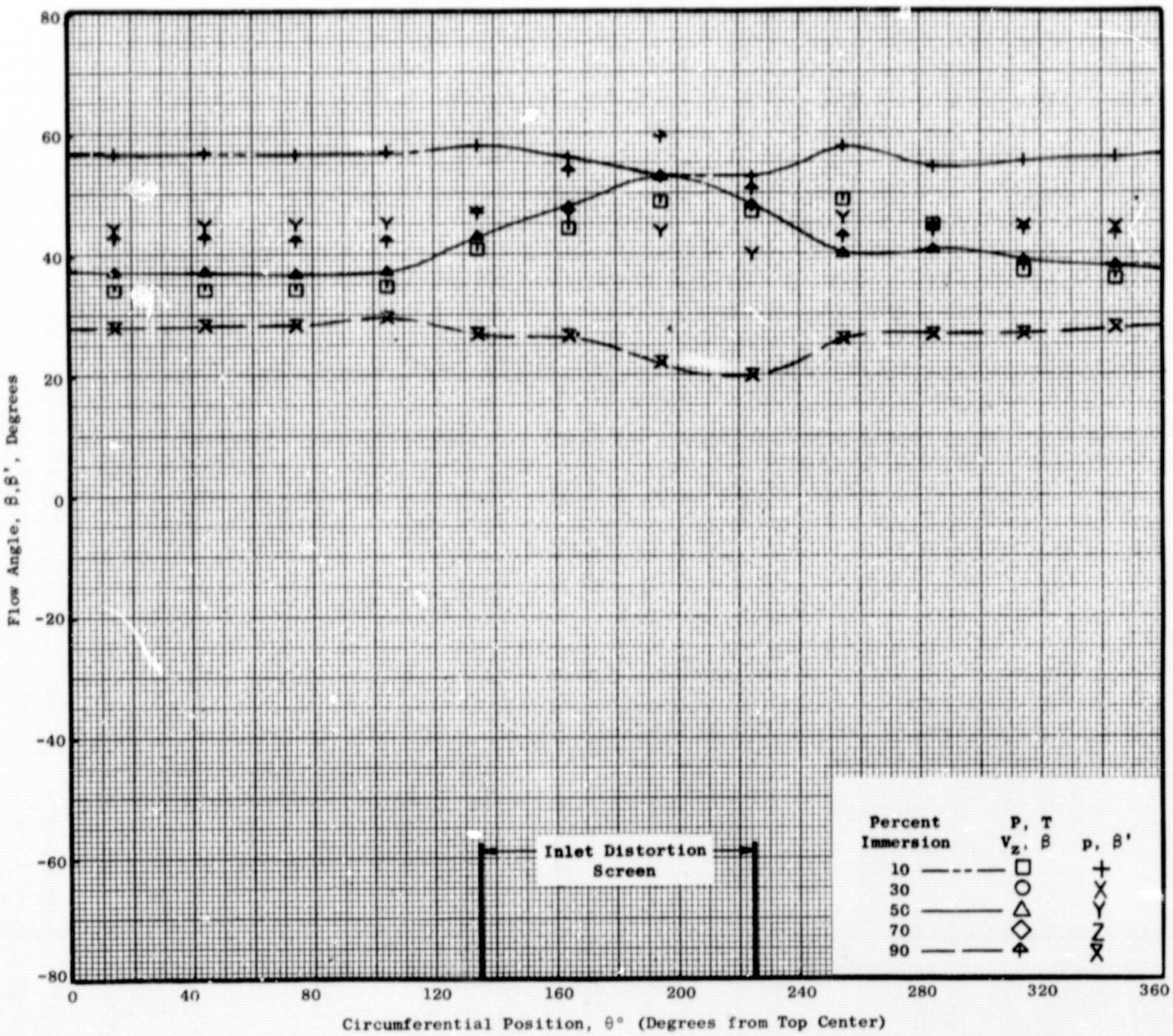

Figure 23(c). Circumferential Distortion Profiles of Flow Conditions at 100 Percent Speed Near Stall with 0°/0° IGV/Stator Schedule at Plane 1.51 (Concluded).

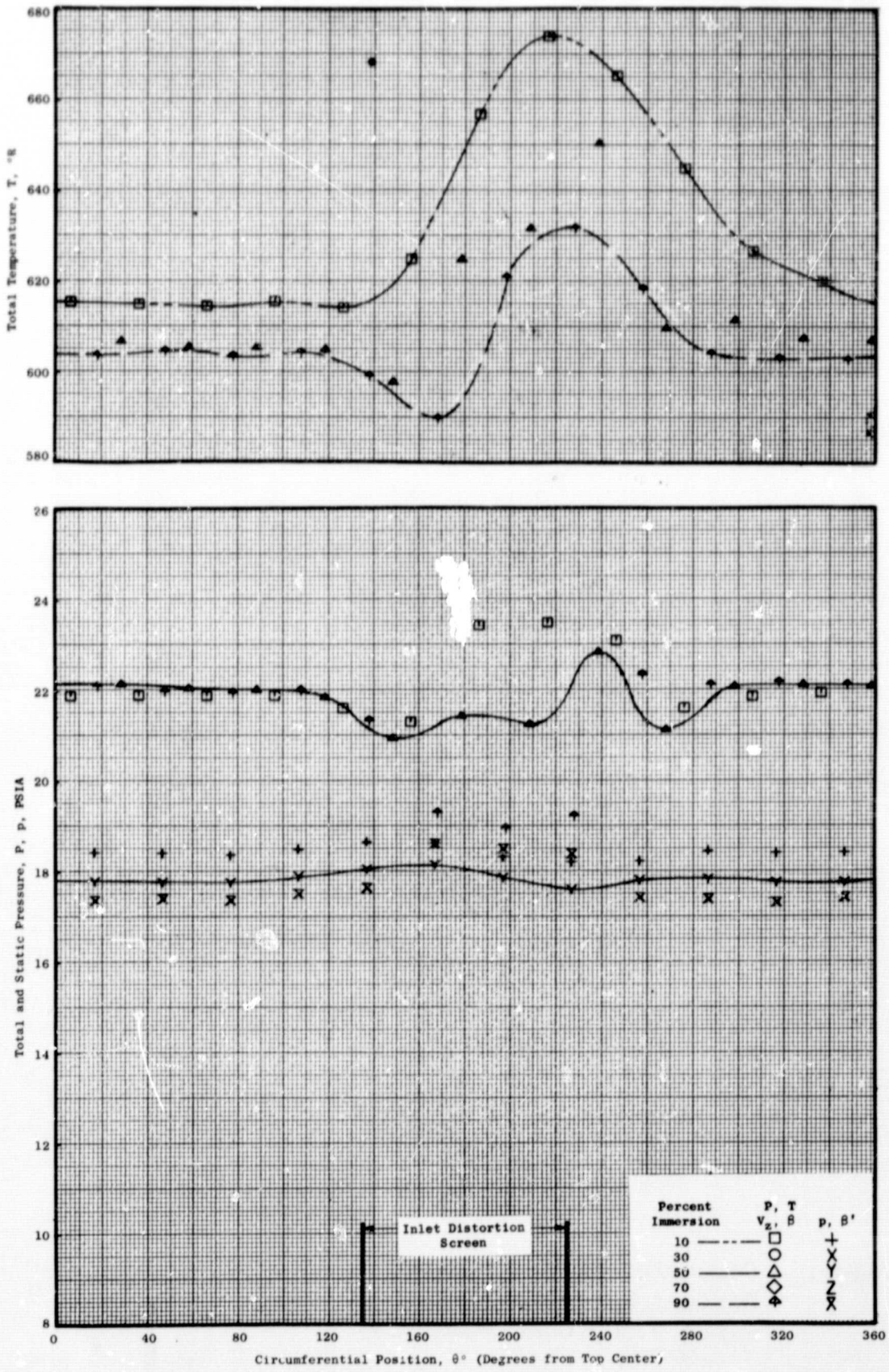

Figure 23 (d). Circumferential Distortion Profiles of Flow Conditions at 100 Percent Speed Near Stall with 0°/0° IGV/Stator Schedule at Plane 2.20.

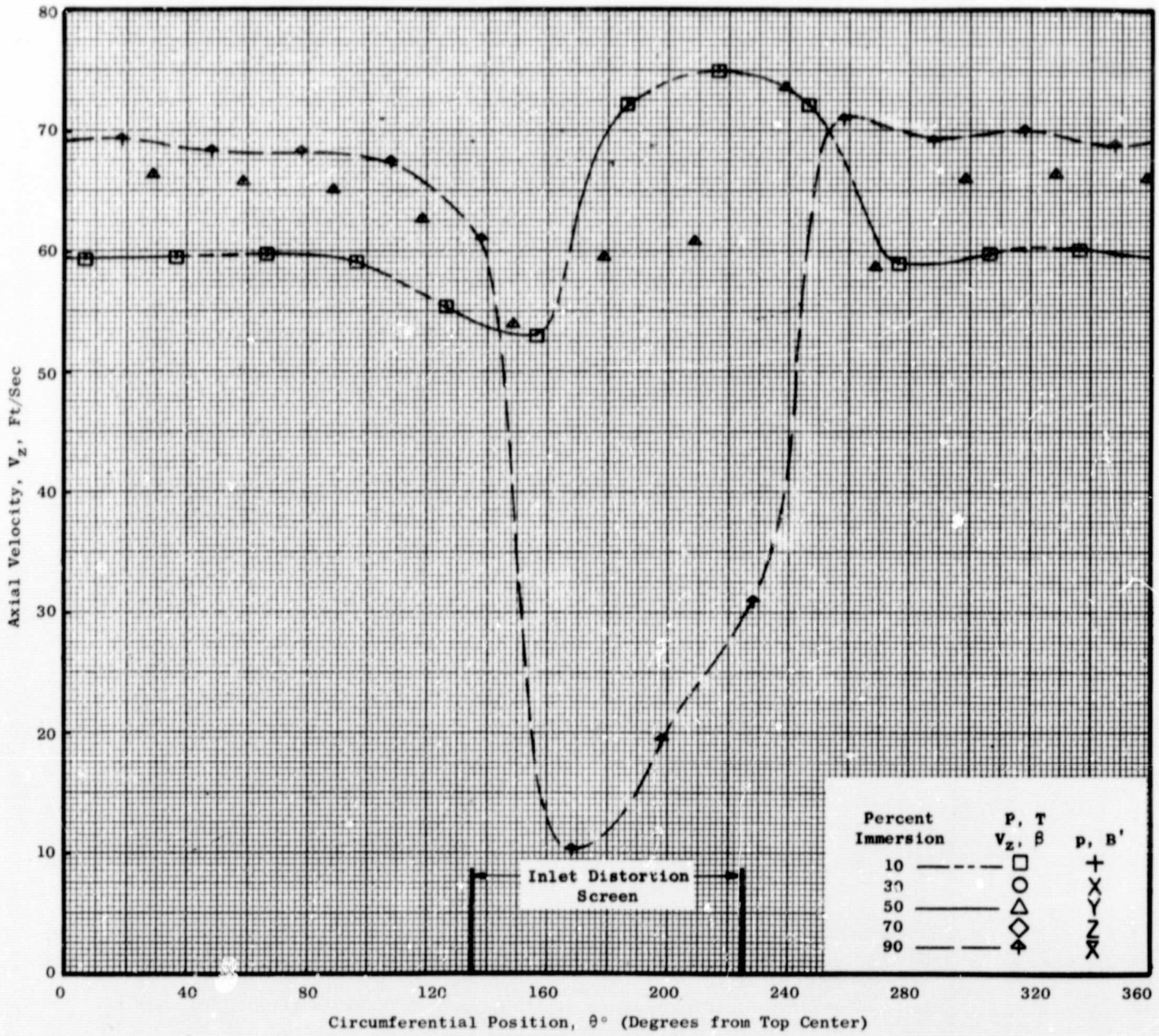

Figure 23(d). Circumferential Distortion Profiles of Flow Conditions at 100 Percent Speed Near Stall with 0°/0° IGV/Stator Schedule at Plane 2.20 (Continued).

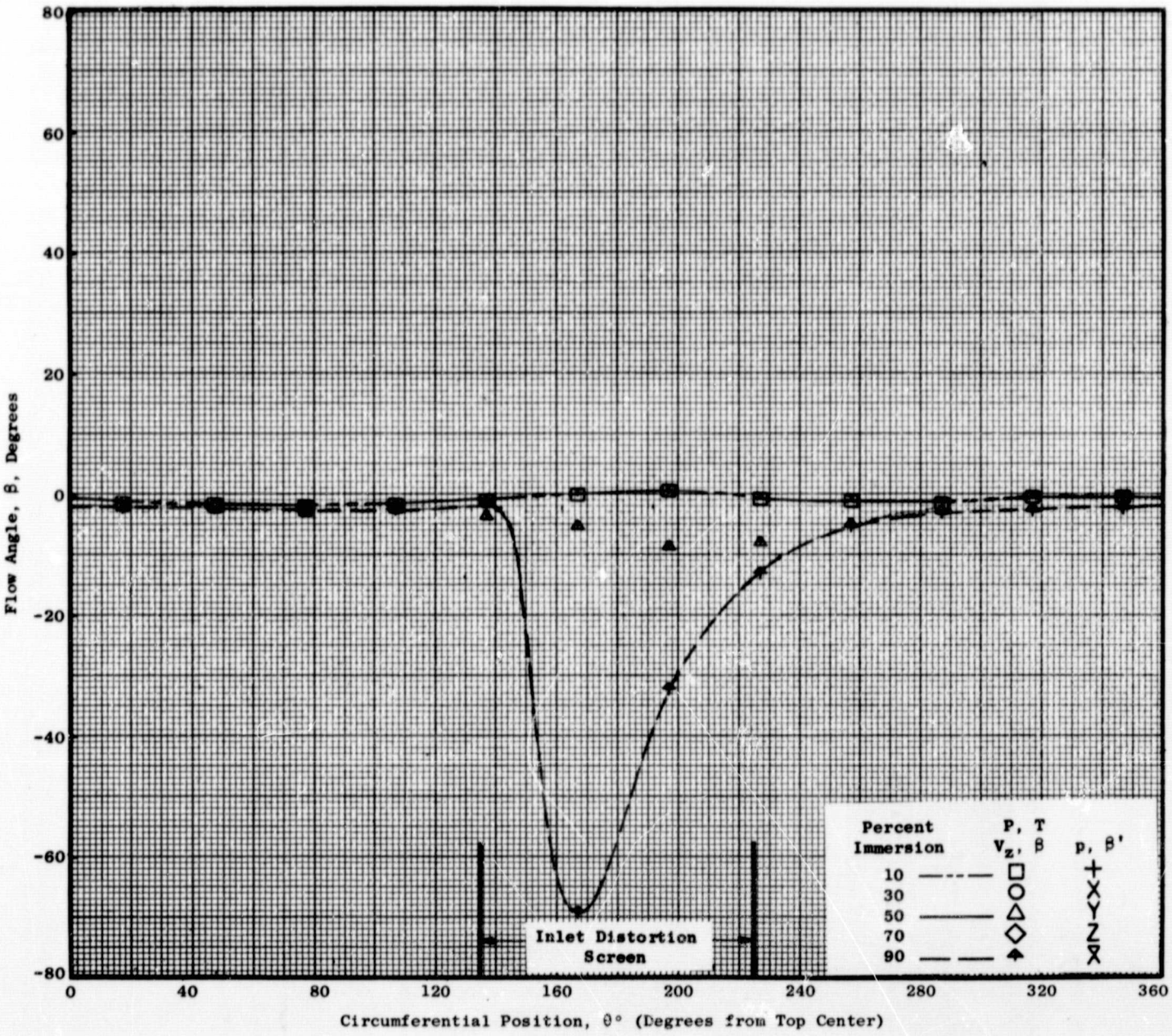

Figure 23(d). Circumferential Distortion Profiles of Flow Conditions at 100 Percent Speed Near Stall with 0°/0° IGV/Stator Schedule at Plane 2.20 (Concluded).

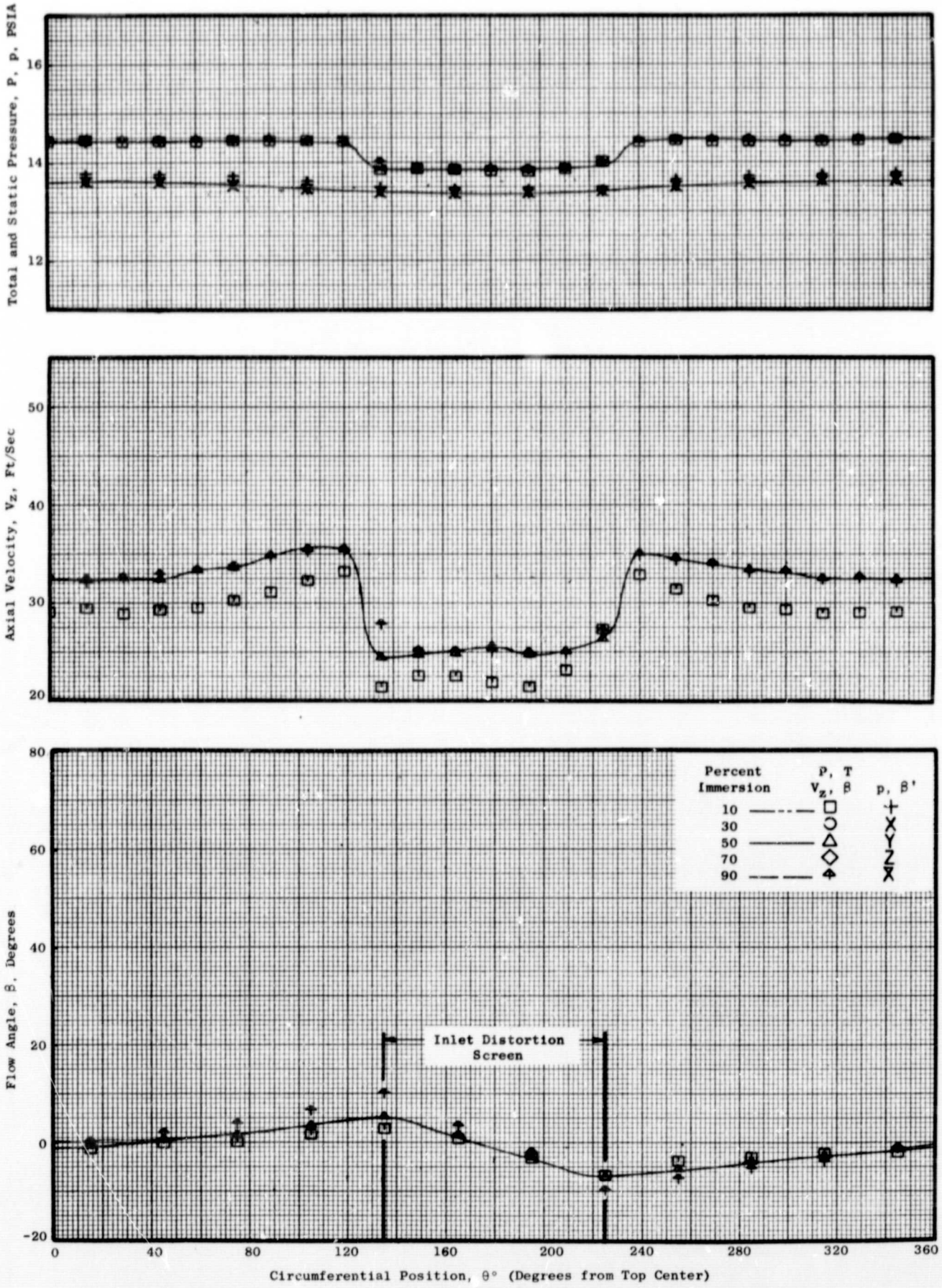

Figure 24(a). Circumferential Distortion Profiles of Flow Conditions at 70 Percent Speed Maximum Flow with 40°/8° IGV/Stator Schedule at Plane 0.18.

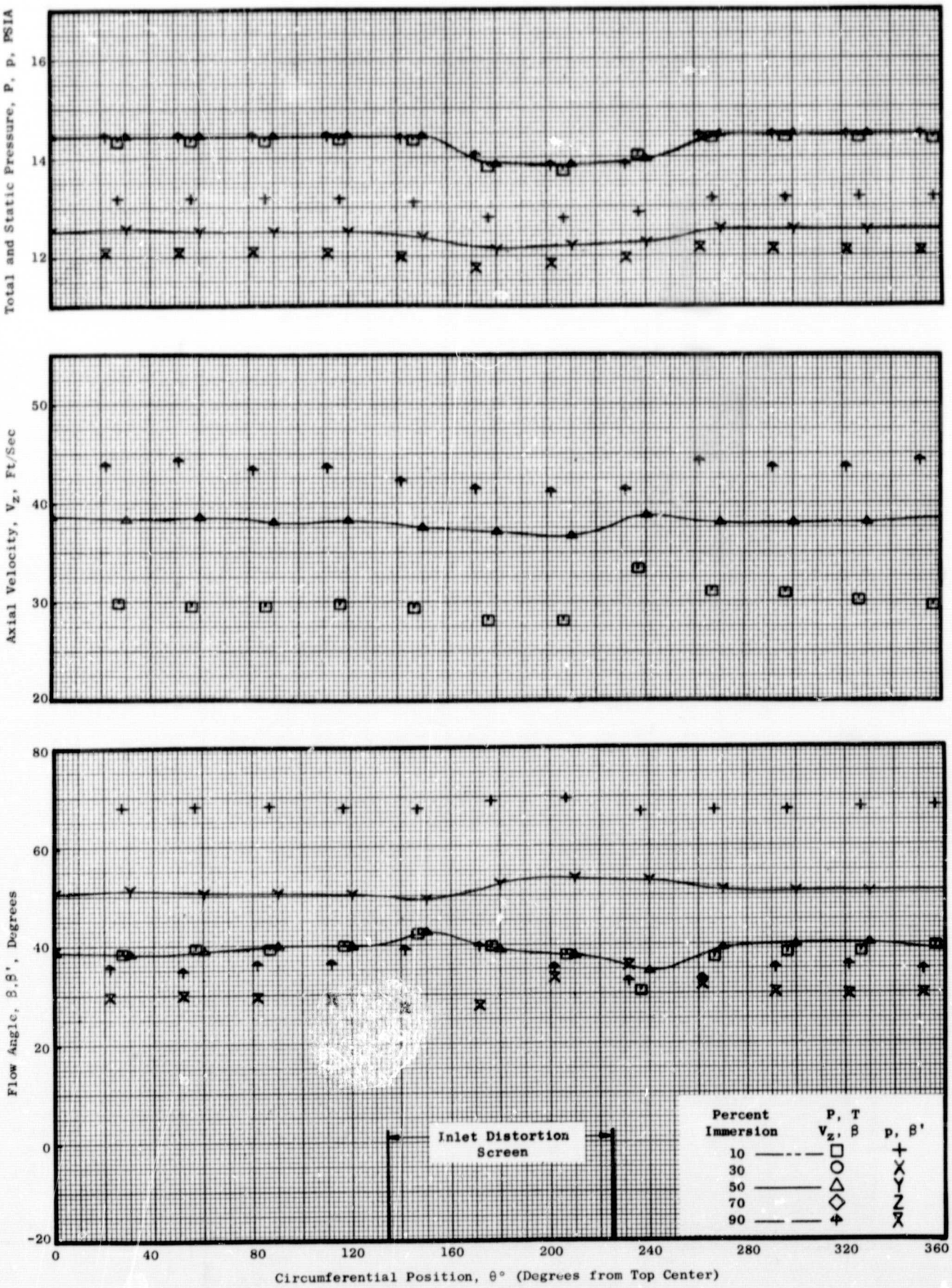

Figure 24(b). Circumferential Distortion Profiles of Flow Conditions at 70 Percent Speed Maximum Flow with 40°/8° IGV/Stator Schedule at Plane 0.95.

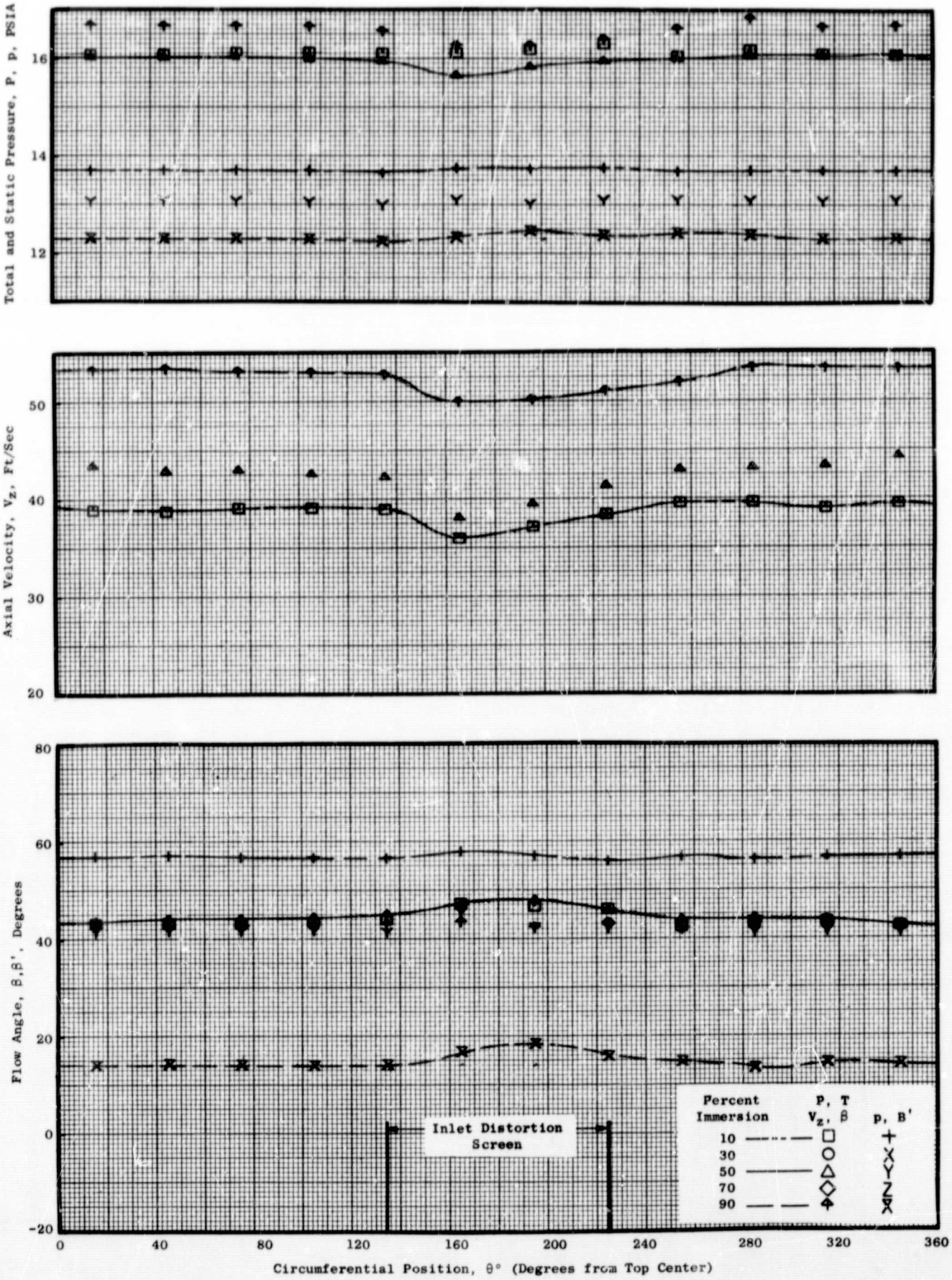

Figure 24(c). Circumferential Distortion Profiles of Flow Conditions at 70 Percent Speed Maximum Flow with 40°/8° IGV/Stator Schedule at Plane 1.51.

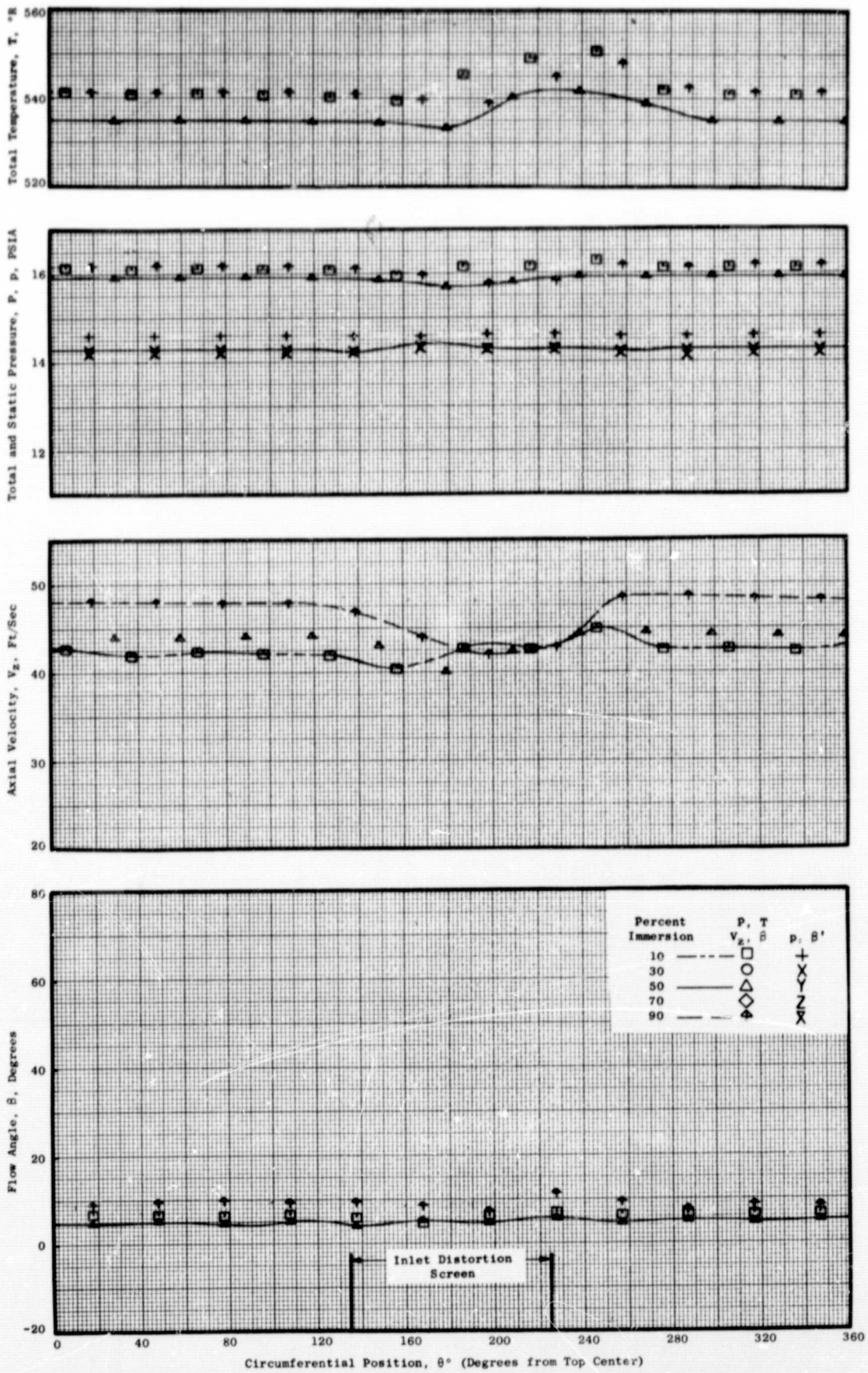

Figure 24 (d). Circumferential Distortion Profiles of Flow Conditions at 70 Percent Speed Maximum Flow with 40°/8° IGV/Stator Schedule at Plane 2.20.

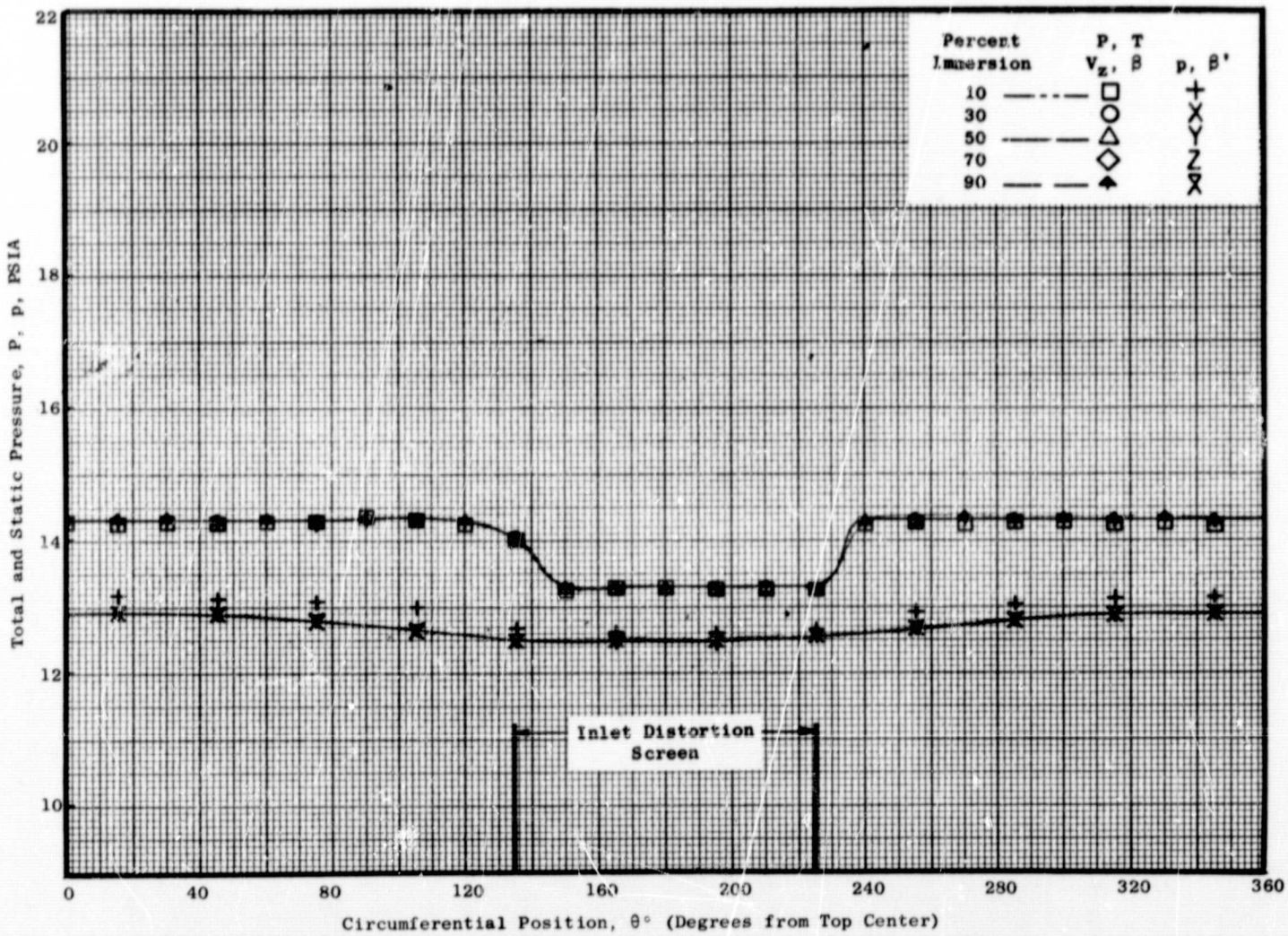

Figure 25(a). Circumferential Distortion Profiles of Flow Conditions at 100 Percent Speed Intermediate Flow with 40°/8° IGV/Stator Schedule at Plane 0.18.

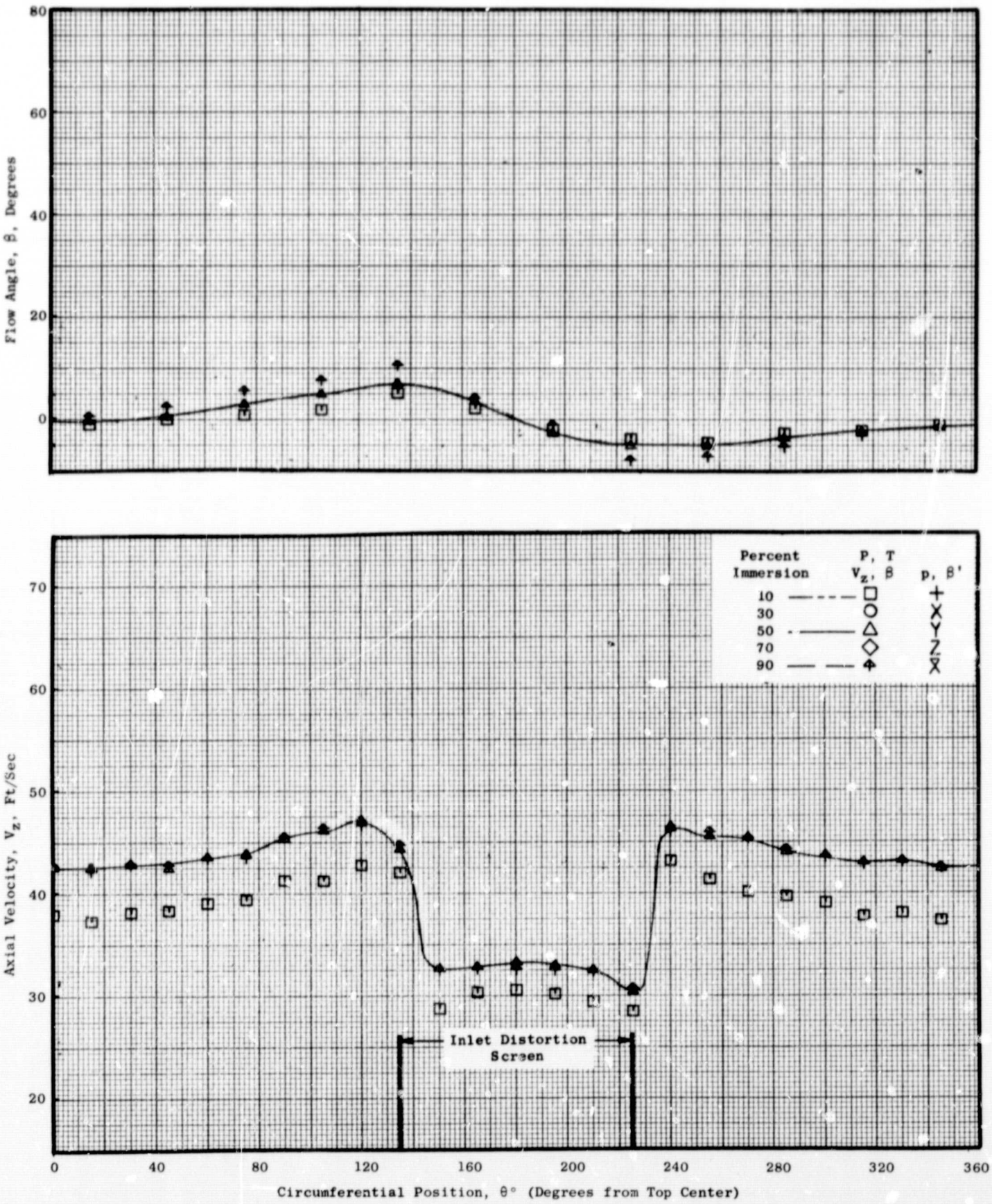

Figure 25(a). Circumferential Distortion Profiles of Flow Conditions at 100 Percent Speed Intermediate Flow with 40°/8° IGV/Stator Schedule at Plane 0.18 (Concluded).

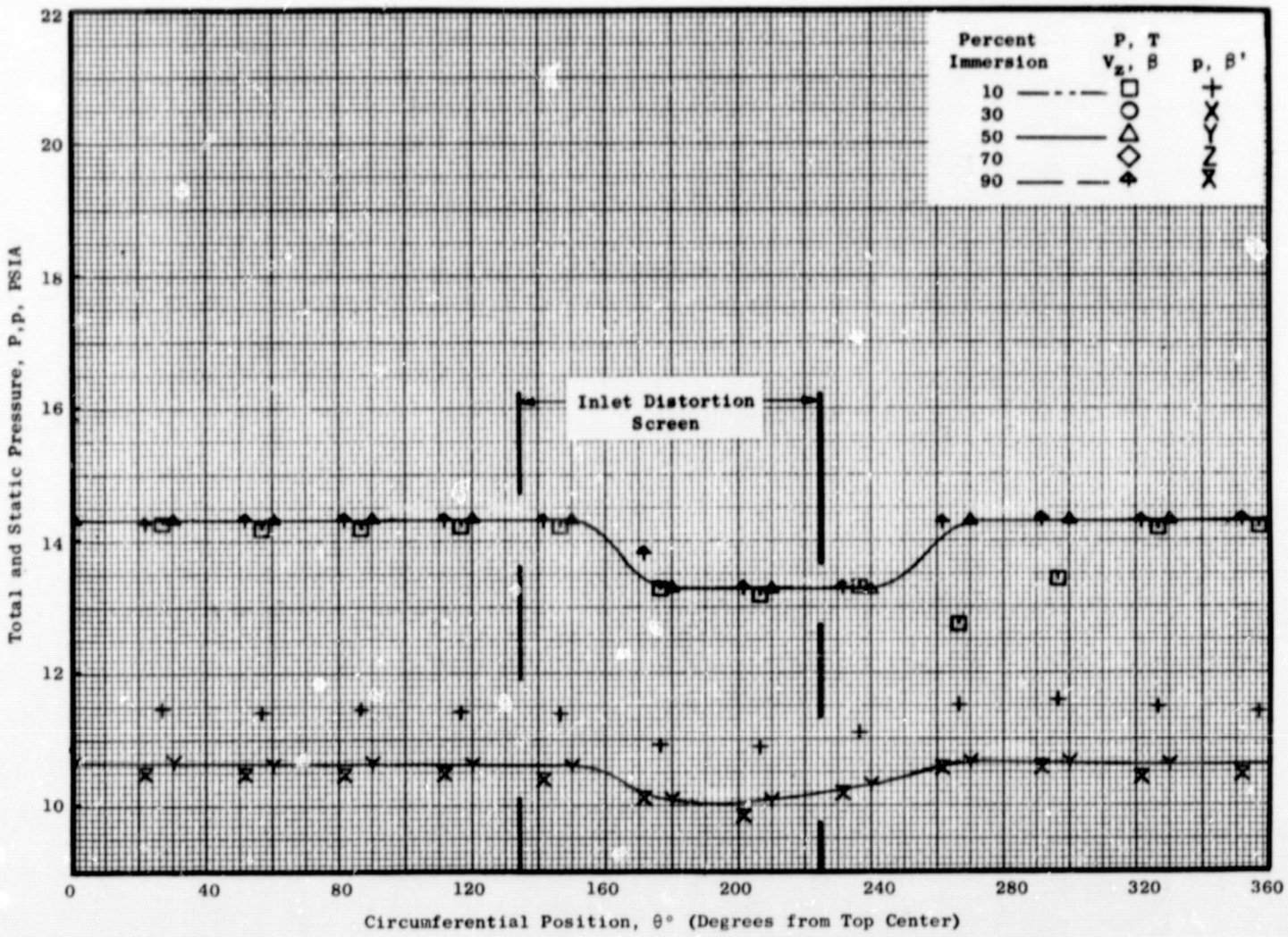

Figure 25(b). Circumferential Distortion Profiles of Flow Conditions at 100 Percent Speed Intermediate Flow with 40°/8° IGV/Stator Schedule at Plane 0.95.

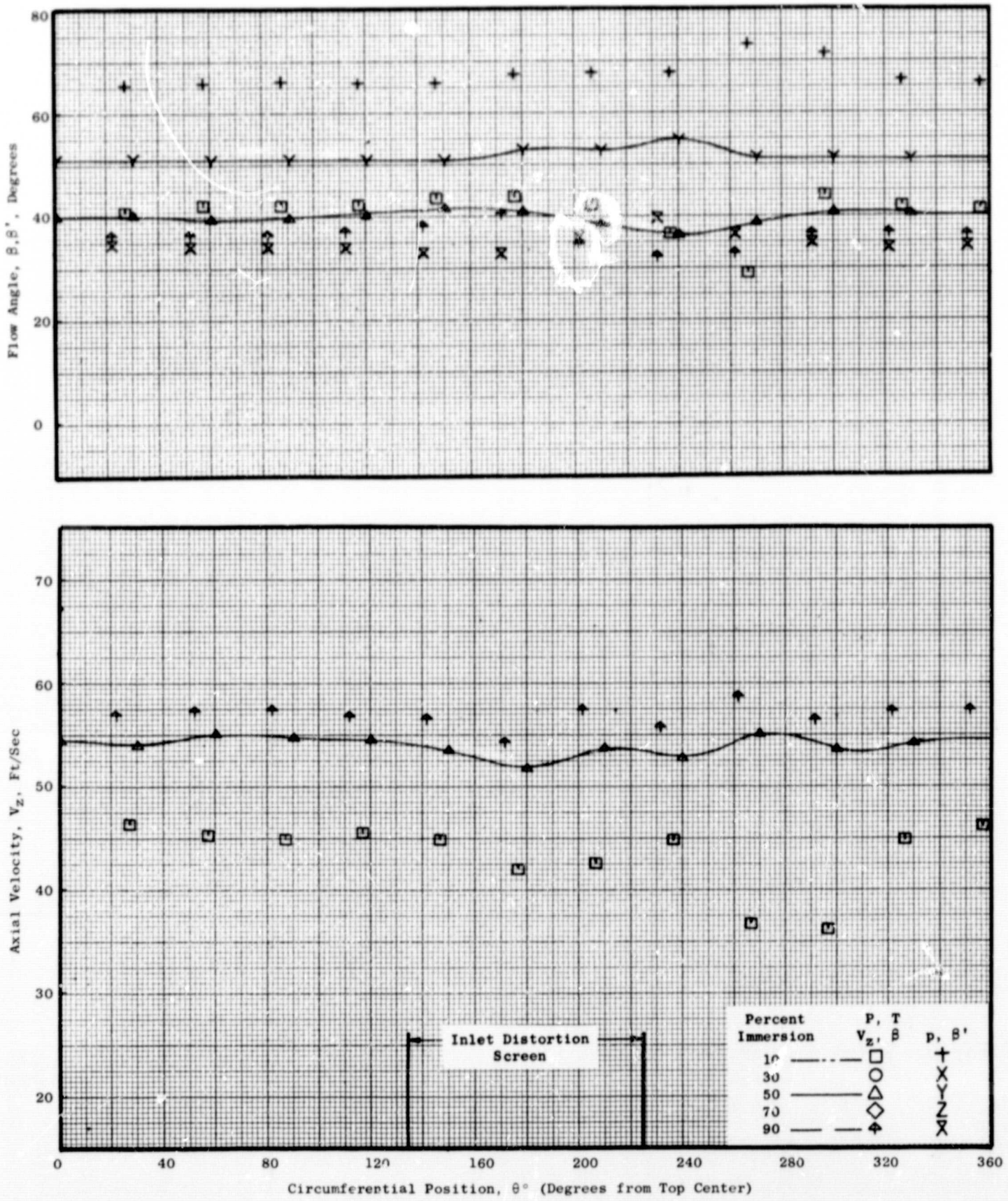

Figure 25(b). Circumferential Distortion Profiles of Flow Conditions at 100 Percent Speed Intermediate Flow with 40°/8° IGV/Stator Schedule at Plane 0.95 (Concluded).

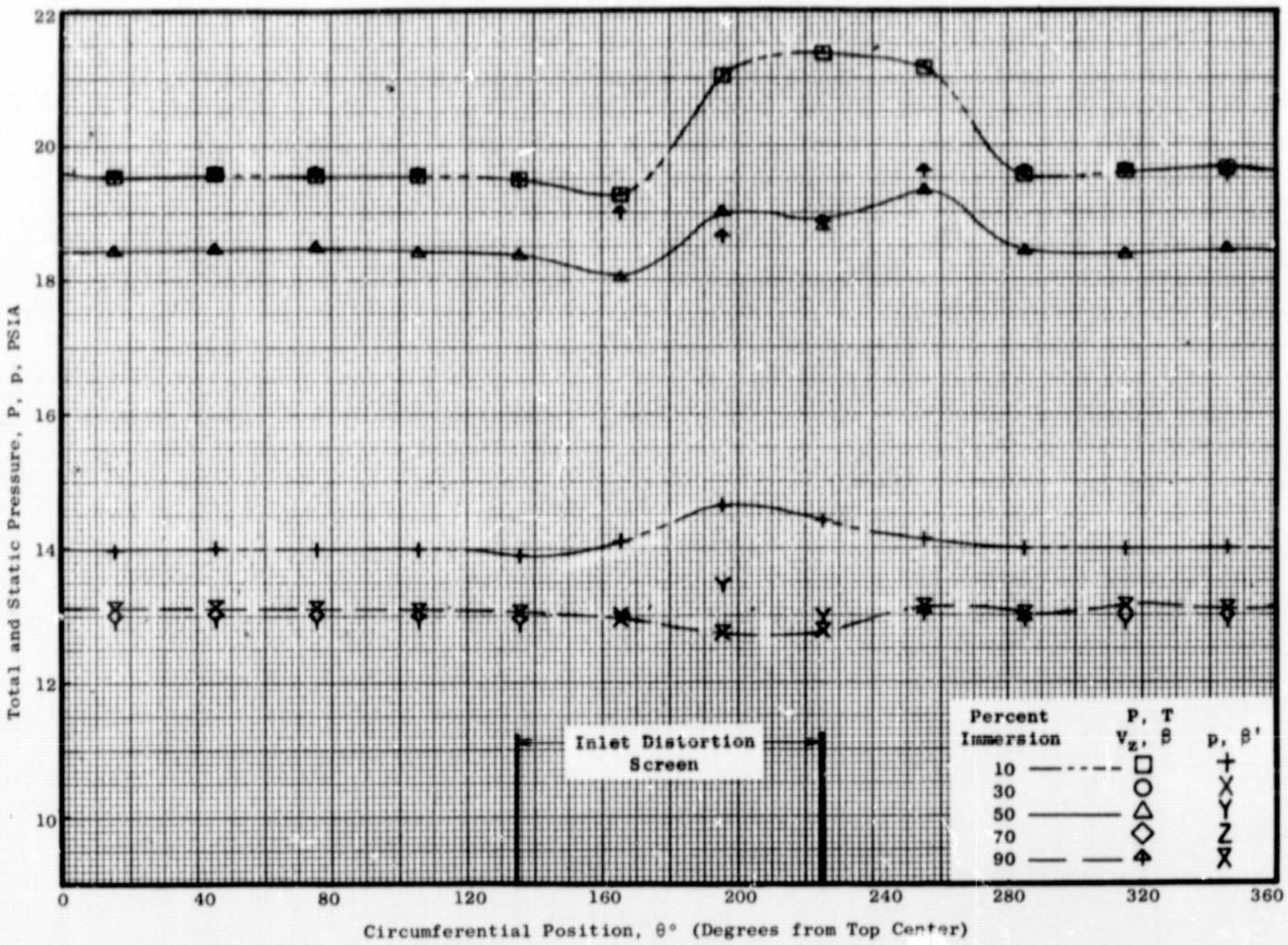

Figure 25(c). Circumferential Distortion Profiles of Flow Conditions at 100 Percent Speed Intermediate Flow with 40°/8° IGV/Stator Schedule at Plane 1.51.

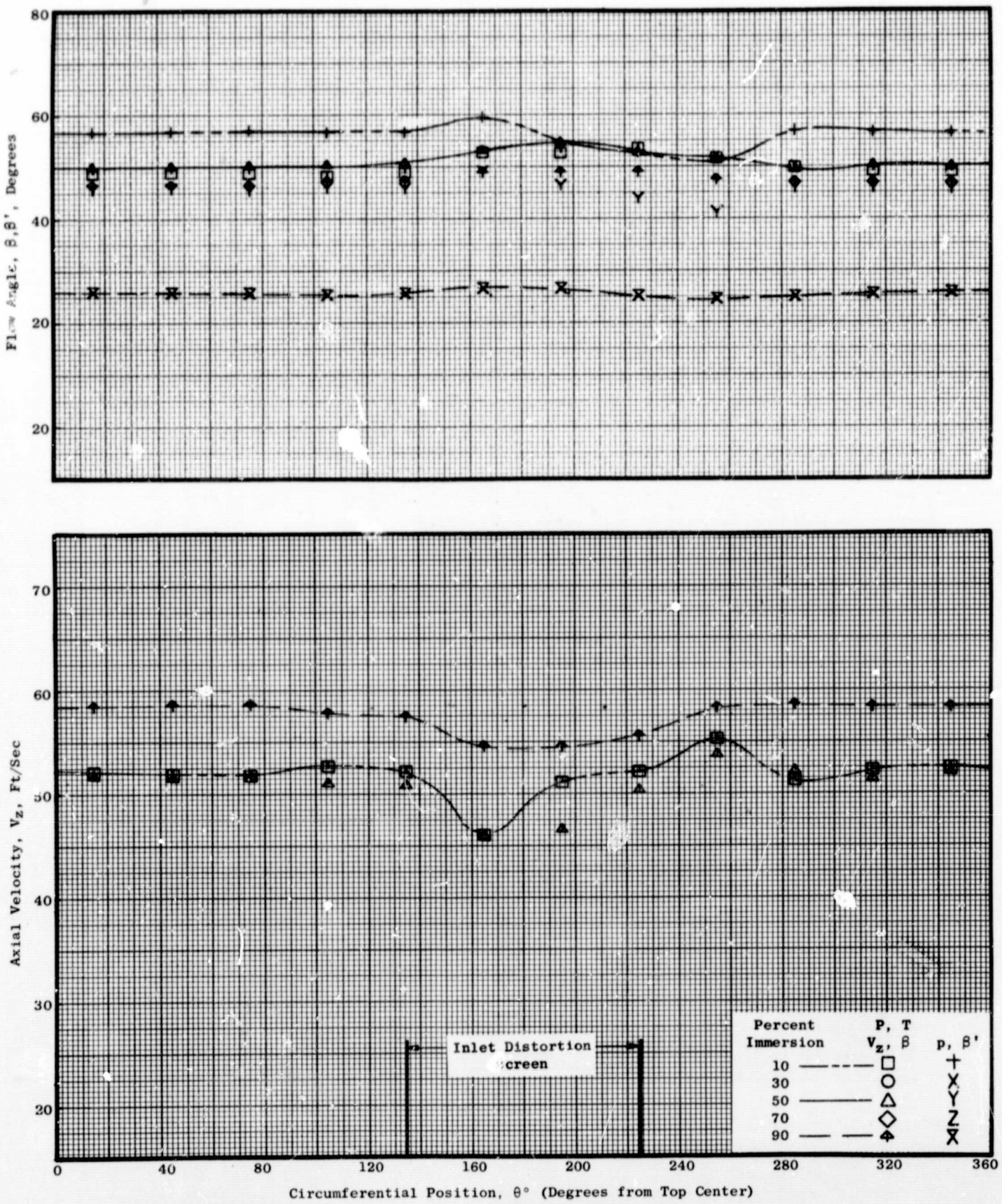

Figure 25(c). Circumferential Distortion Profiles of Flow Conditions at 100 Percent Speed Intermediate Flow with 40°/8° IGV/Stator Schedule at Plane 1.51 (Concluded).

3

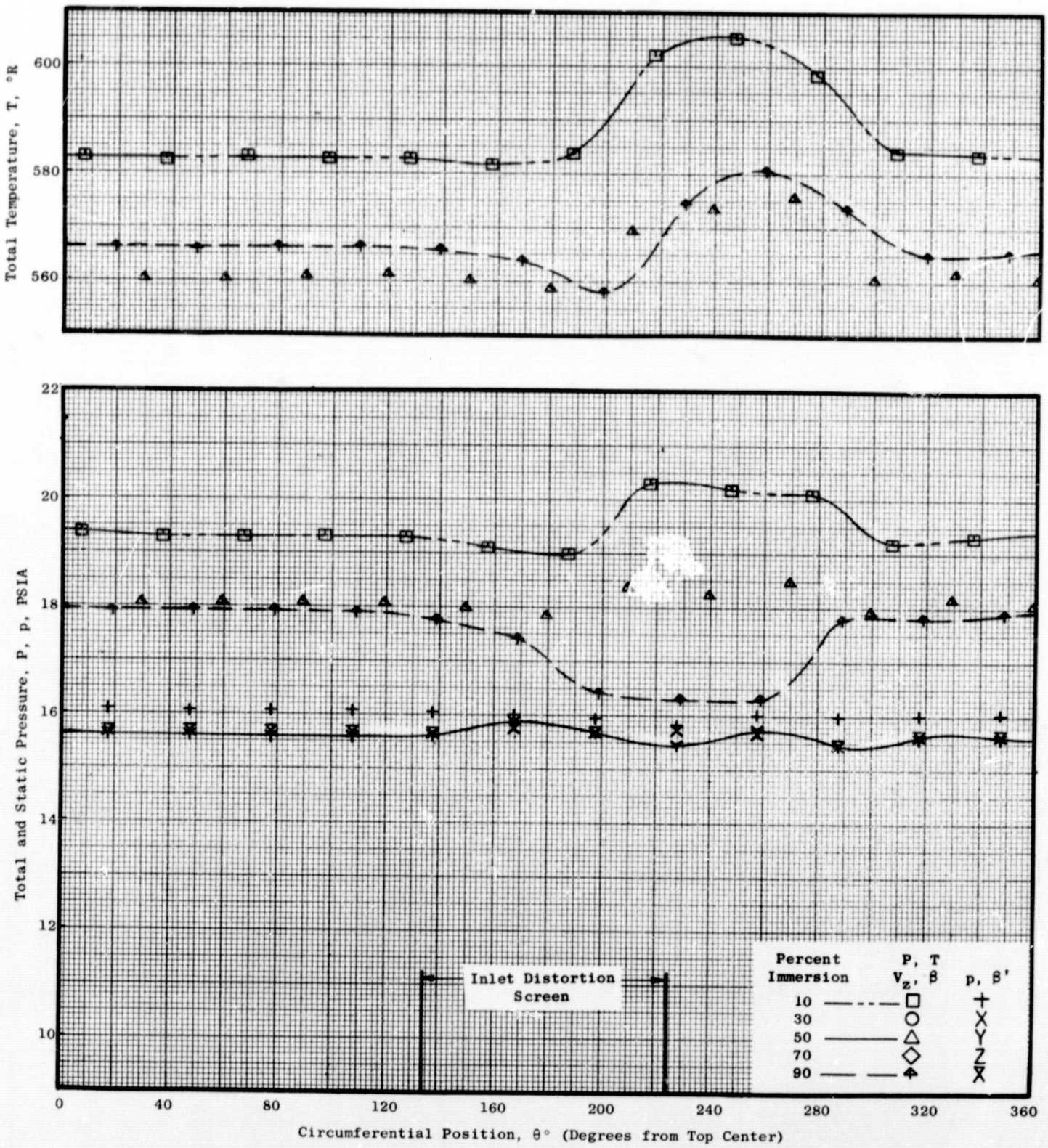

Figure 25(d). Circumferential Distortion Profiles of Flow Conditions at 100 Percent Speed Intermediate Flow with 40°/8° IGV/Stator Schedule at Plane 2.20.

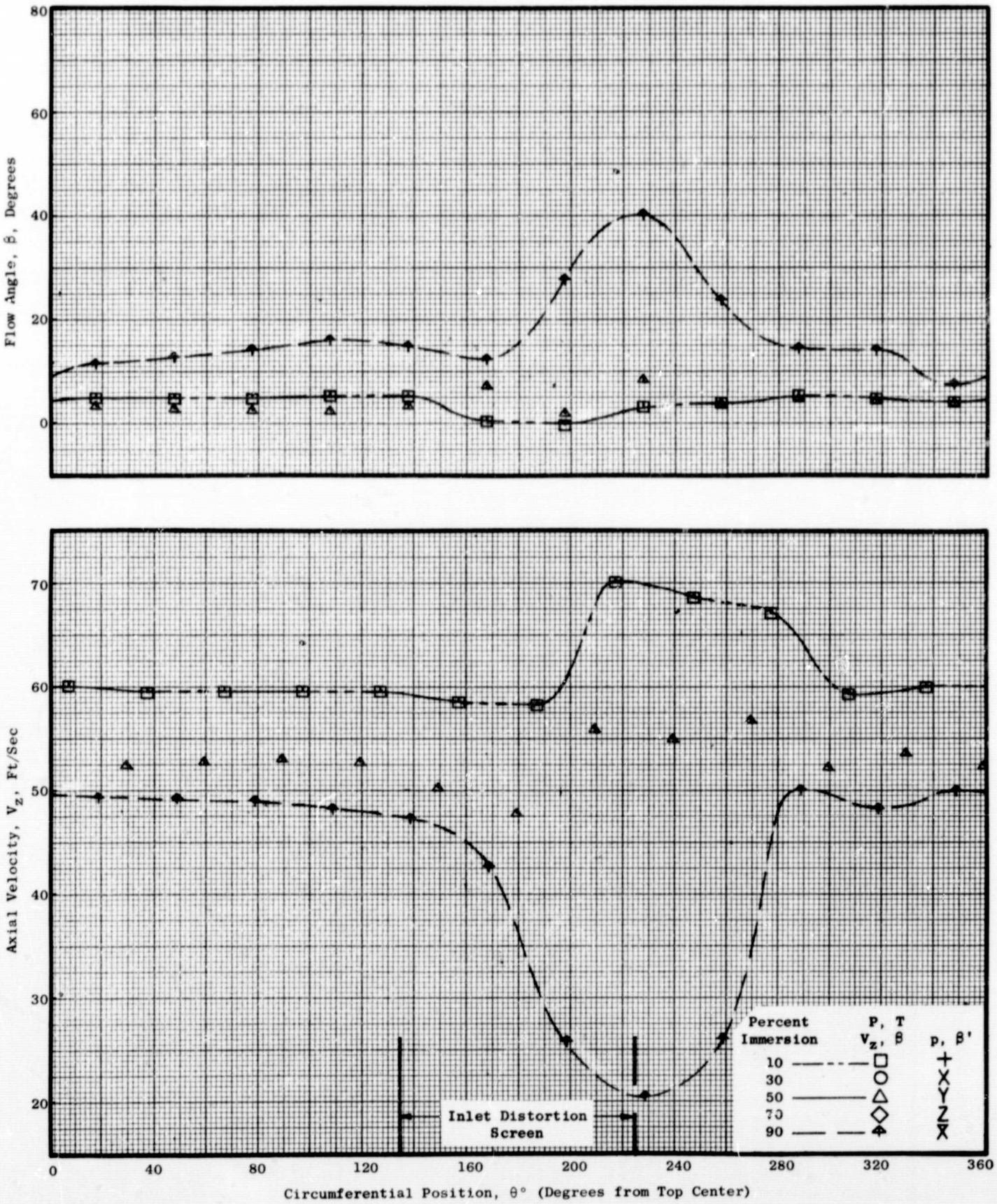

Figure 25(d). Circumferential Distortion Profiles of Flow Conditions at 100 Percent Speed Intermediate Flow with 40°/8° IGV/Stator Schedule at Plane 2.20 (Concluded).

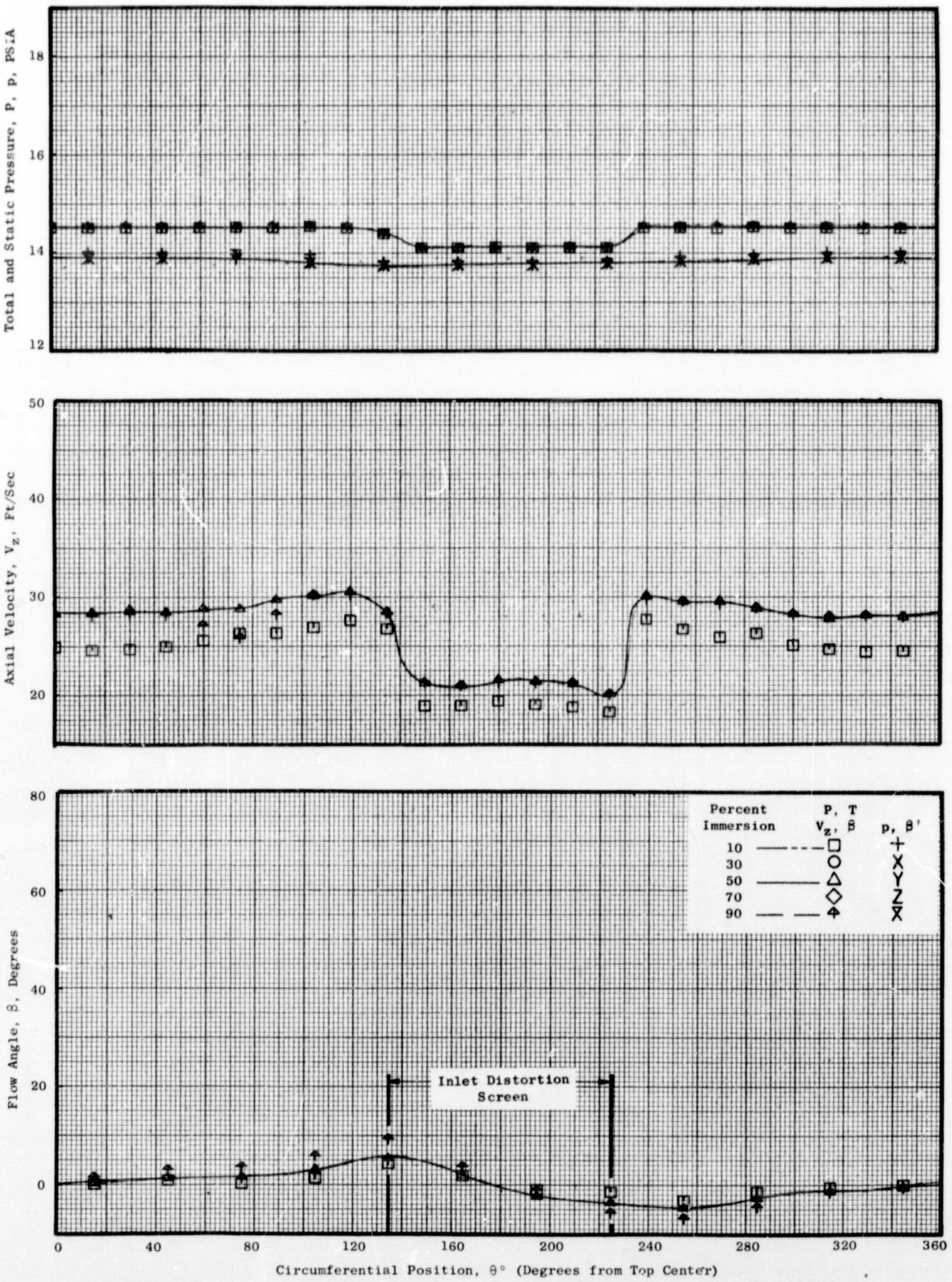

Figure 26(a). Circumferential Distortion Profiles of Flow Conditions at 70 Percent Speed Near Stall with 40°/8° IGV/Stator Schedule at Plane 0.18.

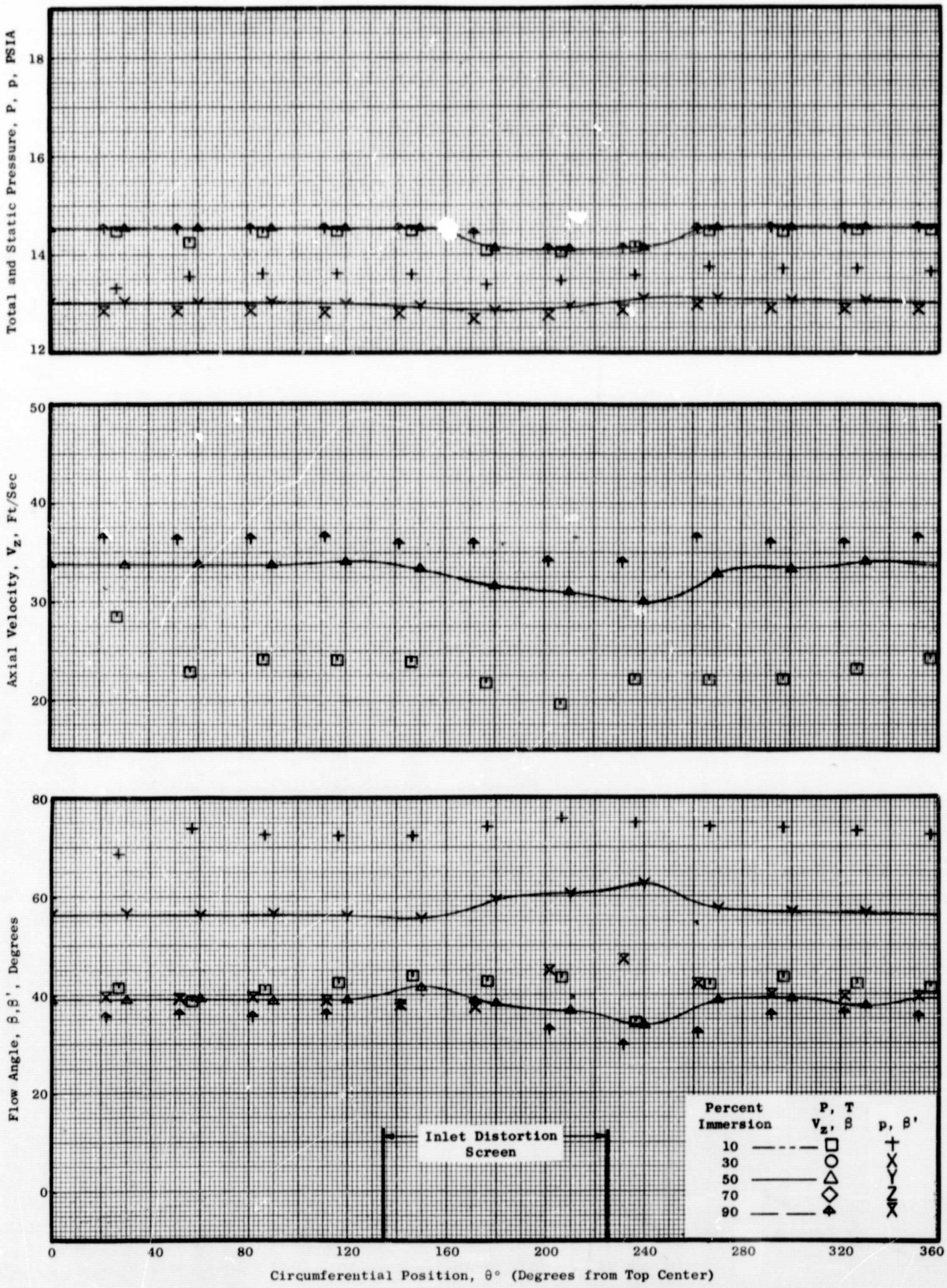

Figure 26(b). Circumferential Distortion Profiles of Flow Conditions at 70 Percent Speed Near Stall with 40°/8° IGV/Stator Schedule at Plane 0.95.

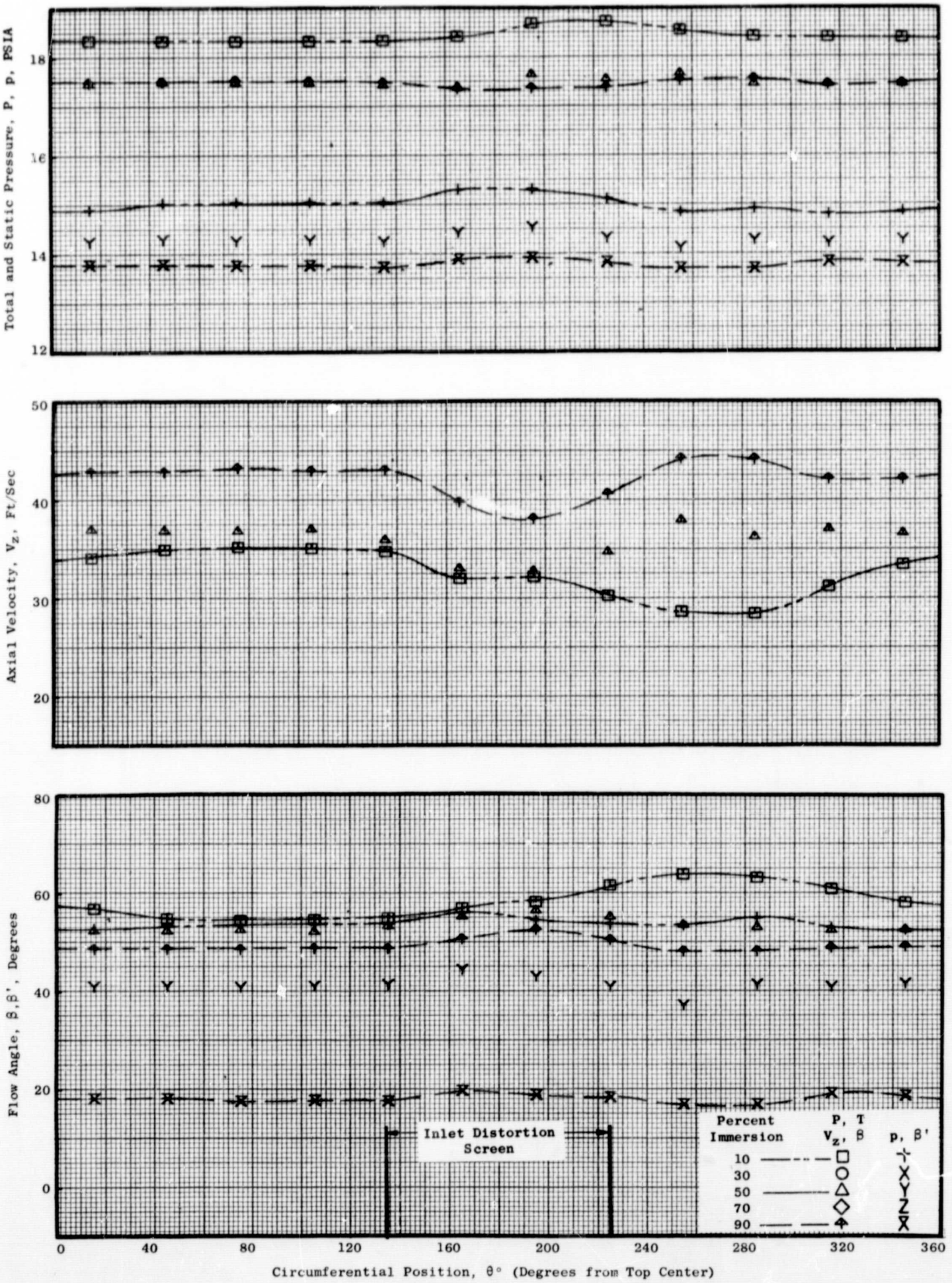

Figure 26(c). Circumferential Distortion Profiles of Flow Conditions at 70 Percent Speed Near Stall with 40°/8° IGV/Stator Schedule at Plane 1.51.

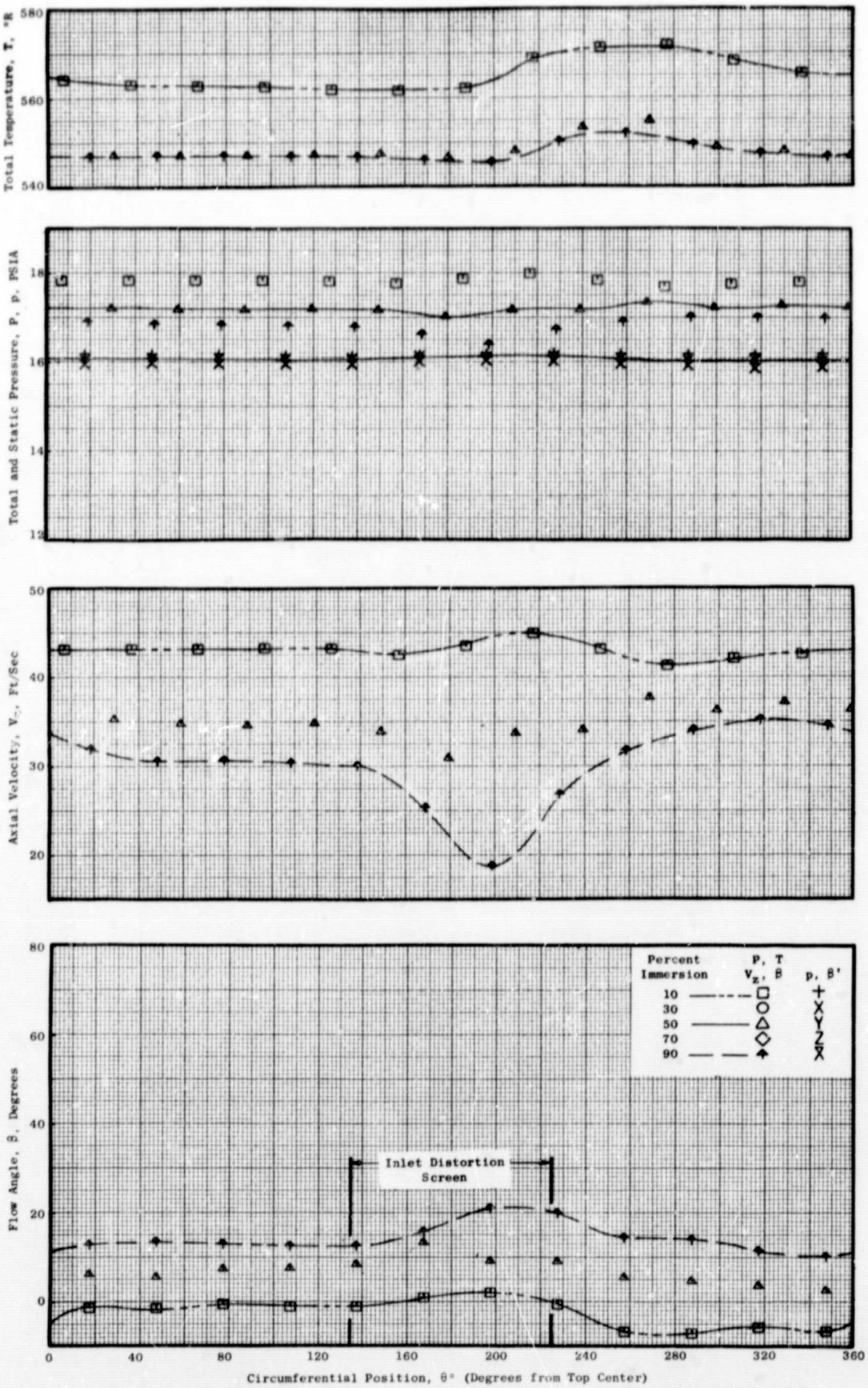

Figure 26 (d). Circumferential Distortion Profiles of Flow Conditions at 70 Percent Speed Near Stall with 40°/8° IGV/Stator Schedule at Plane 2.20.